PhD degree in Systems Medicine (curriculum in Molecular Oncology)

European School of Molecular Medicine (SEMM),

University of Milan and University of Naples "Federico II"

Settore disciplinare: Bio/10

Role of IRSp53 in epithelial polarity establishment and lumen morphogenesis

Syed Abrar Hussain Rizvi

FIRC Institute of Molecular Oncology (IFOM), Milan

Matricola n. R11121

Supervisor: Prof. Giorgio Scita

IFOM, Milan

Internal Advisor: Prof. Elisabetta Dejana

IFOM, Milan

External Advisor: Prof. Holger Gerhardt

MDC, Berlin

Anno accademico 2018-2019

Abstract

Polarity establishment is essential for the normal development and morphogenesis of virtually all epithelial tissues. Loss of epithelial polarity has been implicated in many disorders including tumorigenesis and metastasis.

Epithelial polarity is established by a multifaceted signalling cross-talk between a network of polarity determinants that include cell adhesion molecules, trafficking machinery, polarity complexes and the spindle orientation apparatus. Despite tremendous advance in defining the molecular details of how these processes are controlled, much remains to be understood as to how the coordination between all these components is achieved.

IRSp53, a versatile molecule operating at the membrane-actin interface, has been reported to be involved in the process of epithelial polarity but the mechanisms through which it operates has, however, remained completely elusive. Here, we studied the processes through which IRSp53 plays a role in the establishment of epithelial polarity and lumen morphogenesis in MDCK and Caco-2 derived 3-D cysts. We further extended the relevance of our *in vitro* findings to the kidney morphogenesis in our genetically modified animal models.

We found that IRSP53 is apically restricted at the luminal side of various epithelial tubular and glandular human, murine and zebrafish tissues. Further, IRSp53 is early recruited after the first cell division along the AMIS and essential for the formation of a single apical domain and the localized recruitment of aPKC and Podocalyxin (PDX). Molecularly, IRSp53 exerts this function by binding directly through a positively charged patch on its I-BAR-domain to the inactive form of RAB35, which colocalizes with IRSp53 at the onset of AMIS, and by controlling PDX trafficking. Additionally, membrane- and SH3- mediated interactions are required for proper localization and,

thus, for the function of IRSp53. IRSp53 is also found to localize to the spindle poles and to aid in the proper orientation of the mitotic spindle during cystogenesis. Consistently, IRSp53 depletion causes spindle misorientation, leading to aberrant cell divisions and multi-lumen phenotype during epithelial cystogenesis.

The critical physiological role of IRSp53 in epithelial morphogenesis is corroborated by the finding that genetic deletion of IRSp53 results in abnormal renal tubulogenesis, with profound defects in tubular polarity, architectural organization and lumen formation during both kidney development and in the adult kidneys either in IRSp53 zebrafish mutant lines and in IRSp53 KO murine models. We propose that the proper localisation of IRSp53 is pivotal for the assembly of macromolecular complexes on the apical domain of tubular and glandular epithelia which is, in turn, necessary for the proper kidney development by regulating cell polarity and lumen morphogenesis.

1.1) Phosphate-buffered Saline (PBS 1X)

1.2) Tris-HCl (1 M)

1.3) EDTA (0.5 M)

1.4) Tris-EDTA (TE 10X)

1.5) Tris-Acetate-EDTA (TAE 50X)

1.6) Tris buffered saline (TBS 10X)

1.7) JS lysis buffer

1.8) Laemmli buffer (2X)

1.9) Tris-Glycine buffer (10X)

1.10) Transfer buffer (10X) for Western blotting

1.11) Ponceau solution

2) Basic molecular cloning techniques

2.1) DNA digestion

2.2) Ligation

2.3) Transformation of competent cells

2.4) Minipreps

2.5) Large Scale Plasmid Preparation (Maxipreps)

2.6) PCR (Polymerase Chain Reaction)

2.7) Site directed mutagenesis

2.8) Agarose gel electrophoresis

2.9) DNA elution from agarose gel

2.10) RNA Extraction

2.11) cDNA synthesis

2.12) Quantitative Real time PCR (qRT-PCR)

2.13) Generation of IRSp53 constructs

2.14) Other constructs

3) **Reagents and antibodies**

4) **Cell Culture**

5) **Caco-2 Cyst formation assay**

6) **MDCK cyst formation assay**

7) **Lentiviral infection**

8) **Short interfering RNA (SiRNA experiments)**

9) **Protein Biochemistry**

    9.1) Western Blotting

    9.2) Co-immunoprecipitation

    9.3) Dot blot Assay

10) **Immunofluorescence (IF)**

    10.1) Cell Monolayers on Coverslips

    10.2) Cysts

11) **CRISPR-Cas9 KO Clones**

12) **Analysis of cysts for multi-lumen and spindle orientation**

13) **Calcium Switch experiment**

14) **Animal Models**

    14.1) IRSp53 KO Mice

    14.2) BAIAP2a mutant zebrafish

    14.3) Morpholino microinjections

15) **Imaging techniques**

    13.1) Microscope equipment

    13.2) Epifluorescence time-lapse microscopy

    13.3) Confocal spinning-disc time-lapse microscopy

16) **Statistical analysis**

17) **Histological analysis**

1.9) IRSp53 depletion perturbs the trafficking of Podocalyxin to the apical compartments in epithelial and endothelial cells

1.10) IRSp53 binds to Rab35 that may explain its role in the trafficking of apical proteins during polarization

1.11) IRSp53 binds to Rab35 through its I-BAR domain

1.12) IRSp53-Rab35 interaction controls PODXL trafficking to AMIS to establish a proper apico-basal polarity

1.13) I-BAR, CRIB and SH3 domains are all essential for proper polarization and lumenogenesis during spheroid formation

Part 2: IRSp53 is involved in the proper orientation of mitotic spindle during cystogenesis

2.1) IRSp53 is enriched at the spindle poles both in 2-D monolayers and 3-D spheroids during cell division and is required for the correct orientation of the mitotic spindle during cystogenesis

2.2) I-Bar domain of IRSp53 is required for the localization at the spindle poles, but it is not sufficient for the proper orientation of the spindle

2.3) I-BAR, CRIB & SH3 domains are all required to rescue the mis-orientation of spindle poles in IRSp53 depleted cysts

Part 3: Role of IRSp53 in proper tissue morphogenesis

Figure Index

Introduction

Materials and Methods

Results

List of abbreviations

2-D	two dimensional
3-D	three dimensional
ABI1	Abl-interactor 1
AMIS	apical membrane initiation site
aPKC	atypical protein kinase c
ARP2/3	actin-related protein 2/3
BAIAP2	brain-specific angiogenesis inhibitor 1-associated protein 2
BAR	bin-amphiphysin-Rvs167
Caco2	human colorectal adenocarcinoma cells
CDC42	cell division control protein 42 homolog
Crb	crumbs protein homolog
CRIB	CDC42/RAC interactive binding
Dlg	disks large homolog
ECM	extra-cellular matrix
ENA	enabled protein
EPS8	epidermal growth factor receptor kinase substrate 8
F-ACTIN	filamentous actin
F-BAR	FCH-BAR, Fes/CIP4 homology BAR
FAK	focal adhesion kinase
FH1	formin homology 1 domain
FH2	formin homology 2 domain
FMNL3	formin-like 3
G-ACTIN	globular actin
GAB	G-actin binding domain

GAP	GTPase activating protein
GEF	guanine nucleotide exchange factor
GUV	giant unilamellar vesicles
I-BAR	inverted BAR
IHC	immunohistochemistry
IRSp53	insulin receptor substrate protein of 53 kDa
IRTKS	insulin receptor tyrosine kinase substrate
KD	knock down
KO	knock out
Lgl	lethal giant larvae
LIN7	protein lin-7 homolog
MAD	multi-focal AMIS-like apical domains
MDCK	madin darby canine kidney cells
MEF	mouse embryonic fibroblast
MENA	mammalian enabled
MIM	missing-in-metastasis
N-BAR	N-terminal amphipathic helix BAR
NMDAR	N-methyl-D-aspartate receptor
Pals1	protein associated with LIN7
PAP	pre-apical patch
Par	partitioning defective
PATJ	Pals1-associated tight-junction homolog
PDX	podocalyxin
PDZ	PSD95-DLG1-ZO-1
PH	pleckstrin homology
PIP_2	phosphatidylinositol-(4,5)-bisphosphate

PIP_3	phosphatidylinositol-(3,4,5)-trisphosphate
PK	protein kinase
PP	protein phosphatase
PR	proline-rich
PRD	proline-rich domain
PSD	post synaptic density
PTB	phospho-tyrosine binding
ROCK	RHO-associated protein kinase
SDS-PAGE	SDS polyacrylamide gel electrophoresis
SH3	SRC homology 3 domain
SOS1	son of sevenless homolog 1
TIRF	total internal reflection fluorescence
VAC	vacuolar apical compartment
VASP	vasodilator-stimulated phosphoprotein
WASP	Wiskott-Aldrich syndrome protein
WAVE	WASP-family verprolin homologous
WH2	WASP homology domain 2
WRC	WAVE regulatory complex
WT	wild type
ZO-1	zonula occludens protein 1

Abstract

Polarity establishment is essential for the normal development and morphogenesis of virtually all epithelial tissues. Loss of epithelial polarity has been implicated in many disorders including tumorigenesis and metastasis.

Epithelial polarity is established by a multifaceted signalling cross-talk between a network of polarity determinants that include cell adhesion molecules, trafficking machinery, polarity complexes and the spindle orientation apparatus. Despite tremendous advance in defining the molecular details of how these processes are controlled, much remains to be understood as to how the coordination between all these components is achieved.

IRSp53, a versatile molecule operating at the membrane-actin interface, has been reported to be involved in the process of epithelial polarity but the mechanisms through which it operates has, however, remained completely elusive. Here, we studied the processes through which IRSp53 plays a role in the establishment of epithelial polarity and lumen morphogenesis in MDCK and Caco-2 derived 3-D cysts. We further extended the relevance of our *in vitro* findings to the kidney morphogenesis in our genetically modified animal models.

We found that IRSP53 is apically restricted at the luminal side of various epithelial tubular and glandular human, murine and zebrafish tissues. Further, IRSp53 is early recruited after the first cell division along the AMIS and essential for the formation of a single apical domain and the localized recruitment of aPKC and Podocalyxin (PDX). Molecularly, IRSp53 exerts this function by binding directly through a positively charged patch on its I-BAR-domain to the inactive form of RAB35, which colocalizes with IRSp53 at the onset of AMIS, and by controlling PDX trafficking. Additionally, membrane- and SH3- mediated interactions are required for proper localization and,

thus, for the function of IRSp53. IRSp53 is also found to localize to the spindle poles and to aid in the proper orientation of the mitotic spindle during cystogenesis. Consistently, IRSp53 depletion causes spindle misorientation, leading to aberrant cell divisions and multi-lumen phenotype during epithelial cystogenesis.

The critical physiological role of IRSp53 in epithelial morphogenesis is corroborated by the finding that genetic deletion of IRSp53 results in abnormal renal tubulogenesis, with profound defects in tubular polarity, architectural organization and lumen formation during both kidney development and in the adult kidneys either in IRSp53 zebrafish mutant lines and in IRSp53 KO murine models. We propose that the proper localisation of IRSp53 is pivotal for the assembly of macromolecular complexes on the apical domain of tubular and glandular epithelia which is, in turn, necessary for the proper kidney development by regulating cell polarity and lumen morphogenesis.

Introduction

1) Cell Polarity

Polarity is a common characteristic of all cells ranging from a single celled bacterium to a highly complex neuronal cell in humans [1] [2]. It is primarily achieved by asymmetric partitioning of biomolecules at different sub-cellular localisations through the generation of specialised sub-cellular domains in the cells. It is fundamentally required by all cell types to achieve complex biochemical tasks by sorting them into simpler modules which are then carried out at the respective specialised domains [1, 2].

Some of these specialised sub-cellular domains across a tissue may align along particular orientations to give rise to more complex forms of tissue polarity. This higher order of tissue polarity is required for the development of multifaceted structures such as the network of tubules in renal, hepatic, vascular or glandular tissues, multi-layered sheets of epithelium or the different layers of the brain cortex. Thus, cell polarity can be sub-divided into different types: apico-basal polarity, baso-lateral polarity, front-rear or migrational polarity, planar cell polarity, epithelial polarity. Since, this thesis work focuses mainly on the apico-basal and epithelial polarity, we will limit our discussions to these types of cell polarities only.

Apico-basal polarity is established by an asymmetric arrangement of specialised membrane domains and organelles along the apico-basal axis of epithelial cells. The basal side of the plasma membrane of these epithelial cells is usually attached to a basement membrane via integrins, while the apical side consists of specialised structures, such as microvilli, cilia, ion-pumps, transporters and other factors that are context and tissue specific. The presence of these specialised membrane domains on

the apical and basal surfaces allows a directional flow of molecules, metabolites and other informational cues. Apico-basally polarised cells, in an epithelium, can align in different higher order structures to give rise to epithelial sheets, layers or tubules.

Epithelial tissues are highly polarised layers of cells, usually at the interface of different environments. Polarity is essential in the development and functioning of virtually all these epithelial tissues. It is a pre-requisite for the formation of luminal and tubular structures both *in vivo* and *in vitro.*

At the cellular level polarity is established by a cross-talk of polarity complexes with the cell cytoskeleton, trafficking machinery and cell adhesion molecules [3]. Defects in any of these components or alterations of their coordinated activities result in the perturbation of cell polarity. Importantly, loss of polarity in mammalian tissues has been reported to cause many diseases including, Cystic fibrosis [4], Wilson's disease [5], polycystic Kidney disease [6], tumour development and metastasis [7].

2) Establishment of apico-basal polarity in epithelial tissues

In epithelial cells the establishment of apico-basal polarity is primarily achieved by targeting the different polarity complexes to specific sub-domains on the membrane. The components of three main polarity complexes were identified in elegant genetic experiments using C. *elegans* and *Drosophila* [8, 9]. These complexes are: 1. Partitioning defective (Par) comprising of Par3, Par6 and aPKC; 2. Crumbs, consisting of Crb, Pals1 and PATJ; and 3. Scribble consisting of Scrib, Dlg and Lgl [10, 11]. Par and Crumbs complexes are subapically located, whereas Scribble complex is positioned baso-laterally. These evolutionarily conserved polarity complexes act in a coordinated fashion either through cooperative or antagonistic means to establish the apico-basal polarity in the epithelial cells [12] [10].

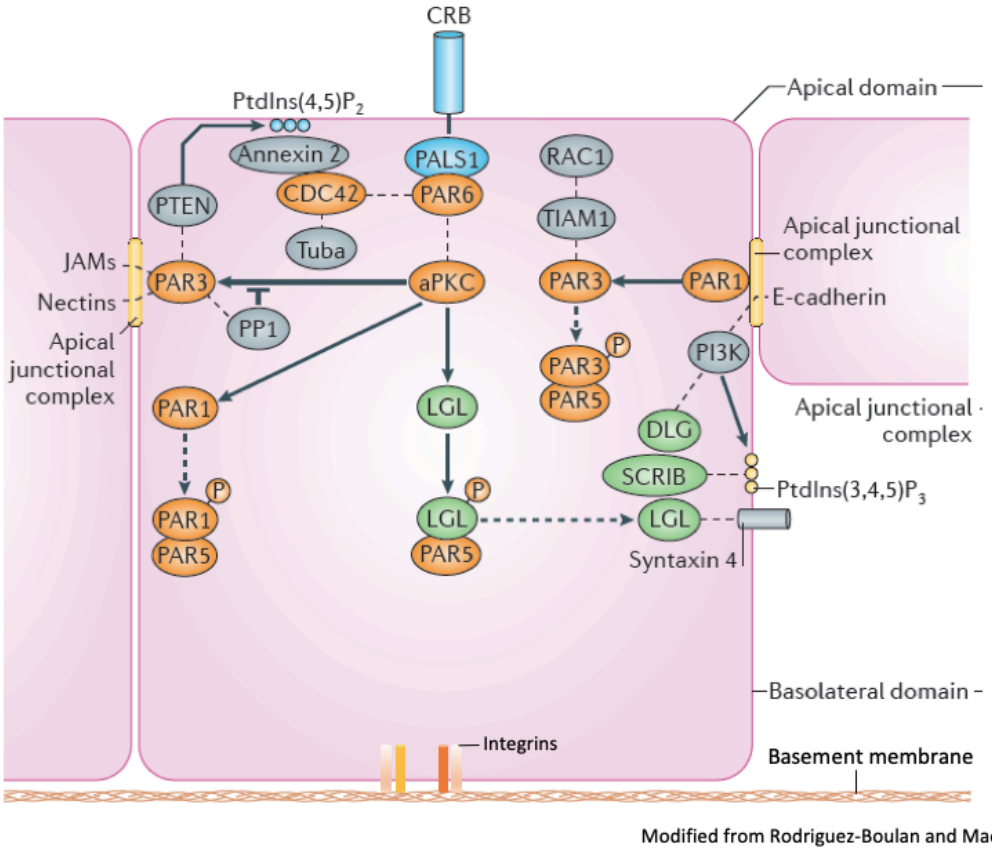

Fig 1: Apico-basal polarity establishment by an interplay between the components of the polarity complexes

CRB recruits PALS1, and through it Par6 as well, at the apical membrane. Par6 along with CDC42, which is recruited by annexin-2 to PIP2 rich apical domain and activated by its GEF – Tuba, activates aPKC. Activated aPKC phosphorylates LGL (a member of the Scribble complex) and PAR3 to exclude them from the apical membrane. PAR3 is recruited to the junctional complex in a PP1 dependant manner where it interacts with PTEN which mediates the enrichment of PIP2 in the apical membrane thus, forming a feedback loop to establish the apical polarity program. (Modified from Rodriguez-Boulan and Macara, 2014)

2.1) Par complex

The Partitioning defective (Par) complex comprises of Par3, Par6 and aPKC. Initially discovered in *C. elegans* embryos for their role in proper partitioning of germline specific P-granules [8]. Par complex was found to be highly conserved throughout evolution and specifically required for the establishment of polarity in mammalian cells [13, 14]. The Par complex is mostly associated with the tight junctions, a specialized type of cell-cell junction found in epithelia, formed by a multi-protein junctional complex, via binding of Par3 to junctional adhesion molecules (JAMs), and is involved in the regulation of apical tight junction formation. Their general function is to prevent leakage of transported solutes including water and to seal the paracellular pathway [15-17]. Par6 and aPKC are recruited by activated CDC42, a small GTPase, upon enrichment of phosphatidylinositol 4,5-bisphosphate [Ptdln(4,5)P_2] at the apical membrane to initiate polarity and lumenogenesis in 3-D cysts [18]. CDC42, which is activated apically by its guanine nucleotide exchange factor (GEF), Tuba [19], also controls the activation of aPKC at the apical membrane. Activated CDC42 binds to Par6, relieving its inhibition of aPKC kinase activity, which is important for the establishment of epithelial polarity [20, 21]. Activated aPKC phosphorylates Par3, which is then free to leave the apical Par complex and to bind at the adherens junctions separately [22, 23]. aPKC also phosphorylates Par1 and the notch-antagonist and endocytic protein Numb to exclude them from the apical domains for the proper establishment of polarity [24] [25]. Par1 is known to phosphorylate Par3 to exclude it from the adherens junctions. Par1 was also shown to phosphorylate IRSp53 in MDCK cells, which leads to its inactivation and cytoplasmic sequestration by 14-3-3 binding [26]. Par complex protein, Par6, can also directly interact with the components of Crumbs complex, Crb3 and Pals1, allowing a functional cross-talk and integration of the signalling pathways for the overall polarity establishment [27] [28, 29]

2.2) Crumbs Complex

Crumbs protein complex consists of Crb, Pals1 and PATJ, earlier identified as apical membrane proteins required for the proper organisation of epithelia in drosophila [9]. Crb is an apical transmembrane protein having three isoforms in mammalian cells with Crb3, most widely expressed in the epithelial tissues [27]. Pals1 (Protein associated with LIN seven 1) is a linker protein that binds directly, via its PDZ domain, to Crb3 for proper polarisation and lumenogenesis of epithelial cells [30, 31]. Pals1 mediates E-cadherin trafficking to the cell surface for adherens junction formation [32]. PATJ (Pals1 associated tight junction) is a scaffolding protein containing multiple PDZ domains. It is involved in regulating the localisation of polarity proteins and tight junctions via its interaction with Claudin1, JAM-A and ZO-3 [33, 34]. Its downregulation leads to the mislocalization of Crb3 and Pals1 from apical membranes and cell junction suggesting its role as a linker for Crumbs complex to these domains [35].

2.3) Scribble complex

The Scribble complex is composed of Scrib (Scribble), Dlg (Discs large) and Lgl (Lethal giant larvae) which are mainly localised at the baso-lateral domain of the epithelial cells [36-38]. Scrib directly interacts, via its 16 LRRs (leucine rich repeats) on N-terminus, with Lgl2 in polarised mammary epithelial cells [39]. Whereas, only an indirect interaction of Scrib with Dlg, via a protein called as GUK-holder, has been shown in *Drosophila* neurons [40]. Scrib is targeted to the baso-lateral membranes in an E-cadherin dependent manner via its LRRs [36]. Dlg is known to co-localise with E-cadherin at the lateral membranes of polarised epithelial cells to regulate junctional

integrity [41]. Scribble and Par complexes mutually antagonise each other to regulate the boundaries of apical and basolateral domains. This is achieved partly by binding of Lgl to Par6/aPKC in absence of Par3, to restrict aPKC activity to the apical domains. Whereas, aPKC in turn phosphorylates Lgl to inactivate and restrict it to the baso-lateral membrane [42, 43]

3) Role of ECM and integrin signalling in epithelial cell polarity

In this chapter, I will describe general principles through which cells sense extracellular cues and transduce them into signalling pathways, in turn, affecting the establishment of a proper polarity. I will focus on the best characterized cell-substrate adhesion receptors, Integrins, without getting into the detailed analysis of the plethora of mechanisms and routes mediating their chemico-mechanical sensing roles.

Most of the cells in tissues are surrounded by fibrillar proteins, such Laminin, Collagen, Fibronectin, proteoglycans, forming intricate networks known as the Extra Cellular matrix (ECM), that in addition to physically supporting the tissues also acts as local reservoirs of various growth factors. ECM molecules can be deposited by tissue-associated fibroblasts and many other cell types within the tissue, including the epithelial cells themselves. ECM molecules play an important role in providing specific biochemical and physical cues to cells about their surrounding environment. Among the various cell-receptors capable of sensing and interpreting these cues, the best characterized are cell surface receptors known as ‘Integrins’. Integrins are heterodimeric plasma membrane proteins composed of an alpha and a beta chain, which act as mechano- and biochemical-sensors of the cells by relaying the signals from ECM in an outside-in fashion through the dynamic assembly of multiprotein complexes at their cytoplasmic domains. These complexes are intrinsic components of a complex signal transduction system, which enables the cells to precisely respond

to microenvironmental cues by impinging primarily on the cellular cytoskeletal architecture and dynamics [44, 45].

Epithelial cells usually face different types of ECMs along their differentially organized apical and baso-lateral domains. Usually from their basal side, epithelial cells are in contact with a specialised ECM surface, known as basement membrane, which is composed of an intricate and dense meshwork of Collagen IV, Laminins, proteoglycans and nidogen. Cells recognise these ECM molecules via specific dimeric isoforms of Integrins that provide spatial cues for the establishment of an apico-basal axis in accordance with this orientation [46]. Since, most of the polarised epithelial cells face different environments on their apical and basal sides, the ability to appropriately sense the ECM is very important for the establishment of a proper polarity program. Consistently, this outside-in signalling from ECM has been shown to be essential for polarisation and development of 3-D cysts *in vitro* [47, 48]. Additional mechanisms that rely on outside-in signalling are also at play. For example, a mechanism to segregate the apical domains from the baso-lateral domains involves the co-ordinated maturation of cell-cell contacts by Cadherins with respect to the integrin mediated contacts with the ECM [49] [47] [48]. A case in point of 'adhesion cross-talk' between cell-cell and cell-ECM contact is provided by the signalling axis mediated by Rap1 GTPase. This GTPase has been shown to be positioned at a critical decision point at the cross-roads between integrin and E-cadherin-mediated adhesion and signalling has a major impact on the establishment of epithelial polarity [50]. Indeed, in dominant negative RAC1 expressing MDCKII cells, the constitutive activation of Rap1 causes reversal of inverted polarity. However, despite the defects in epithelial polarity are reversed, the defects in Laminin deposition are not corrected, suggesting an outside-in signalling independent of ECM sensing [51].

Since, epithelial cells are also capable of controlling the deposition and maturation of their ECM they can also establish polarity by an inside-out signalling mechanism through this process. Accordingly, Epithelial cells are known to respond to the isotropic ECM signals from Collagen I by activation of β1-integrin and RAC1 activity. Upon activation, RAC1, in turn, become able to regulate the secretion of Laminins necessary for the assembly of a basement membrane at the basal side of these cells [52] [53]. Notably, among the various effectors RAC1 uses in regulating this process, it was also shown to bind to the adaptor protein IRSp53 [54]. This interaction triggers an ill-defined signalling pathway that promotes Laminin secretion. MDCK cells lacking IRSp53 display reduced cell-matrix interactions and decreased Laminin deposition [26].

Thus, epithelial cells are also capable of responding by an inside-out signalling mechanism to modulate the ECM for the establishment of apico-basal polarity. Failure of this inside-out mechanism by RAC1 inactivation or by blocking β1-integrins leads to an inversion of apico-basal polarity [52] [53]. This inversion of polarity is thought to be caused by the mis-localisation of the polarity complexes and their components. For example, Dlg, a member of the baso-lateral protein complex, mis-localises to the apical domains in all cases of inverted polarity, whereas, functional inhibition of β1-integrins by antibodies leads to the mislocalization of Par3 to the cytoplasm [51]. Thus, ECM modulation by an inside-out signalling mechanism is also required for the proper localisation of polarity proteins.

The interaction with ECM is also critical for the establishment of complex tissue morphogenetic program *in vivo*, and specifically to provide the right cues to epithelial cells for the formation of distinct apical and basal domain, in turn essential for higher order structures in the tissues. Perturbation or impairment of Cell-ECM interactions as a consequence, for example, of the loss of deficiency in certain α/β-integrins or in the Integrin associated protein, ‘Talin’, which connects them to the cytoskeleton, leads to

multiple lumina in Drosophila trachea [55]. ECM remodelling also plays a central role in epithelial branching morphogenesis during development of kidneys, lungs, pancreas and mammary glands [56] [57]. Thus, both outside-in and inside-out signalling by ECM and cell surface molecules seem to play an important role for epithelial tissue development and morphogenesis.

4) MDCK polarisation and cyst development

In this chapter, I will describe general principles of MDCK cyst formation and mainly focus on some mechanistic aspects of polarisation mediating the apical domain specification through transcytosis of the apical determinants.

MDCK cells when plated as single cells on a gel of ECM (Matrigel) and surrounded by Matrigel-containing media, undergo polarisation and lumen morphogenesis to form cysts. These cysts are spherical cell monolayers enclosing a central lumen [58]. The cells interpret the extracellular cues from the ECM, transform them into an intracellular signalling cascade to generate an axis of polarity. Once this axis is established by an outside-in mechanism, the next crucial step is the formation of a central lumen enclosed by an apical membrane mutually formed by the apical domains of the cell-monolayer [59]. Therefore, all the apical domains must align in a proper orientation once the axis of polarity is established. The apical domains are determined by transcytosis of apical membrane determinants like gp135/PDX and aPKC etc from the ECM-facing plasma membrane to the apical membrane. These apical proteins are deposited on the intervening membrane formed between the cells which gives rise to the first apical domain. This apical domain is called AMIS (Apical Membrane Initiation Site) and is the site of *de novo* lumen formation [60].

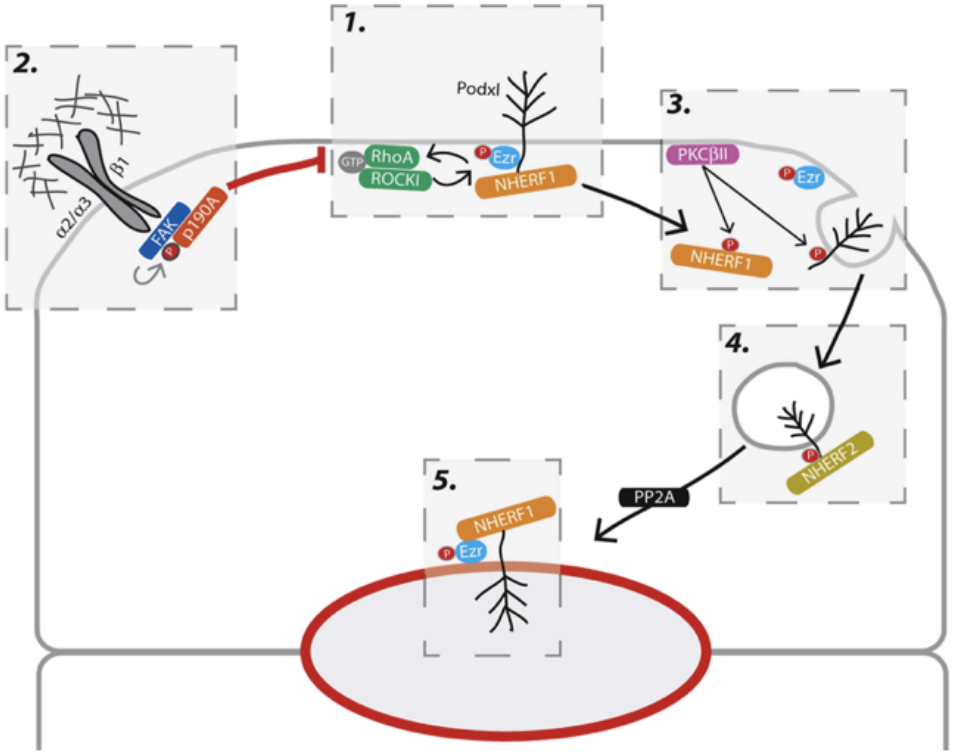

Modified from, Bryant, et al., 2014

Fig. 2: Model depicting the transcytosis of Podocalyxin (Podxl) during early polarisation of MDCK cysts

(1) RHO-ROCK-I phosphorylation stabilise Podxl-NHERF1-pEzrin complex at the cell periphery, (2) RHO-GTP downregulation by an integrin-RHO-GAP module leads to destabilisation of this complex at the periphery, (3) Phosphorylation of Podxl-NHERF1-Ezrin complex by PKCβII leads to the dissociation of this complex which triggers endocytosis of Podxl, (4) Podxl and NHERF2 are trafficked to the apical domain, and (5) Transcytosis of Podxl to the apical domain leads to the formation of AMIS, where PP2A dependent re-association of the Podxl-NHERF1-Ezrin complex is achieved.

Initially, at the first cell division, a two-cell stage with an inverted polarity is formed. This is due to the localisation of apical markers, such as F-actin, PDX, Crb, at the outer ECM bordering surface of the plasma membrane, while basolateral markers, such as E-cadherin, Na/K-ATPase and Occludin, are localized at cell-cell interface of the two newly formed daughter cells [60]. The signalling triggered by the activation of small GTPase RHOA and its effector RHO kinase-associated protein kinase-I (ROCK-I) at the ECM facing cell membrane may account for the stabilization of PDX at this site. In fact, RHOA/ROCK-I signalling, among various changes, leads to the phosphorylation

and activation of Ezrin (pEzrin) at the membrane [61] [62]. pEzrin binds PDX, NHERF1/EBP50 into a complex with actin cytoskeleton at the outer ECM-facing membrane [63]. An outside-in signalling by ECM sensing integrin receptors might trigger a reversal of polarity via transcytosis. This maybe initiated mainly due to the activation of α2β1/α3β1-integrin receptors that become activated following their engagement with the ECM. The signalling downstream of α2β1 results in the activation of the GTPase RAC1, which, as discussed previously, can induce laminin secretion and assembly at the basal side of the epithelial cells [53] [64]. Blocking the signalling downstream of β1-integrins or RAC1 leads to disruption of Laminin deposition and assembly, and causes an inversion of apico-basal polarity [52, 53]. Laminin assembly around the ECM-facing cell membrane may also inhibit RHOA-ROCK activity through the focal adhesion kinase (FAK)-dependant recruitment of p190A-RHO-GAP [61] [62]. This also, reduces the phosphorylation status, and thereby the activity, of Ezrin at the cell-ECM interface and relieving of the PDX-NHERF1/EBP50-Ezrin complex, allowing the endocytosis of apical proteins like PDX and their deposition at the AMIS [61] [62]. These apical proteins are then transcytosed to the apical domain with the help of an array of RAB-GTPases. Along this endocytic route, RAB-GTPases, their effectors, microtubules, motor proteins, exocyst complex and CDC42/Par complex all play important roles in the proper trafficking and deposition of the apical proteins at the AMIS [65] [66]. RAB35 physically interacts with PDX and is involved in its trafficking into RAB11a-positive vesicles to which RAB8a is also recruited by its GEF Rabin8. Failure of PDX translocation due to the knock-down of RAB35 has been shown to induce inverted polarity in the cysts [67, 68]. Axn2 and CDC42, activated by its GEF Tuba, associate with these vesicles to help in their transport towards, what will become the apical membrane. CDC42 binds to inverted formin 2 (INF2) to regulate the apical trafficking of these vesicles with the help of MAL2, which is an essential component of

the apical transcytosis machinery [69] [70] [71]. The motor protein, Myo-5B, also binds Rab8a/11a on these vesicles and may help in moving them along F-actin trails towards the apical domain. This process has been shown to be required for the normal polarisation and lumenogenesis of MDCK cysts [72, 73].

Taken together, this set of findings suggest that INF2 may help to generate a thrust for the vesicle movement by actin polymerisation and also create trails along the way on which other apical vesicles may travel with the help of Myo-5B. At the apical surface, these vesicles are docked by the binding of RAB8a/RAB11a to the exocyst complex subunit Sec15a with the help of Par3-aPKC to form the AMIS [61] [74]. CDC42 also binds Par6 and Par3, which may help to link it with Par3-aPKC-Exocyst complex at the AMIS [60]. Interaction of the Exocyst and Par complex may direct Exocyst-dependent vesicle docking events transiently to AMIS, allowing the apical determinants to establish the axis of polarity, before both these complexes re-localise to the tight junctions [60]. Par6 and aPKC form a complex with CDC42, which is activated apically by its GEF Tuba in a Rab8a/Rab11a dependent mechanism [60, 75]. However, it's not clear how RABs may actually control the activity of CDC42 GEFs. Also, CDC42 in alliance with Annexin2 (Anx2), controls apical trafficking of RAB11a/RAB8a containing vesicles [60]. This suggests that a molecular-interplay, in the form of a feedback loop, exists to ensure a proper polarisation mechanism through transcytosis of apical protein containing vesicles. These vesicles also carry atypical protein kinase C (aPKC)-iota, its activator phosphoinositide-dependent protein kinase 1 (PDK1) [76] [73], and the Ste20-like protein kinase Mst4 [76] which contribute to the structural differentiation and further stabilization of the apical domain by phosphorylation of Ezrin [63].

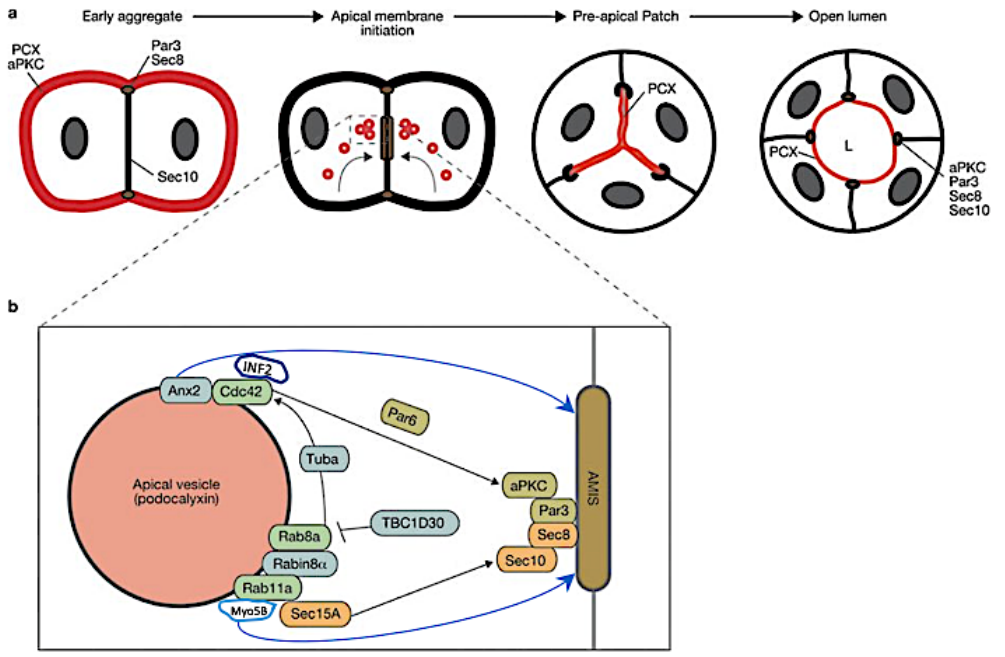

Modified from, Bryant, et al., 2010

Fig. 3: Schematic of the stages of MDCK cyst development

(**a**) Schematic showing different stages of polarization and lumen morphogenesis in MDCK cysts. Initially, Podocalyxin (PCX, marked in red), along with other apical determinants is localized to the periphery of cells undergoing cystogenesis. These apical determinants are internalised into transcytotic vesicles and delivered to the AMIS. Accumulation of PCX at AMIS leads to its progression into a PAP. Expansion due to the repulsion of negatively charged PCX molecules on the opposing membranes allows opening of the luminal space. Red lines, PCX; black lines, plasma membrane; grey ovals, nuclei; brown ovals, tight junctions; brown rectangle, AMIS; L, lumen. (**b**) schematic representation of the molecular determinants of the transcytosis process involved in delivery of apical protein containing vesicles to the AMIS during polarisation.

As a result of this transcytosis, the apical proteins start to accumulate at the apical membrane to give rise to an AMIS. At the apical domain, PDX, which is a negatively charged transmembrane glycoprotein, acts as an anti-adhesin. PDX molecules on the membranes of the opposite cells at the apical domain, experience a repulsive force because of the negative charges. This repulsive force is able to push these membranes apart to open up a space in between adjacent cells, thus forming a Pre-Apical Patch (PAP). PAP is an apical domain where the PDX localization starts to be noticeable from the lumen itself. As local concentration of PDX at the PAP increases,

the space between the membranes starts to expand [60]. A polarised secretion of fluids into this luminal space gives rise to a fully formed lumen enclosed within the apical domains of the cell monolayer. Upon expansion of the cysts, subsequent divisions in the monolayer of cells must be properly aligned to the already established apico-basal axis of the dividing cells. This requires a proper co-ordination of the cell divisions by a near perpendicular alignment of their plane of division with respect to the apico-basal axis. We will discuss more on the process of lumenogenesis and further growth of the cysts by cell divisions in the following chapter.

5) Caco-2 cyst development and lumen morphogenesis

In this chapter, I will describe the general principles of Caco-2 cyst polarisation and lumen morphogenesis. Since, the mechanism of apical trafficking was described in the previous chapter, here, I will focus more on the role of mitotic spindle orientation and polarised secretion of fluids in the proper polarisation and lumen morphogenesis of these epithelial cysts.

Caco-2 (originally named, Cancer coli-2; Fogh, et al., 1977 [77]) are human epithelial colorectal adenocarcinoma cells which retain the ability to polarise and functionally differentiate, towards confluency, into a layer of enterocytes with apical microvilli [78]. These cells have been extensively used to model intestinal barrier functions for drug uptake as polarised monolayers [79, 80]. Caco-2 cells when embedded as single cells in a three-dimensional matrix of collagen and Matrigel generate polarized cysts with a single central lumen [81, 82]. The steps of polarisation in these cysts follow overall the same pattern as that of the MDCK cysts described in the previous chapter. In Caco-2 cells, at the single cell stage, their apical markers such as aPKC and F-actin are localised at their outer ECM-facing membrane. The first cell division acts as a trigger to break-down this arrangement and rapidly translocate these apical determinants to the newly formed intervening membrane between the two cells. In Caco-2, this relocalization may be achieved during the cytokinesis stage, so that an apical domain consisting of aPKC, ZO-1 and demarcated by E-cadherin on either side, is already formed at the two-cell stage [82]. Irrespective of some minor differences in Caco-2 and MDCK polarisation, the basic mechanism of the apical trafficking appears to be strikingly similar in both the systems. Interestingly, the regulators of apical trafficking in MDCK cysts have also been shown to be important for the trafficking of apical determinants and proper polarisation in the gut of animal models *in vivo* and in

Caco-2 cells *in vitro* at least in 2-D cultures (reviewed in, Amy Christine Engevik and James R. Goldenring, 2018 [83]).

As Caco-2 cells proliferate further to form a cyst, the cell-divisions are oriented in such a way that the apical domain is maintained exclusively at the centre and the basal domain at the periphery, thus, creating an apico-basal axis of polarity in the cysts [82]. This alignment is maintained in subsequent divisions by positioning the mitotic spindle at the near perpendicular orientation with respect the apico-basal axis. This arrangement is analogous to the planar or symmetric cell divisions in epithelial monolayers. The proper orientation of these epithelial cell divisions is achieved by a coordinated interplay between the cell polarisation machinery with the mitotic spindle [84].

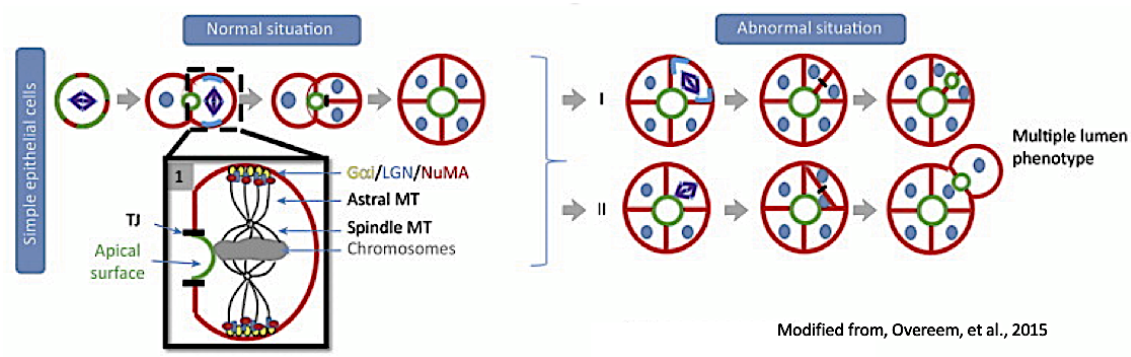

Fig. 4: Schematic representation depicting the role of spindle orientation during polarisation and lumen morphogenesis of epithelial cells

The orientation of the mitotic spindle poles determines the axis of cell division and controls the positioning of the apical lumen. Epithelial cells orientate the axis of their mitotic spindle (and thus the axis of the cell divisions) perpendicular to the apico-basal axis. This leads to the orientation of the daughter cells in the same apico-basal axis. Perturbation of this process by aberrant spindle orientation leads to out-of-plane cell-divisions and the formation of ectopic apical lumens. Spindle orientation during mitosis is regulated in part by the recruitment of Gαi, LGN, and NuMA to the polar cell cortex (Insert 1). Abbreviations: LGN, leu-gly-asn repeat protein, also known as GPSM2 (G protein signalling modulator 2); NuMA, nuclear mitotic apparatus protein

The centrosomes or the spindle-poles organise the mitotic spindle by nucleating three types of microtubules (MTs); 1) Kinetochore MTs, attach to the chromosomes to

move them to the opposite pole; 2) Polar MTs, overlap in anti-parallel fashion over the mid plane and help to bind the whole assembly together and 3) Astral MTs that link this whole assembly to the cell cortex and thus help in its proper positioning during the mitosis. Astral MTs bind to a conserved protein complex consisting of Gαi subunit of the hetero-trimeric G-proteins, LGN (Leu-Gly-Asn repeat protein, also known as GPSM2; G-protein signalling modulator 2), and NuMA (nuclear mitotic apparatus protein), which, in a Par3/aPKC-dependent manner, controls spindle orientation by anchoring them to the lateral cell cortex [85] [86].

Gα is known to bind the plasma membrane through its myristoyl group [87], thus paving the way for the cortical assembly of Gαi-LGN-NuMA. Only GDP-bound form of Gαi is able to interact with LGN. Gαi-GEF; Ric-8A (Resistance to inhibitors of cholinesterase 8A) generates a pool of Gαi-GDP which binds to LGN and targets it to the cortex. LGN acts as a molecular scaffold which brings in NuMA [88]. Cortical NuMA mediates the interaction with Dynein which binds to the astral MTs. Thus, helping in the proper positioning of the centrosomes [89]. The minus-end directed movement of the Dynein anchored at the membrane by Gαi-LGN-NuMA results in the traction forces pulling on astral MTs towards the poles to reinforce the spindle assembly with the cell cortex [89]. aPKC can phosphorylate LGN, which binds to 14-3-3 and can no longer bind to Gαi, thus resulting in its exclusion from the apical domains. Par3, which recruits aPKC to the apical domain, is also required for the proper spindle orientation in MDCK cells [86]. Interestingly, CDC42, which binds to Par6/aPKC complex to activate aPKC [90], has also been shown to be essential for the proper orientation of the mitotic spindle in Caco-2 cysts [82]. Depletion of CDC42 in Caco-2 cysts results in an aberrant multi-lumen phenotype [82]. Recent studies in HeLa cells has shown that Ran-GTP prevents the cortical enrichment of NuMA-LGN above the metaphasic plate, thus confining their localisation to the polar cortex adjacent to the spindle poles only [91].

Thus, a coordinated mechanism of action by the polarity proteins and the spindle apparatus may be at play to establish and maintain the overall apico-basal polarity during cystogenesis.

The next step in the process of cystogenesis is the opening up of a central lumen at the pre-apical patch which, as described in the previous chapter, is achieved with the help of a repulsive force generated by negatively charged Sialomucins, including PDX at the opposing apical membranes [60]. The expansion of the lumen in the epithelial cysts occurs through a process of internal expansion due to fluid accumulation, driven by polarized ion transport [82]. This is achieved by the apical distribution of the ion channels, like cystic fibrosis transmembrane conductance regulator (CFTR), Na^+/K^+ ATPase, H^+/K^+ transporters etc. CFTR secretes chloride ions, which creates a negative charge inside the lumen. This may follow an efflux of Na^+, K^+ and H^+ ions to neutralise the charge, resulting in a very high concentration of these ions inside the lumen. This, in turn increases the osmotic potential inside the lumen and thus drives the accumulation of fluids and the lumen expansion [82, 92]. Even though, the polarisation and the formation of the apical domains is achieved quite early, the process of lumen expansion is slow and inefficient in case of Caco-2 cysts. In this system, usually less than 50% of Caco-2 cysts develop a lumen after 12 days in culture. However, this process can be accelerated by the stimulation of cAMP signalling with cholera toxin (CTX) treatment at day 6 for 12 hours, which can induce lumen expansion in about 90% of the cysts at day 7 [82]. CTX induces ADP-ribosylation and thus inactivation of the GTPase activity of Gαs subunit causing a constitutive production of cAMP through Adenylate cyclase (Ac). This leads to activation of PKA, which, in turn, phosphorylates CFTR leading to continuous efflux of Cl^- ions into the lumen [82, 93]. Consistently, 6-Bnz which is a cAMP analogue that specifically activates PKA also induces rapid lumen formation. While Ouabain, an inhibitor of the Na^+/K^+ ATPase, completely abolishes the

lumen expansion [82]. Polarised secretion of fluids to drive the expansion lumen seems to be an evolutionarily conserved mechanism in a wide range of epithelial tissues such as the Drosophila retina [94] and trachea [95, 96] the zebrafish neural tube [97] and the gut [92].

6) IRSp53

IRSp53 (insulin receptor tyrosine kinase substrate of 53kDa) is a multi-domain protein, operating at the membrane-actin interface to induce deformations of the cell membrane, by sensing and promoting membrane curvature and coordinating the actin polymerisation machinery. IRSp53 is encoded by BAIAP2 (Brain-specific angiogenesis inhibitor 1-associated protein 2) gene in humans and mice. While, in zebrafish, this gene is duplicated into two paralogues, referred to as BAIAP2a (B2a) and BAIAP2b (B2b).

IRSp53 was originally identified in a screen of substrates, phosphorylated by insulin and insulin-like growth factor-1 (IGF-1) signalling. It is the founding member of the IMD (IRSp53-missing in metastasis homology domain) containing-family of proteins, which constitute an unconventional sub-group of a larger family of BAR (Bin-amphypysin-Rvs167) domain containing proteins [98]. IMD containing sub-group features an inverted-BAR domain, thus, also known as I-BAR domain containing proteins [54]. BAR domains are capable of binding phospholipid-rich membranes and to deform it by forming banana shaped dimers, which can assemble into a helix. These membrane deformations naturally lead to invaginations, thereby facilitating the process of endocytosis [99]. In contrast to the normal BAR domains, I-BAR domains form zeppelin shaped dimers, which assemble into similar multimeric helix (formed by intertwined dimers organized in a head-to-tail multimer) but with an opposite polarity leading to the formation of membrane protrusions instead. Apart from I-BAR (IMD) domain, IRSp53 consists of mainly three other functional domains; an unconventional CDC42 and RAC interactive binding motif (CRIB) domain which is extended to include a set of prolines and is thus called as CRIB-PR, Src homology-3 (SH3) and PSD-95, DLG and ZO-1 (PDZ) binding motif, which will be discussed in the proceeding sub-chapters.

The gene encoding IRSp53 undergoes alternative splicing events to give rise to at least four known isoforms (L, M, S and T) which differ in their C-termini. The S-isoform contains a PDZ binding motif, while as M and L-isoforms contain a WH2-like motif (which possesses actin-binding properties). The T-isoform, identified in MCF7 breast cancer cell line with unknown function, lacks both of these motifs [54].

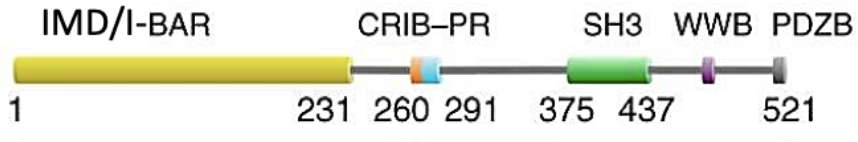

Fig. 5: Schematic representation of the structure of IRSp53

Schematic showing the arrangement of the domains; I-BAR, CRIB-PR, SH3, WW-binding domains and PDZ-binding motif in S-isoform of IRSp53 (modified from Kast et al., 2014).

IRSp53 is expressed in wide range of tissues like spleen, lungs, liver, testis and brain in mammals. It is particularly enriched in the brain cortex, hippocampus, striatum and cerebellum [100] [101, 102]. IRSp53 is abundant in the synaptic terminals of the post excitatory neurons, where it is involved in the assembly of post-synaptic density (PSD) complex, which transforms the excitatory stimulus into the downstream signalling pathways. It may also play a role in regulating actin-rich dendritic spines and synapse formation in the neurons [103]. IRSp53 is also implicated in CDC42-mediated filopodia and RAC1-dependent lamellipodia formation [54].

At the organismal levels, the loss of IRSp53, which is particularly abundant in the central nervous system, causes a variety of neurological alterations which have been the subject of intense investigations. IRSp53 KO mice display many neurological defects including enhanced NMDAR (N-methyl-D-aspartate receptor) function, decreased synaptic plasticity which lead to learning deficits, memory loss, social and

cognitive dysfunction, despite no apparent structural shortcomings in the dendritic spines of their neurons [101] [104]. Hippocampal neurons in IRSp53 KO mice display abnormally stable actin filaments, which may increase the localization of NMDAR at the synapsis and suppress their activity-dependent removal (cofilin resistance); mice lacking EPS8 and WAVE1, two interactors of IRSp53, also show altered NMDAR function [101, 104, 105]. In humans, IRSp53 has been implicated in wide range of psychiatric disorders, including autism spectrum disorder, schizophrenia, attention deficit hyperactivity disorder [104].

6.1) I-BAR/IMD domain

N-terminus of IRSp53 consists of an I-BAR (inverse-BAR, or IMD, IRSp53-MIM homology) domain, which is able to form zeppelin shaped dimers. I-BAR domain is known to bind membrane lipids, actin and RAC1 through its positively charged residues, concentrated at its C-terminal sites. Other positively charged residues in this domain form two complementary planes along the surface. One of these surfaces is able to bend the membrane into a convex shape leading to membrane deformations [54, 106]. These deformations together with the ability of IRSp53 to serve as a scaffold for the localization and activation of the actin branched WAVE regulatory complex (WRC) [54, 106], can facilitate the formation of lamellipodia for cell spreading or migration. I-BAR has also been reported to deform membrane into tubular structures *in vitro* and for filopodia formation in cells [107, 108] [109], by binding to its PIP_2 rich internal leaflet [110]. In addition to binding these membrane domains, I-BAR domain can itself induce PIP_2 clustering at the membrane [110]. Overexpression of I-BAR or IRSp53, in cells can induce F-actin and PIP_2 dependant filopodia formation [107, 111] [112]. However, deletion of I-BAR or substitution of its terminal K142,143,146,147

residues with glutamic acid (4K I-BAR* mutant) in IRSp53, which preserves its overall conformation, abolishes the filopodia formation in COS7 cells [113] [106].

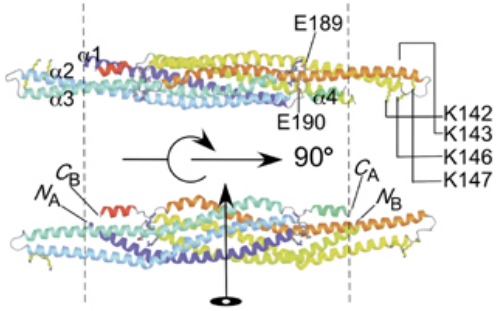

Fig. 6: Structure of the I-BAR domain of IRSp53

Ribbon representation of two orthogonal views of an I-BAR dimer. The helices have been colour-ramped; blue to green (chain A) and yellow to red (chain B). The core region of the dimer is demarcated by the two vertical dashed lines (modified from Millard et al., 2005).

Apart from generating the membrane protrusions, I-BAR domain is also able to sense the membrane curvature and preferentially accumulates on the membrane domains with a negative curvature [114]. It can also generate tubules *in vitro* in the GUVs (Giant unilamellar vesicles). Additionally, I-BAR encapsulated in GUVs can generate membrane tubes, if concentrated enough. Under these conditions, the I-Bar can reduce the force needed to sustain and stabilize the tubules. Deformations induced by I-BAR proteins seems to be concentration-dependent, reinforcing the notion that I-BAR dimers can associate into higher order oligomers [107, 115].

6.2) CRIB domain

IRSp53 contains a shorter non-canonical, CRIB (CDC42 and RAC interactive binding) motif, with only three N-terminal consensus residues and a C-terminal half containing a proline-rich (PR) sequence. This CRIB-PR (referred as CRIB, hereafter) motif is able to bind active CDC42 [116] but not RAC1 probably due to the less conservation of the consensus sequence and the overlap with the PR motif. Moreover, the PR motif of this

domain is able to bind switch-I – switch-II region of CDC42, that undergoes conformational change in response to the GTP/GDP-binding. Since, only GTP bound CDC42 is able to bind CRIB-PR, thus PR motif of this domain is involved in the nucleotide-state sensing of CDC42 [112, 116]. PR can also bind the SH3 domain of IRSp53 resulting in an autoinhibition of the protein. Binding of GTP-CDC42 induces a conformational change to a more open state and relieves IRSp53 from its auto-inhibition [116]. Since, CDC42 through its prenylated residues can tether to the plasma membrane, thus both I-BAR and CRIB domains are thought to be responsible for the membrane localization of IRSp53.

6.3) SH3 Domain

SH3 (SRC homology 3) domain is known to interact with a wide range of proteins containing PR sequence. It is usually found in proteins that mediate the formation of large protein complexes. IRSp53 SH3 domain is also known to bind to a growing list of actin-regulating proteins and other neuronal proteins via their proline-rich sequences. These include: WAVE1 [117], WAVE2 [118], N-WASP [117], Mena [108], EPS8 (EPS8/ABI1/SOS1) [109, 119], mDia [120] [117], Espin [121], Shank1 [100] [122], Shank3 [102], synaptopodin [123], SPIN90 [124], DRPLA/atrophin-1 [125], BAI1 [126], EspFU [127], IQ-ArfGEF/BRAG1 [128], WIRE [129], huntingtin [130], cypin [131], SH2B1 [115], dynamin1 [132]. Thus, IRSp53 can be regarded as an adaptor protein, capable of binding various proteins via its SH3 domain to assemble multi-protein complexes and target them along the specific domains on the membrane with the help of its I-BAR and CRIB domains. Interactors of SH3 domain of IRSp53 have been implicated in many biological processes, including filopodia formation by Mena,

EPS8 and mDia; lamellipodia extension via WAVE proteins and neuronal spine morphogenesis via Shank proteins [54] [100] [102].

The region between CRIB and SH3 contains different phosphorylation sites, involved in Tiam1 and 14-3-3 binding upon the phosphorylation of these residues. Upon 14-3-3 binding, IRSp53 is sequestered in the cytoplasm in an inactive state and abrogation of the interactions with SH3 binding partners [26] [133].

6.4) PDZ-binding motif

The C-terminal of IRSp53 contains a PDZ (PSD-95, DLG and ZO-1) domain-binding motif (referred to as PDZ, hereafter). This motif is responsible for the binding of IRSp53 with a number of proteins containing PDZ domains; PSD-95, PSD-93/Chapsyn-110 [103], LIN7 (or MALS) [134], SAP97 [134].

Through its PDZ-binding domain, IRSp53 can assemble a large PSD scaffolding/signalling complex in the post-synaptic excitatory neurons to regulate the dendritic spine morphogenesis downstream of RAC1 and CDC42 [103] [135]. Additionally, the PDZ motif has been shown to facilitate the interaction of IRSp53 with MALS/Lin-7, which is a part of a larger cell adhesion complex mediating the proper cell–cell adhesions in the epithelial cells [134].

7) Cellular functions of IRSp53

IRSp53 is a membrane binding adaptor protein having actin remodelling capabilities to induce reorganisation of membrane domains in response to various signals. Thus, it is involved in many diverse the cellular processes like axon path finding, neurite extension, dendritic spine morphogenesis, cell migration, tumour cell invasion, cell polarity, phagocytosis and myogenic differentiation [54]. These processes require the integration of RHO-family GTPase signalling with the remodelling of actin filaments underneath the plasma membrane to generate lamellipodia [136] [108] [111] or filopodia [137] [138]. Apart from this, IRSp53 has also been implicated in facilitating the endocytosis through clathrin and dynamin-independent CLIC/GEEC pathway. It has been proposed that IRSp53 is recruited at the neck of these endocytic vesicles where it is activated by CDC42 and aids in the activation of branched polymerization of actin, mediated by the Arp2/3 complex in a process that leads to the neck constriction and scission of vesicles [139]

IRSp53 induces filopodia formation downstream of CDC42 signalling, working synergistically with Mena [108]. IRSp53 fails to induce filopodia formation in N-WASP KO fibroblasts or Ena/Mena/VASP KO cells, suggesting that IRSp53 is able to convert CDC42 signalling into actin remodelling mechanism and generate filopodia as an output of this signal [117]. Since, the extension of dendrites and axons is preceded by filopodia formation, IRSp53 can facilitate these processes by integrating various signals into the actin remodelling events to induce filopodia formation. IRSp53 has been shown to interact with the scaffolding protein SH2B1, which acts downstream of neurotrophin receptors, to enhance the neuronal outgrowth and dendritic branching in cultured hippocampal neurons [115]. Consistently, primary neurons from IRSp53 null mice display reduced dendritic processes and a delay in the formation of post synaptic clusters. On the other hand, IRSp53 overexpression increases the spine density and

their size in cultured hippocampal neurons [102]. This is due to the formation of CDC42 dependent, Shank1-IRSp53-PSD-95 complex [103, 135] to facilitate the dendritic spine development.

IRSp53 binds RAC1 through its I-BAR domain and to the WAVE2 through its SH3 domain, forming a complex, which is involved in enhancing the membrane ruffling and lamellipodia formation [137]. Tiam1 (a RAC-GEF) enhances the signalling via this axis by specifically facilitating RAC1-GTP binding to IRSp53 which further promotes IRSp53:RAC1-GTP:WAVE2 complex formation [140]. Moreover, the loss of IRSp53 inhibits lamellipodia formation [106]. IRSp53 also interacts with EPS8 and enhances EPS8-ABI1-SOS1 mediated activation of RAC1, suggesting that IRSp53 can act as a crucial mediator of a feedback loop both upstream and downstream of RAC to sustain its activation. This signalling axis has been shown to promote motility and invasiveness of the malignant tumour cells [119].

The localisation of the EPS8:IRSp53 complex is under the regulation of CDC42. Simultaneous expression of IRSp53 and EPS8 in cells enhances the protrusive activity of IRSp53, leading to the formation of longer, branched protrusions, which do not form on expression of only I-BAR or EPS8 alone [109]. *In vitro*, EPS8 bundling activity is synergistically enhanced by the presence of full-length IRSp53, but not I-BAR deleted mutant form of IRSp53 [109].

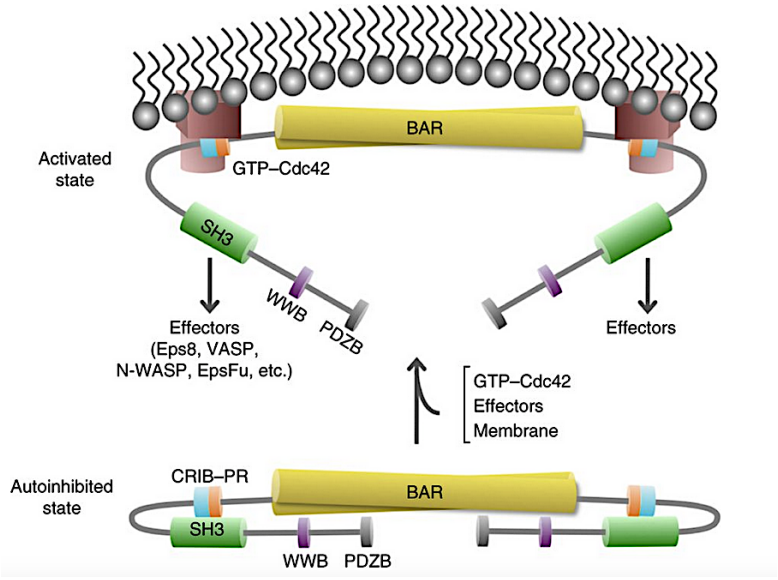

Fig. 7: Model for the activation of IRSp53 dimer

Schematic representation of an IRSp53 dimerised through its I-BAR (BAR in the figure) domain in a closed conformation of an autoinhibited state (lower) due to the binding of its SH3 domain with the PR-binding motif. This inhibition is relieved due to the binding of GTP-CDC42 at the CRIB-PR domain which no longer able to bind the SH3 domain, changes its conformation to an open state (modified from Kast, et al., 2014).

IRSp53 senses and binds, via its I-BAR domain, to promote the membrane deformations, where it restrains the growth of the barbed ends of the actin filaments by its weak capping activity, which is further reinforced the binding and localized recruitment of the strong capper EPS8 [109] [141]. The subsequent binding of activated CDC42 is sufficient to inhibit the capping activity of IRSp53 and to induce a conformational change [112] [116] which causes the protein to transit from a close to an open structure. The latter change facilitates, in turn, the binding, through the now liberated SH3 domain, of the linear actin elongator-VASP family of proteins [142]. This also promotes the formation of IRSp53 multimers at the negative curved plasma membrane, that causes the clustering of VASP, which is critical to enhance the linear actin-elongation activity. Therefore, the actin filaments formed, are extended and subsequently bundled by proteins such as Fascin, generating the forces necessary to

push the PM outward for the extension of filopodia. [112]. Consistent with this mode of action and the well-established role of filopodia as steering and mechanical sensors during directed motility, the genetic loss of IRSp53 impairs wound healing of mouse embryo fibroblasts, while it significantly delays epidermal skin repair by impacting on the migratory property of keratinocyte in IRSp53 null mice [112]. Of note, IRSp53 removal has also been linked to impaired macrophage chemotactic activity [143] and their migration to the wound bed [112], suggesting that multiple cell types rely *in vivo* on the activity of this protein.

8) Role of IRSp53 in MDCK cyst morphogenesis and polarity

IRSp53 has been shown to be phosphorylated by Par1b leading to its inactivation and sequestration in the cytoplasm by 14-3-3 binding. PAR1b, a serine/threonine kinase, regulates epithelial apico-basal polarity and lumen formation [144]. Par1b over expression in MDCK cysts leads to an inverted polarity phenotype marked by disrupted Laminin staining, retention of PDX at the basal membrane and formation of multiple lumina [26]. These phenotypes were mimicked by the silencing of IRSp53 in these cysts and rescued by introducing a non-phosphorylatable version of IRSp53 in Par1b overexpressing cells. This suggests that the Par1b phosphorylation and subsequent inactivation of IRSp53 due to 14-3-3 binding is the underlying cause of this perturbation in polarity [26]. However, the molecular mechanism through which IRSp53 inactivation causes these defects has remained entirely mysterious.

Aims of the study

IRSp53 has been reported to play a role in the assembly of cell-cell and cell-ECM adhesions downstream of the Polarity-regulating kinase Par1b, and to be required for the polarized architectural organization and morphogenesis of MDCK epithelial cells *in vitro* [26, 145]. However, the molecular pathways and interactors that IRSp53 uses in controlling these processes and its physiological relevance at the organismal level have remained poorly understood. In this thesis work, we aimed to investigate the role of IRSp53 in the establishment of polarity and lumen morphogenesis in epithelial systems.

We specifically devised a strategy aimed at uncovering the underlying molecular processes and mechanisms through which IRSp53 contributes in the proper polarity establishment and lumen morphogenesis. To this end, we initially took advantage of the 3-D epithelial cysts, derived from Caco-2 and MDCK cell lines, which recapitulate the epithelial polarisation and lumen morphogenesis *in vitro*. In the final part of this study, we extended the finding obtained using in vitro cell culture models at organismal levels and specifically focussed on providing evidence of the physiological implications of IRSp53-dependent processes. To this end, we used different zebrafish and mouse models to study the effect on the epithelial (renal) morphology using different genetic approaches.

Materials and Methods

1) Solutions:-

1.1) Phosphate-buffered Saline (PBS 1X)

137 mM NaCl

2.7 mM KCl

10 mM Na_2HPO_4

1.8 mM KH_2PO_4

The solution is prepared by dissolving 8 g of NaCl, 0.2 g of KCl, 1.44 g of Na_2HPO_4 and 0.24 g of KH_2PO_4 in 800 ml of distilled water. The pH is adjusted to 7.4 with HCl and deionised H_2O is added to make up the final volume to 1 litre.

1.2) Tris-HCl (1 M)

The solution is prepared by dissolving 121.1 g of Tris base in 800 ml distilled H_2O. The pH is adjusted (depending on the requirement) with HCl, and deionised H_2O is added to make up the final volume to 1 litre.

1.3) EDTA (0.5 M)

To prepare EDTA at 0.5 M (pH 8.0): Add 186.1 g of disodium EDTA•2H2O to 800 mL of H2O. Stir vigorously on a magnetic stirrer. Adjust the pH to 8.0 with NaOH (~20 g of NaOH pellets). Make up the final volume to 1 litre. The disodium salt of EDTA will not go into solution until the pH of the solution is adjusted to ~8.0 by the addition of NaOH.

1.4) Tris-EDTA (TE 10X)

100 mM Tris-HCl (desired pH; 7.4 – 8.0)

10 mM EDTA (pH 8.0)

1.5) Tris-Acetate-EDTA (TAE 50X)

2 M Tris base

50 mM EDTA

1 M Acetic Acid

Mix 242 g of Tris base, 57.1 mL of Acetic acid and 100 mL of 0.5 M EDTA in 800 mL of deionised water and make up the final volume to 1 L. The pH of this buffer is around 8.5 & need not to be adjusted.

1.6) Tris buffered saline (TBS 10X)

247.6 mM Tris base

1.37 M NaCl

27 mM KCl

Dissolve 30 g Tris, 80 g NaCl and 2 g KCl in about 800 mL of deionized water. Adjust pH to 7.6 with 1 M HCl. Add deionized water to make up the final volume to 1L. Dilute 1:10 for the (1X) working solution.

1.7) JS lysis buffer

50 mM Hepes pH 7.5

150 mM NaCl

1% Glycerol

1% triton

1.5 mM MgCl2

5 mM EGTA

To this solution protease inhibitors and phosphatase inhibitors were freshly added as below;

Protease Inhibitor Cocktail

1 mM DTT

20 mM sodium pyrophosphate (pH 7.5)

50 mM NaF

0.5 M sodium orthovanadate in HEPES pH 7.5

1.8) Laemmli buffer (2X)

4% SDS

20% glycerol

10% 2-mercaptoethanol

0.125 M Tris HCl pH approx. 6.8

0.004% bromophenol blue (BPB)

Laemmli buffer used directly for cell lysis was prepared without BPB and 2-mercaptoethanol, as these solutions interfere with the protein quantification assays. Complete buffer containing these solutions were added to the protein samples before processing them for SDS-PAGE.

1.9) Tris-Glycine buffer (10X)

144 g/L Glycine

30 g/L Tris base

1% SDS

1.10) Transfer buffer (10X) for Western blotting

144 g/L Glycine

30 g/L Tris base

The buffer was used at 1X concentration along with 20% v/v of methanol in the final volume.

1.11) Ponceau solution

0.1% (w/v) Ponceau

5% Acetic acid

2) Basic molecular cloning techniques

2.1) DNA digestion

1-2 μg of DNA was digested for 1 hour at 37°C with 10 units of a specific restriction endonuclease (NEB). Reaction volume was adjusted to 20 μl with the appropriate 10X NEB buffer and ddH_2O. The sequences consisting of two different restriction sites were double digested with both the enzymes in a single reaction mix containing a suitable buffer having 100% activity for both the enzymes.

2.2) Ligation

Ligation was performed with Quick Ligation kit (NEB). 50 ng of vector was mixed with a 3-fold molar excess of the insert. The volume of the mix was adjusted to 10µl with nuclease free water (NFW). 10 µl of 2X Quick Ligation Buffer and 1 µl of Quick T4 DNA Ligase was added to the mix. The reaction mix was centrifuged briefly and incubated at room temperature (25°C) for 5 minutes. The reaction was stopped by immediately chilling it on ice. The ligated DNA was then either used directly to transform the competent cells or stored at –20°C for later usage.

2.3) Transformation of competent cells

E. coli one shot Top10 cells (Thermo Fisher Scientific) were used for cloning and large-scale DNA preparation, while *E. coli* BL21 Rosetta (DE3) cells (Promega) were used for protein production. The transformation protocol used for both the strains was as follows:

50 µl of fresh competent cells were thawed on ice. 50ng of the plasmid DNA or 5µl of the ligation reaction (as described above) were added directly to the cells and incubated on ice for 20 minutes. The cells were subjected to a heat shock at 42°C for 45 seconds. Cells were chilled on ice for 5 minutes and 0.2 mL of SOC (Super Optimal broth with Catabolite repression) media was added to the transformed cells to let them recover at 37°C for 60 minutes (with 200 rpm shaking). 50 µl of the transformed cells or in case of low efficiency transformations, entire cells briefly spinned down at 5000Xg for 5 minutes and resuspended in 50µl of SOC, were plated onto agar plates containing appropriate antibiotics. Plates were incubated overnight at 37°C.

SOC medium (pH 7.5):

2% Bactotryptone

0.5% Yeast extract

10 mM NaCl

2.5 mM KCl

10 mM $MgCl_2$

10 mM $MgSO_4$

20 mM glucose

2.4) Minipreps

Transformed colonies were picked individually with sterile tips or inoculating loops to inoculate 5 mL of LB (Lysogeny Broth or Luria-Bertani medium) containing appropriate antibiotics in 15mL Falcon tubes. The culture was grown overnight at 37°C in a shaker incubator at 250 rpm. Cells from a total of 4.5 ml cell culture were pelleted down thrice for 30 seconds each at max speed in 1.5ml tubes. The remaining 0.5ml was stored at 4ºC for further usage. Plasmid DNA was extracted from the cells by alkaline lysis method and isolated by binding on silica columns using Wizard Plus SV Minipreps kit (Promega). The final elution was made in 50μl of milli-Q water. DNA was checked by agarose gel electrophoresis using 5μl of the eluate and quantified using a NanoDrop™ 2000 Spectrophotometer.

LB medium:

1% Bactotryptone

0.5% Yeast extract

1% NaCl

pH 7.25

2.5) Large Scale Plasmid Preparation (Maxi-preps)

E. coli transformant colonies or the stored cultures from the miniprep (see above) containing the desired plasmid were cultured overnight in 500 mL LB containing appropriate antibiotics at 37ºC & 200rpm. The cells were harvested by centrifuging the cultures at 6000Xg for 15 minutes at 4ºC. Plasmid DNA was extracted from the cells by alkaline lysis method and isolated by binding on silica columns using Qiagen Maxi-prep kit (Qiagen, Valencia, CA) according to the manufacturer's instructions. The isolated DNA was finally eluted in Tris EDTA buffer, pelleted down, washed with 70% ethanol and resuspended in 500µl of milli-Q water. DNA was quantified using a NanoDrop™ 2000 Spectrophotometer and checked by agarose gel electrophoresis of 1µg of the DNA.

2.6) PCR (Polymerase Chain Reaction)

Sense and antisense oligos, 20-30 nucleotides long, were designed, one annealing in 5' (forward) and the other at 3' (reverse) position of the target sequence with the help of Primer3Plus online software. The primer pairs designed were of similar length and annealing temperature. The primer pairs were diluted to 10µm each in a single primer mix. The target DNA sequence was amplified in a PCR reaction in an automated thermal cycler (GeneAmp PCR system 9700, Applied Biosystems). The reactions were carried out with a high-fidelity DNA polymerase (Q5® or Phusion®, NEB) for the downstream applications like cloning etc or with a normal Taq polymerase (GoTaq® Promega) for other applications (like genotyping etc) that do not require high fidelity.

Q5® Hot-start

Reaction mixture

Q5 2X Master Mix	12.5µl
10µM primer mix	1.25µl
DNA Templ	100ng
NFW	up to 25µl

Phusion® High-Fidelity DNA Polymerase (NEB).

Reaction mixture

5x Phusion HF buffer	10 µl
DNA template	10-20 ng
Primer mix (10µm)	0.5 µM
dNTPs mix	0.2 mM
Phusion® Polymerase (NEB)	1 U
Nuclease free H_2O	to a final volume of 50 µl

Cycling parameters:

Step	Temperature	Time	N° of cycles
A)	denaturation at 98°C	30 seconds	1
B)	denaturation at 98°C	10 seconds	
	annealing at *x*°C	30 seconds	25
	extension at 72°C	(30 seconds/each kb of target length)	
C)	extension at 72°C	5 minutes	1

GoTaq® G2

Reaction mixture

2X GoTaq® G2 Master Mix	12.5µl
10µM primer mix	1 µl
DNA Templ	100ng
NFW	upto 25µl

Cycling parameters:

Step	Temperature	Time	N° of cycles
A)	denaturation at 95°C	5 minutes	1
B)	denaturation at 95°C	30 seconds	
	annealing at *x*°C	30 seconds	25
	extension at 72°C	(1min/each kb of target length)	
C)	extension at 72°C	7 minutes	1

2.7) Site directed mutagenesis

Site directed mutagenesis was performed using the Quick-Change mutagenesis kit (Stratagene), following manufacturer's instructions. A sense and an antisense oligo of about 30-45 nucleotides each, carrying the desired mutation in the middle of the sequence, were designed and used in a PCR reaction with wild type construct as the template. PCR was performed using the Pfu DNA Polymerase (Promega).

Reaction mixture

10X Pfu buffer	10 µl
DNA template	10-100 ng
primer forward	0.125 µM
primer reverse	0.125 µM
dNTPs mix	0.2 mM
Phusion Polymerase (NEB)	3 U
Nuclease free H_2O	to a final volume of 50 µl

Amplification was carried out for 18 PCR cycles with a denaturation step of 30 seconds at 95°C, followed by an annealing step of 1 minute at 55°C and extension step at 68°C for 2 minutes/Kb of the target sequence.

After amplification, 2 µl of DpnI restriction enzyme (NEB), which selectively cuts methylated DNA at the GATC sequence, was added to digest the wild type template DNA. After one-hour incubation at 37˚C, the PCR product was checked by DNA electrophoresis and used to transform competent *E. coli* Top10 cells (Thermo Fisher Scientific) as described previously. Single colonies were screened for the presence of the desired mutation and the absence of other unwanted base changes by DNA sequencing.

2.8) Agarose gel electrophoresis

Agarose gel electrophoresis of DNA samples was carried out in 0.8%-2% agarose gels along with DNA markers. Gels were made in TAE buffer containing 0.3 µg/mL ethidium bromide or GelRed™ Nucleic Acid 1:10000 (Biotium, Italy). The DNA samples were loaded along with DNA loading dye (30% (v/v) glycerol, 0.25% (w/v) bromophenol blue, 0.25% (w/v) xylene cyanol FF) and run at 80-100V until desired separation was achieved. DNA bands were visualized and imaged with a gel-doc (EuroClone).

2.9) DNA elution from agarose gel

Separate DNA bands were cut out from agarose gel after the electrophoresis. Isolation of the DNA from the gel was performed using Wizard® SV Gel and PCR Clean-Up System (Promega), following the manufacturer's instructions.

2.10) RNA Extraction

RNA extraction of samples was carried out with TRIzol™ (Thermofisher) according to the manufacturer's guidelines. The samples were lysed in an appropriate volume of TRIzol™ reagent by repeated pipetting and incubating at RT for 10 minutes. In case of zebrafish embryos, the samples were disrupted by passing through insulin syringe at least thrice before the incubation step. The lysed samples were either frozen at -80º C or directly processed for the RNA extraction.

The RNA pellet obtained at the end of extraction was airdried and resuspended in 50µl of pre-warmed NFW. The RNA was dissolved completely by incubating the samples at 60º C for 5' on a heat-block with gentle shaking.

The concentration and the quality of RNA was checked using the nanodrop spectrophotometer and by running ~1µg of the samples on 2% agarose gel.

2.11) cDNA synthesis

1-2µg of total RNA was reverse transcribed to synthesize cDNA either with SuperScript™ VILO™ master mix (ThermoFisher Scientific) or with High Capacity cDNA Reverse transcription kit following the manufacturer's protocol.

2.12) Quantitative Real time PCR (qRT-PCR)

500 nanogram of RNA was retrotranscribed using "Quanta, VWR" kit. For some samples RT minus was made to check the absence of genomic DNA.

For gene expression analysis, 5ng of cDNA was amplified (in triplicates) in a reaction volume of 10 uL containing the following reagents: 5ul of "TaqMan® Fast Advanced Master Mix, Thermofisher", 0.5 ul of "TaqMan Gene expression assay 20x, Thermofisher" (for details see the list below). Real-time PCR was carried out on the 7900HT Fast Real-Time PCR (Thermofisher), using a pre-PCR step of 20s at 95°C, followed by 40 cycles of 1s at 95°C and 20s at 60°C. Samples were amplified with primers and probes for each target and for all the targets one NTC sample was run.

Raw data (Ct) were analyzed with "Biogazelle qbase plus" software and the fold change was expressed as CNRQ (Calibrated Normalized Relative Quantity) with Standard Error (SE).

The entire process (extraction, retro-transcription, gene expression and data analysis) was performed by the qPCR-Service at Cogentech-Milano

Baiap2a: Dr03426793_m1

Baiap2l1a: Dr03074526_m1

Baiap2l1b: Dr03423996_m1

Actb1: Dr03432610_m1

Baiap2b:

Fw AAAAGTGGAGTTGGATGTTCGCTAT

Rev AGACTTTCTCCTTTACTTTTGTGTTCCA

Probe CTTCAGAGCTGCATTTAA

2.13) Generation of IRSp53 constructs

IRSp53 constructs used in the experiments encode for the S (short) isoform that contains a PDZ binding domain at the C-terminus. Flag–IRSp53 was a gift from S. Ahmed (Neural Stem Cell Laboratory, Institute of Medical Biology, Singapore) and it was used to subclone IRSp53 in pBABE vector (Cell Biolabs). pEGFP–IRSp53 was a gift from H. Nakagawa (Austrian Academy of Sciences, Vienna Austria) and used to subclone IRSp53 in pTrcHis-A (Thermo Fisher Scientific) or pmCherry-C1 (Clonetech) vectors, performing BamHI-BamHI digestions.

IRSp53 deletion constructs were generated by PCR, using pTrcHisA-IRSp53 vector as a template. To clone the different constructs, specific primers flanked by BamHI and EcoRI sites (or EcoRI and SalI sites) were designed. DNA fragments were then sub-cloned in an empty pGEX-6P-1 (Amersham) vector. The primers used are listed in the table below:

1-250 aa	Fwd: 5'-GCGGATCCTCTTTGTCTCGCTCAGAGGA-3' Rev: 5'-GCGAATTCTCAGTTGCTGGCCACCTGCTG-3'
1-290 aa	Fwd: 5'-GCGGATCCTCTTTGTCTCGCTCAGAGGA-3' Rev: 5'-GCGAATTCTCACATCCGCCCCACGAACG-3'
1-309 aa	Fwd: 5'-GCGGATCCTCTCTGTCTCGCTCAGAGGA-3' Rev: 5'-GCGAATTCGTCCTCGCCATCCGGGCC-3'

1-339 aa	Fwd: 5'-GCGGATCCTCTCTGTCTCGCTCAGAGGA-3' Rev: 5'-GCGAATTCGTTGGAGTAGGAGTCGCTGA-3'
1-374 aa	Fwd: 5'-GCGGATCCTCTCTGTCTCGCTCAGAGGA-3' Rev: 5'-GCGAATTCATTGCGCTCCAGGCCGGC-3'
1-437 aa	Fwd: 5'-GCGGATCCTCTTTGTCTCGCTCAGAGGA-3' Rev: 5'-GCGAATTCTCAACTGCCATCGCTGTCCA-3'
290-521 aa	Fwd: 5'-GCGGATCCATGTCTGCCCAGGAGAGCAC-3' Rev: 5'-GCGAATTCTCACACTGTGGACACCAGC-3'
375-437 aa	Fwd: 5'-GCGAATTCGGCCGTATGCGGGTGAAGGC-3' Rev: 5'-GCGTCGACTCAACTGCCATCGCTGTCCA-3'

IRSp53 W413G mutant was generated by site directed mutagenesis as described previously.

2.14) Other constructs

CDC42 N17 and L61 were cloned in pRK5 vector (with myc-tag) for mammalian expression, CDC42 was cloned in pGEX vector for bacterial purification. VASP was cloned in pEGFP vector for mammalian expression and in pGEX/pTRCHisA for bacterial purification. EPS8 was cloned in pFL vector (kindly gifted by A. Musacchio, Max Planck Institute, Dortmund) carrying His-tag motif for baculovirus expression.

pFUW lentiviral vectors encoding GFP, GFP-IRSp53 WT and GFP-IRSp53 mutants (in I-BAR domain: 4KtoE on positions 142, 143, 146, 147, CRIB domain: I268N, SH3 domain: I403P, PDZ domain: V522G) were gifts from Hans-Jurgen Kreienkamp (University of Hamburg). Apple-RAB11a was kindly given by K. Mostov (University of California, San Francisco).

3) Reagents and antibodies

The monoclonal anti-IRSp53 was generated against the purified full-length, His-tagged protein [109]. Other antibodies used were: rabbit polyclonal anti-IRSp53 (Sigma), monoclonal anti-EPS8 (Transduction Laboratories), anti-vinculin (Sigma), anti-tubulin (Sigma), anti-myc (Babco), anti-VASP (Cell Signaling), rabbit polyclonal anti-aPKC ζ (C-20, Santa Cruz Biotechnology), anti-ZO-1 (Thermo Fisher Scientific), anti-podocalyxin (3F2/D8, DSHB, University of Iowa, deposited by G. Ojakian), anti-βcatenin (Sigma), anti-GFP (gift from Jan Faix, Hannover), anti-EEA-1 (N-19, Santa Cruz Biotechnology), anti-Giantin (Covenance), anti-RAB7 (Cell Signaling), anti-Lamp1 (Sigma).

Secondary antibodies conjugated to horseradish peroxidase were from Bio-Rad; FITC- and Cy3-secondary antibodies from Jackson ImmunoResearch, AlexaFluor 488 was from Molecular Probes, TRITC- and FITC-conjugated phalloidin were from Sigma. Growth Factor Reduced Matrigel™ Matrix Basement Membrane and Collagen I were from BD Biosciences. Laminin, gelatin and fibronectin were from Sigma.

4) Cell Culture:

HeLa cells were grown in Minimum Essential Medium (MEM Thermo Fisher Scientific) supplemented with 10% FBS (EuroClone), 1% non-essential amino acids and 1% Sodium Pyruvate.

Immortalized mouse embryo fibroblasts (MEFs) were grown in Dulbecco's Modified Eagle Medium (DMEM, Lonza) supplemented with 10% FBS (EuroClone) and 2 mM L-Glutamine (EuroClone).

MDCK cells were grown in Dulbecco's Modified Eagle Medium (DMEM, Lonza) supplemented with 5% FBS (EuroClone) and 2 mM L-Glutamine (EuroClone).

MDCK Tet-Off cell line T23 containing IRSp53 shRNAmir (kind gift of A. Musch, Albert Einstein College of Medicine, New York), described in [26], were grown in Dulbecco's Modified Eagle Medium (DMEM, Lonza) supplemented with 10% FBS (EuroClone), 2 mM L-Glutamine (EuroClone) and doxycycline 200 ng/ml. IRSp53 KD was induced by doxycycline removal (in presence of 50 μM enoxacine).

Caco2 cells were grown in Dulbecco's modified Eagle's medium (DMEM, Thermo Fisher Scientific) supplemented with 20% FBS (EuroClone), 2 mM L-Glutamine (EuroClone) and 1% non-essential amino-acids.

HEK-293T and phoenix cells were grown in Dulbecco's modified Eagle's medium (DMEM, Lonza) supplemented with 10% FBS (EuroClone) and 2 mM L-Glutamine.

All cells were grown at 37°C in humidified atmosphere with 5% CO_2.

5) Caco-2 Cyst formation assay:

The cells were trypsinised, mechanically disrupted by pipetting repeatedly to break the clusters and counted under a microscope using cell counting slides.

The cells were passed through 40μm cell strainers and the volume was adjusted to get a cell-density of 200,000 cells/ml of media.

The cells were suspended, to give a final density of 60000 cells/ml in a solution of matrix which was prepared as under;

	Vol./Well	Final concentration
Caco-2 (200,000/ml)	75µl	15000 cells/Well
HEPES (1M)	5µl	0.02M
Collagen I (9.4mg/ml)	26.5µl	1mg/ml
Matrigel (10mg/ml)	125µl	50% v/v
Caco-2 Media	18.5µl	make up to 250µl

The solution was kept on ice after its preparation until plating it in the wells. After adding the cells, the solution was mixed well to ensure homogenous distribution of the cells in the matrix. 250µl of the solution was plated in the wells of Ibidi chamber slides in duplicates.

The matrix was let to solidify by incubating the slides at 37ºC for 30 mins.

250µl of Caco-2 media was added on top of the solidified matrix in each well.

The cells were let to grow and form the cysts at 37°C in a 5% CO_2 incubator over a period of 7 days. The media in the wells was changed with fresh media every other day. On day 6, 250ul of media supplemented with 0.1mg/ml of cholera toxin was added on top of the matrix in each well. Cholera toxin activates chloride channels on the luminal membrane letting the Cl^- ions to accumulate in the lumen and thus drives the positively charged ions into the lumen as well. Higher concentration of the ions into the lumen increases the osmotic pressure, accumulation of the fluids and eventually the expansion of the lumen (procedure modified from Jaffe et al. 2008 [82]).

The cysts were fixed in 2% PFA after 24hours of the addition of cholera toxin (for complete fixing and staining procedures, see the section on IF staining).

6) MDCK cyst formation assay

MDCK cells were trypsinised and re-plated the day before to obtain actively growing cells on the day of experiment. Growth Factor Reduced Matrigel™ Matrix Basement Membrane (BD Biosciences) was thawed overnight in ice at 4°C and handled with ice with cold tips only. Each well of µ-slide 8-well chamber slide (Ibidi) was pre-coated with 15 µl Matrigel and allowed to solidify for 30 minutes at 37°C. Meanwhile, the cells were detached with trypsin and carefully re-suspended as single cells by pipetting and flowing through a cell strainer (of 40 µm pore size). Cells were resuspended in MDCK media containing 2% (v/v) Matrigel and 250 µl of this cell suspension was plated in each well of the chamber slide. The cells were let to grow and allowed to form the cysts at 37°C in a 5% CO_2 incubator. The media was replaced every two days until the end of the experiment. Cysts were fixed after 6 days or at earlier time points, as indicated in the experiments. [60]

7) Lentiviral infection

MDCK and Caco-2 cells were subjected to lentiviral infection with pFUW vectors encoding for GFP-IRSp53 WT or its mutated forms. Lentiviruses were produced by transfecting HEK-293T cells with 25 µg of the vector of interest, 9 µg ENV, 16.25 µg pMDL, 6.25 µg REV (for virus packaging). 48 and 72 hours after transfection, supernatants containing virus particles were collected and passed through a 0.45 µm filter. Supernatants were supplemented with 8 µg/ml Polybrene (Sigma) and added to cultured cells, four cycles of infection were performed. GFP-constructs expression was checked by Western blot analysis and immunofluorescence.

8) Short interfering RNA (siRNA) experiments

MDCK cells were seeded the day before transfection (150000 cells/well in 6 well format). siRNAs (small interfering RNAs) delivery was achieved by mixing 10 nM of specific siRNAs with Opti-MEM and Lipofectamine RNAiMAX Transfection Reagent (Thermo-Fisher Scientific) according to manufacturer's instruction. Equal amount of the scrambled siRNA was used as a negative control. KD efficiency was checked by Western blot analysis. Oligos were purchased from Thermo-Fisher Scientific, oligos details as follows:

IRSp53 (canine): CCAAGGAACTCGGAGACGTTCTCTT

Scrambled: TCGAATACGAACATTTATTT

9) Protein Biochemistry

9.1) Western Blotting

Cells/tissues/embryos were lysed either in JS buffer and incubated on ice for 10 mins or directly in 2X Laemmli buffer and then heated at 94ºC for 10 mins to ensure complete lysis of the samples. The lysis buffers were freshly added with Protease inhibitor cocktail to prevent the degradation of proteins. In case the lysates were too viscous, the samples were subjected to ultrasonication for 5 cycles of 5 seconds each at intervals of 5 seconds. Lysates were centrifuged at 12000 rpm for 10 mins at 4˚C to remove the debris. The cleared lysates were transferred to fresh vials and the protein concentration of each sample was measured by Bradford assay, using BSA solutions as the standard. Equal amounts of the protein were loaded on SDS-Polyacrylamide gel and run by electrophoresis to separate the proteins of different molecular weights. The proteins thus separated on the gel were transferred to nitrocellulose membrane using a wet-transfer system. Membranes were blocked for unspecific antibody binding using 5% skimmed milk in TBST (0.1% Tween) for 30 mins at RT. Blocked membranes

were incubated in the primary antibody (diluted to the appropriate concentration) in the blocking solution for 1hr at room temperature or overnight at 4°C. After washing thrice in TBST, the blots were incubated with HRP conjugated secondary antibodies for 1 hr at room temperature. The blot was washed again as previously, developed using Enhanced Chemi-Luminescent Substrate (ECL) and imaged using a chemidoc.

9.2) Co-immunoprecipitation:

HeLa cells, HEK293 or MDCK cells expressing GFP-Rab35 and Flag-IRSp53 were either stimulated by GF or kept as unstimulated. The cells were lysed in IP lysis buffer [40mM HEPES, 150mM NaCl, 5mM $MgCl_2$, 2mM EDTA, 1% Glycerol, 10mM Sodium pyrophosphate, 10mM NaVn, 50mM NaF, 2mM PMSF, 1% Triton X-100, 1mM DTT and 1X PIC]. Proteins were immuno-precipitated from 1000ug of cell lysates with 5ug of primary antibody for 2 hours at 4^0C, followed by 1-hour incubation in 20ul of 50% slurry of Protein-G agarose beads and centrifugation at 5000rpm for 1 min at 4°C. The beads were washed thrice with IP buffer and loaded on SDS-PAGE after lysing in 15ul of 1X SDS loading buffer. The following steps were done in the same way as the western blotting.

9.3) Dot blot Assay:

Purified GST-Rab35, Q73L and S22N proteins were spotted on a nitrocellulose membrane, dried and blocked in 5% Skimmed Milk in (1X) TBST for 1 hour at RT. The membranes were washed thrice in TBST and each spot was overlaid with the solution containing 100nM of purified IRSp53 in TBST containing 1% Skimmed milk and incubated for 1 hour at 4°C with continuous rocking. The membranes were again washed thrice with TBST as previously and incubated with anti-IRSp53 antibody. The

primary antibody was also washed out with TBST washes and the blots were incubated in the secondary antibody conjugated with HRP. The blots were washed once again and developed in ECL, as in the western blotting.

10) Immunofluorescence (IF):

10.1) Cell Monolayers on Coverslips;

Cells plated on coverslips were fixed in 4% Paraformaldehyde (PFA) in PBS for 10 mins at room temperature, washed thrice in 1X PBS for 5 mins each at RT. The cells were either stored in 1X PBS at 4ºC or directly processed for the IF staining as follows;

The cells were permeabilized in IF Blocking buffer (1%BSA+0.3%TritonX-100 in 1XPBS) at room temperature for 30 mins followed by washing thrice with 1X PBS and incubation in primary antibody for 30 minutes at RT or O/N at 4ºC. The cells were washed again with 1X PBS as previously and incubated in secondary antibodies for 30mins at room temperature. The dilutions of both primary and secondary antibodies were made in IF blocking buffer. DAPI and Phalloidin were added in the secondary antibody solution, whenever required. The coverslips were mounted on glass slides, either in VectaShield hardset or in Mowiol.

10.2) Cysts;

Caco-2 cysts were fixed in 2% PFA (in PBS) for 15 minutes at room temperature followed by three washes with PBS-Glycine (0.75mg/ml of Glycine in PBS) for 5 mins each to quench the unreacted PFA. This was followed by one more wash with PBS for 5 minutes at room temperature.

The cysts were stored in PBS-NaN_3 for 2 days at room temperature to allow stabilization of the matrix. Cysts were permeabilized with 0.5% Triton X-100 in PBS for

20 minutes and washed thrice with PBS at room temperature. Blocking was done in 10% goat serum in IF buffer (NaN_3 0.052mg/ml, Triton X-100 0.2%, 0.05% Tween-20, BSA 0.1mg/ml in PBS) at room temperature for 1-1.5 hours. The cysts were incubated in 100µl/well of primary antibodies, diluted (1:100) in IF buffer, overnight at room temperature. The unbound antibodies were washed out by three washes in IF buffer for 5 mins each. This was followed by 1-hour incubation with secondary antibodies (1:100) and phalloidin (1:10) also in IF buffer at room temperature. Again, the unbound antibodies and phalloidin were removed by three more washes with IF buffer as previously. The nuclei were stained with 1:500 DAPI in PBS for 5 minutes followed by another wash with PBS.

Post-fixation with 2% PFA for 9 minutes at room temperature was done to reduce the diffusion of antibodies. This was followed by three PBS-Glycine washes and a rinse with PBS. The cysts were stored in PBS in dark till imaging.

11) CRISPR-Cas9 KO Clones:

Caco-2 cells were transfected using Lipofectamine 2000 with CRISPR vector expressing both Cas9-RFP and sgRNA targeting IRSp53. After 48hrs of transfection, RFP positive cells were sorted by FACS (MoFlo Astrois, Beckman Coulter) and plated in 96 well plates as single cells in 30 separate wells. The wells with single colony formation were further cultured at gradually increasing scales. The clones that were able to reach the final steps of amplification, were frozen and analysed for the levels of IRSp53 by western blotting (as described in the results section). Clones #3 and #12 showed very efficient downregulation of IRSp53 expression and were used for the IRSp53 depleted conditions.

12) Analysis of cysts for multi-lumen and spindle orientation:

The cysts were counted on the 7th day under a light microscope on a per field basis. The focus of the objective was slowly shifted from bottom to top of the matrix, while counting the number of the single and multi-lumen cysts that appear in the field. For each sample, the counting was done at least at 2-3 such fields.

The spindle orientation analysis was done on the confocal images of the Caco-2 cysts treated with RO-3306 to arrest the dividing cells in mitotic phase. The angle bisecting the spindle pole axis from the centre of the cyst was calculated with the help of ImageJ (NIH) software. Around 60 cysts were analysed for each sample and percentage of multi-luminal cysts was calculated out of the total cysts observed.

13) Calcium Switch experiment:

MDCK cells Ctrl and IRSp53 KD were plated on coverslips in a 12 well plate at a density of 80000/well. The next day, media was removed from the wells and the cells were washed with DPBS. Calcium free MDCK media was added in the wells and the cells were let to grow until the desired timepoint, as usual. The cells were fixed, in 4% PFA, at different time-points after the calcium switch.

14) Animal Models

All the animal studies were carried out according to the ministry of health, government of Italy's, guidelines for the welfare of laboratory animals. The projects for the animal studies were approved by the ministry under project #598/2015 for the mice studies and #219/2016-PR for the zebrafish studies.

14.1) IRSp53 KO Mice:

IRSp53 KO mice were generated using an ES cell line XG-757 (BayGenomics, S. Francisco) harbouring an insertion of exon trapping construct of a β-geo (β -

galactosidase–NeoR fusion) cassette between exons 3 and 4 of mouse Irsp53 (described in Sawallisch et al., 2009 [102]). Injection of these ES cells into the blastocysts yielded offsprings with an efficient germline transmission. Genotyping was performed using a forward primer in exon 3, one reverse primer in intron 3 for the WT allele, and one reverse primer in the exon trap insertion for the mutant allele. Eventually homozygous mutants for IRSp53 were obtained with a complete functional loss of the protein.

14.2) BAIAP2a mutant zebrafish:

Zebrafish BAIAP2a mutants (sa1139) were generated by ENU (N-ethyl-N-nitrosourea) mutagenesis at European Zebrafish Resource Centre (EZRC). The mutation was identified as a single A>T nonsense mutation in the 7th exon of BAIAP2a gene, resulting in premature termination of the BAIAP2a protein translation. The mutants were out-crossed with AB wild-type zebrafish to clear them of any background mutations. The progeny of these out-crosses was screened by genotyping (as described below) and the heterozygous embryos with BAPA2a$^{+/-}$ genotype were selected after each cross. The heterozygous fish, obtained from the out-crosses, were finally in-crossed (BAIPA2a$^{+/-}$ **X** BAIPA2a$^{+/-}$) to obtain BAIAP2a null fish in the WT background. This BAIAP2a$^{-/-}$ line was further expanded by in-crossing the homozygous mutants (BAIAP2a$^{-/-}$ **X** BAIAP2a$^{-/-}$) to obtain a progeny all having BAIAP2a$^{-/-}$ genotype.

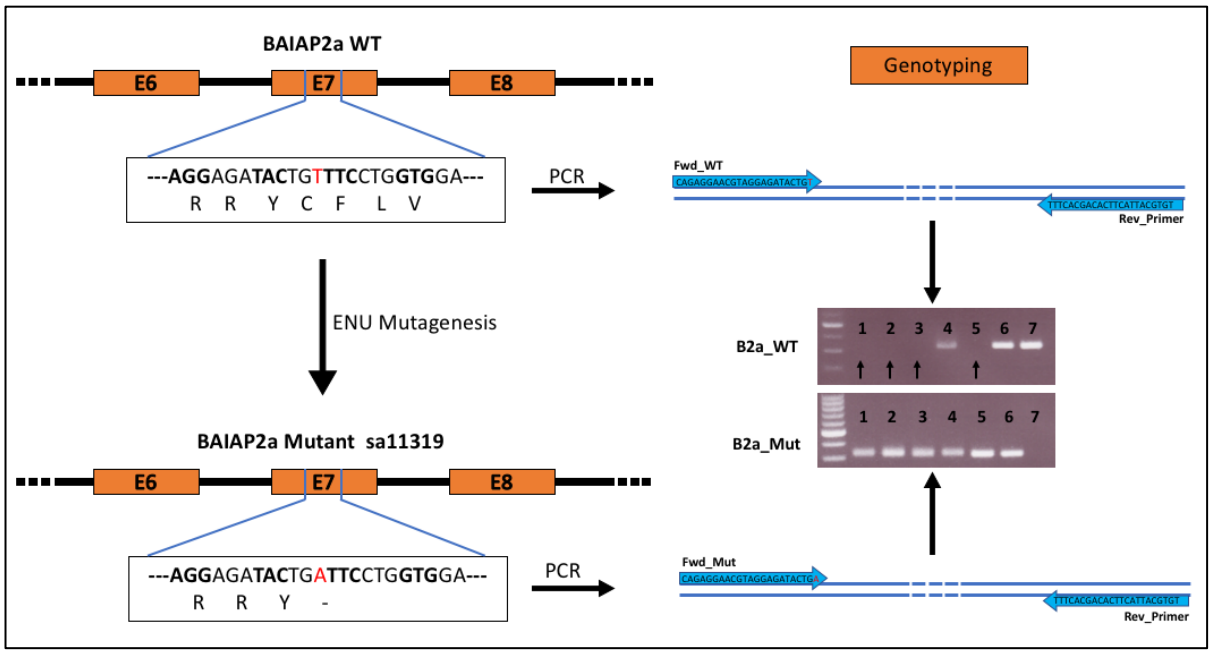

Fig. 8: Schematic of the zebrafish B2a mutant line generation

Left panel, shows the schematic of zebrafish mutagenesis at the B2a genetic locus. The upper gene represents a normal WT allele while as the lower one represents the mutated allele. DNA sequence in the boxes represents the locus of the mutation (shown in red) at the exon-7, while as the sequence underneath the DNA sequence represents the protein sequence, which is prematurely terminated in the mutant allele by the non-sense mutation.

Right panel, represents the screening procedure to identify the mutant alleles through genotyping PCR as described in the materials and methods section. The representative image of the gel from a screening depicts the specificity of the PCR for WT and Mutant alleles. Zebrafish #1, #2, #3 & #5 do not possess a WT allele as confirmed by the absence of the PCR amplification in these lanes, while as, #4 & #6, showing amplification in both the alleles, are heterozygous and #7 is a WT without any mutant allele.

The mutants were screened by genotyping PCR of genomic DNA, extracted from the clippings of their tail fins. The genotyping was carried out by two separate PCR reactions for each sample, using different forward primers for each reaction (5'-CAGAGGAACGTAGGAGATACTGT-3' for the amplification of WT gene sequence and 5'-CAGAGGAACGTAGGAGATACTGA-3' for the mutant sequence) with a common reverse primer (5'- TGTGCATTACTTCACAGCACTTT-3') for both the PCR reactions. The 3' ends of both forward primers, WT and mutant coincide with the locus of the point mutation in BAIAP2a gene and thus are able to amplify their respective products in the PCR, based on the presence or absence of the mutation in the gene sequence.

On running the PCR products in 2% agarose gel, WT samples show a band in the reactions containing the WT forward primer, the homozygous mutant samples show a band only in the reaction containing mutant forward primer whereas the heterozygous mutants show a band in both the reactions.

BAIAP2a$^{-/-}$ mutants were also crossed with Tg(KDRL:GFP) and Tg(CldnB:GFP) zebrafish to create BAIAP2a mutant lines in these genetic backgrounds as well. The former transgenic line expresses GFP in its vasculature under a KDRL promoter whereas the latter expresses GFP in its pronephric ducts under CldnB promoter. The out-cross generated heterozygous BAIAP2a$^{+/-}$ in these genetic backgrounds and were selected for the GFP expression during the embryonic stages. The heterozygous fish were then in-bred and screened as previously, to obtain BAIAP2a$^{-/-}$ homozygous mutant lines in WT genetic backgrounds.

12.3) Morpholino microinjections:

Freshly fertilized embryos were obtained, for microinjections, by breeding adult zebrafish in the breeding tanks. The solutions for microinjections were back loaded in microcapillaries, pulled into very fine needles with the help of a puller, and injected in 1-2 cell stage embryos with the help of a microinjector and a micromanipulator under a stereomicroscope. ~2nl of 0.3mM morpholino solution was injected into the yolk of each embryo. The embryos were let to grow in E3 medium at 28.5ºC until they reached the desired stage.

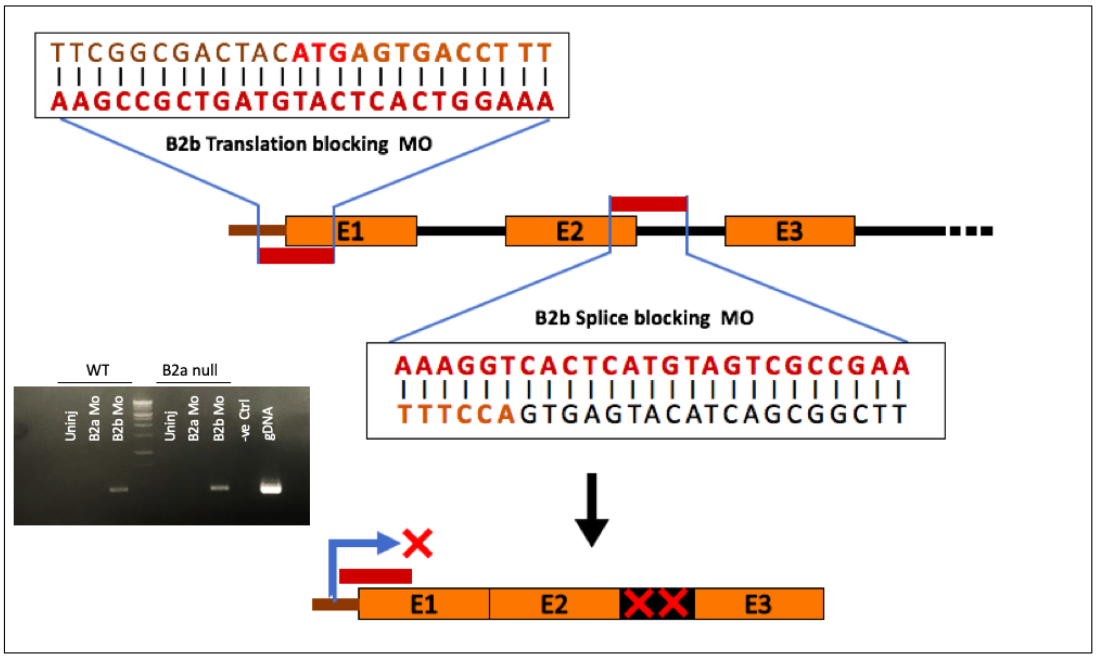

Fig.9: Schematic of gene knock-down by anti-sense morpholinos

Schematic depicting mechanism of gene knockdown by translation blocking and splice blocking morpholinos. The top box shows the B2b pre-mRNA sequence (upper) flanking the translation start site (shown in red), bound by the anti-sense B2b translation blocking morpholino (Mo). Targeting of translation start site in mRNA results in the stalling of translation machinery and downregulation of the protein (as shown below). The box in the centre shows B2b gene locus targeted by (E2i2i) splice blocking Mo (shown in crimson) resulting in the mis-spliced gene product (as shown below). This likely results in either a non-sense or a frame-shift mutation and the subsequent downregulation of the gene function. The gel image, on the left, shows the PCR amplification of an intron-exon B2b gene-locus only in B2b Mo injected embryos and the purified genomic DNA (gDNA), used as a positive control. While as no such amplification occurs either in uninjected (uninj) or B2a Mo injected embryos at 4 days after injection. cDNA synthesis reaction without a reverse transcriptase for total RNA of a WT zebrafish was used as a negative control.

15) Imaging techniques

13.1) Microscopy equipment

AX70 (Olympus) microscope equipped with a 12-bit b/w camera (FviewII, Olympus) was used to take the wide-field fluorescence images of the samples. Confocal images were taken with a Leica TSC SP2 AOBS confocal microscope using Leica Confocal Software. The microscope was equipped with violet (405 nm laser diode), blue (argon,

488 nm), yellow (561 nm Solid State Laser), and red (633 nm HeNe Laser) excitation laser lines. A 40x oil-immersion objective lens (Leica) was used for image acquisition of MDCK and Caco2 organoids. Time-lapse analysis was performed as explained in the following subchapters.

13.2) Epifluorescence time-lapse microscopy

Cells electroporated with various expression vectors, using Neon™ transfection system (Thermo Fisher Scientific) according to the manufacturer's instructions, were seeded on laminin (40 µg/ml). After 24 h, images were acquired for 5 min at 10 sec time intervals using a Leica inverted Microscope DMI6000B with adaptive focus control system driven by Leica Las AF software; an HCX PLAPO 63X (N.A.=1.47) objective was used with an Andor camera iXon DU-885 EM CCD. All experiments were performed using an environmental microscope incubator set to 37°C and 5% CO_2 perfusion.

13.3) Confocal spinning-disc time-lapse microscopy

Cells were electroporated and seeded on laminin as described above. After 24 h, images were acquired (10 min, 0.55 sec time interval) with an UltraVIEW VoX (Perkin Elmer) spinning disk confocal unit, equipped with an EclipseTi inverted microscope (Nikon), a C9100-50 emCCD camera (Hamamatsu) and driven by Velocity software (Improvision, Perkin Elmer). Images were acquired with a 100x oil immersion objectives (Nikon Apo TIRF, NA 1.49). All the experiments were performed using an environmental microscope incubator (OKOLab) set to 37°C and 5% CO_2 perfusion.

16) Statistical analysis

All data are mean ± S.D. from at least three independent experiments, except for wherever specified. Student's t-test was done to calculate the p-values (*$p<0.05$, **$p<0.01$ & ***$p<0.001$).

17) Histological analysis

Tissues of Human, mouse and zebrafish were fixed in 4% paraformaldehyde, dehydrated in an increasing gradient of Ethanol and embedded in paraffin for microtome sectioning. Adult zebrafish were decalcified using MicroDec™ D0052 (DiaPath, Italy) for 36 hours before embedding. The sections were deparaffinized in Xylene and rehydrated gradually in a decreasing gradient of Ethanol and finally 100% distilled water. The fully rehydrated sections were stained Haematoxylin and Eosin for 2 minutes. For IHC, the samples were incubated with the antibodies, overnight at 4ºC, after antigen unmasking and blocking steps. The sections were washed thrice in TBS and probed with the HRP-conjugated secondary antibodies. The signal was detected using DAB peroxidase solution and counterstained with Haematoxylin for the nuclear staining. The stained samples were washed in distilled water and dehydrated again as previously. The samples were cleared in Xylene, mounted with a coverslip and analysed under a light microscope.

RESULTS

Part 1: IRSp53 is involved in the establishment of polarity by coordinating the trafficking of apical proteins and a proper AMIS formation

1.1) IRSp53 localizes to the apical membrane surrounding the lumen of epithelial tissues in humans and mice

Polarity establishment is important for the proper development and functioning of tissues and therefore, central to the organogenesis in humans and other animals. Many proteins involved in the establishment of polarity like aPKC, Podocalyxin (PDX), Par complex etc. are distributed in a very asymmetric manner in the polarised cells and tissues. The asymmetric distribution of these canonical polarity determinants helps in the establishment of overall apico-basal polarity in glandular tissues for proper morphogenesis and functioning [12]. To assess a potential physiological implication of IRSp53 in defining the polarity of tissues *in vivo*, we first examined its localization and distribution across various human and mouse tissues. Immunohistochemistry (IHC) of tissue microarrays of human prostate, kidneys, gastric mucosa, salivary and mammary glands revealed that IRSp53 is invariably and specifically localized in a very polarised fashion, at the apical side of the luminal membrane in all the tissues tested (Fig.1.1). To understand if this peculiar distribution of IRSp53 was also present across the homologous murine tissues, we performed IHC analysis of mouse kidneys, gastric mucosa, colon and breast tissues with α-IRSp53 antibody. A similar pattern of highly polarised and restricted localisation of IRSp53 was evident in all these murine tissues as well. Indeed, IRSp53 is enriched at the luminal side of all the glands and tubules in murine kidneys, colon, gut and breast tissues (Fig.1.1).

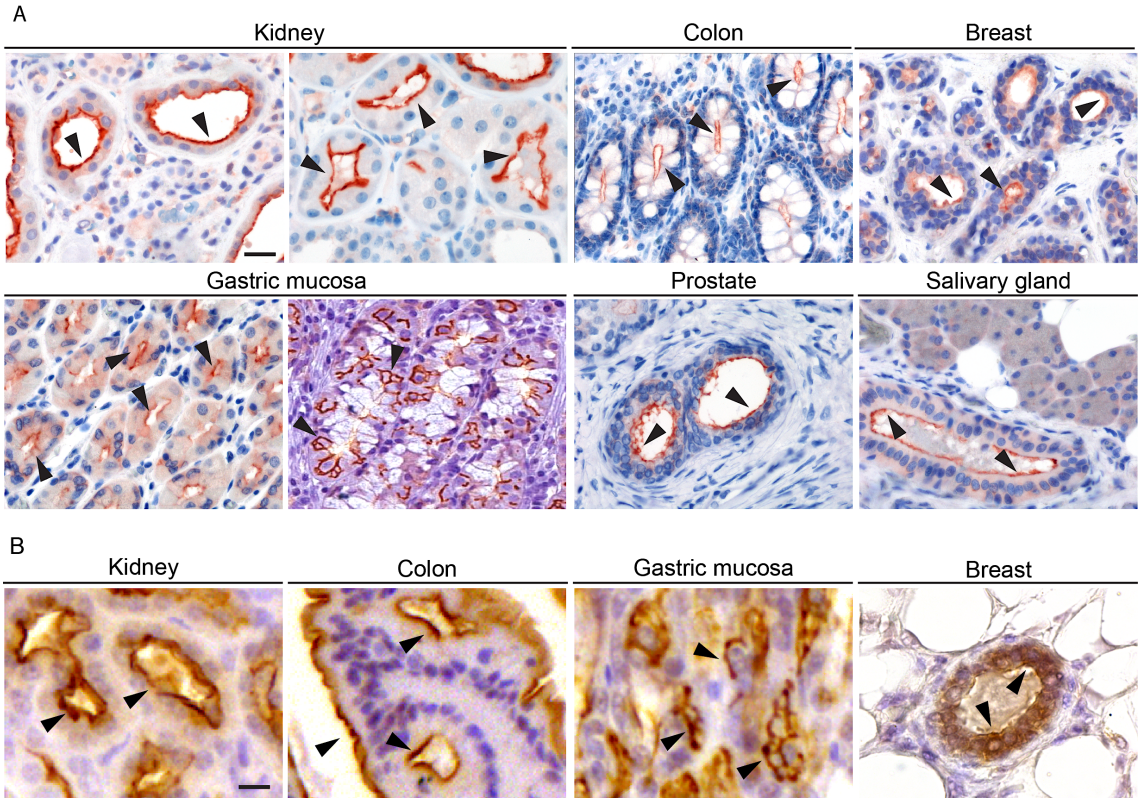

Fig.1.1: IRSp53 is localised at the apical side of lumina in various epithelial and glandular tissues
IHC of human (A) and mouse (B) paraffin sections with anti-IRSp53 antibody to study its localization across various epithelial tissues, as indicated. The staining pattern, red in human tissues and brown in mouse tissues, as pointed out by the arrows, clearly marks the luminal membranes in these tissues. Scale bar = 50μm in both A and B.

1.2) IRSp53 localizes to the apical membrane surrounding the lumen of pronephric ducts of the embryonic kidneys in zebrafish

The highly restricted cellular distribution of IRSp53 suggests that IRSp53 may be functionally relevant in controlling or regulating the process of polarisation and tissue morphogenesis *in vivo*. To address and verify this possibility, we choose to study zebrafish, a genetically tractable model system in which the morphogenetic processes could be monitored from early onset during its development.

The gene encoding for IRSp53 has undergone a duplication in zebrafish, leading to the generation of two distinct loci which have been named BAIAP2a (B2a) and

BAIAP2b (B2b). Firstly, we wanted to understand if the tissue distribution of IRSp53 in zebrafish was similar to what we observed in human and mouse tissues. To do this type of analysis, we first tested our anti-IRSp53 antibodies for cross-reactivity with the zebrafish B2a and B2b. Among the various available commercially or ad-hoc generated antibodies tested, the rabbit Immuno-purified polyclonal antibody (Rab-IP pAb, 1335) displayed very obvious cross reactivity with zebrafish B2a and B2b. Indeed, ectopically expressed myc-tagged B2a and myc-tagged B2b-GFP in IRSp53 KO MEF (Fig.1.2 & 1.2.1) were readily detected with the 1335 antibody, which stained structures identical to the one observed using anti-myc antibody.

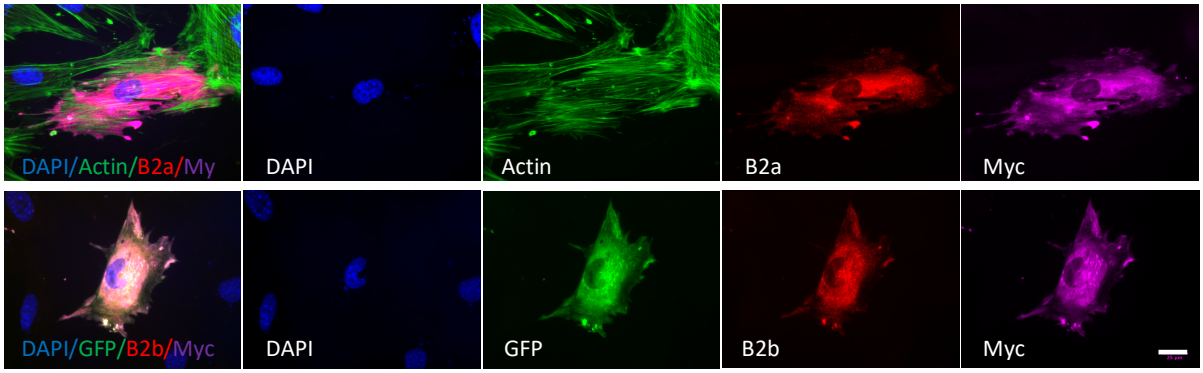

Fig. 1.2: Characterisation of anti-IRSp53 antibody for the cross reactivity with B2a and B2b
IF images of IRSp53 KO MEF, transfected with Myc-B2a or Myc-B2b-GFP. The cells were fixed on coverslips and stained with DAPI, FITC-Phalloidin (only for B2a transfected), Rab_IP 1335 ∝-IRSp53 and ∝-Myc. The signal from Rab_IP 1335 ∝-IRSp53 (Red) completely overlaps with the signal from ∝-Myc antibodies (Magenta). The cells were also stained with DAPI for Nuclei (Blue) and Actin (Green) in case of Myc-B2a. The untransfected cells did not show any staining with the ∝-IRSp53 antibody. Western blot is shown in Fig. 1.2.1. Scale bar = 25µm

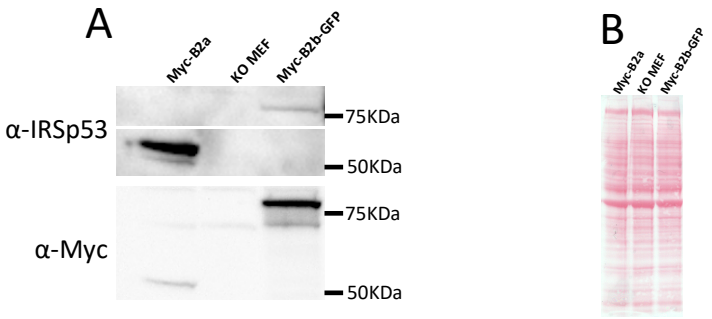

Fig. 1.2.1: Western blotting of IRSp53 KO MEF expressing Zebrafish B2a or B2b

A) IRSp53 KO MEF were transfected with either Myc-B2a or Myc-B2b-GFP, the cells were lysed and the equal amount of the proteins were immunoblotted on a membrane and probed using α-Myc and α-IRSp53 (Rab_IP_1335) antibodies.

B) Ponceau staining of the membrane showing equal amount of the protein loaded in all the three lanes.

Next, we performed immuno-histochemical analysis of zebrafish embryos derived from either WT or B2a knock-out genetic backgrounds and in combination with B2b morpholino knockdowns in these backgrounds. Likewise, in human and murine tissues, the localization of IRSp53 was prominently restricted at the luminal side of the pronephric ducts in zebrafish embryos during development (Fig.1.2.2). More Importantly, the embryos depleted for both the proteins did not show any staining, thus confirming the specificity of the antibodies in zebrafish. However, we could not detect any signal in the B2a null embryos as well. This latter result indicates that either the expression of B2b during zebrafish development is low or that the antibodies we employed have a lower affinity for B2b (or a combination of these factors). Notably, analysis of mRNA expression across various stages of Zebrafish embryo development suggest the B2b is expressed at significantly lower levels with respect to B2a (Fig. 1.2.3).

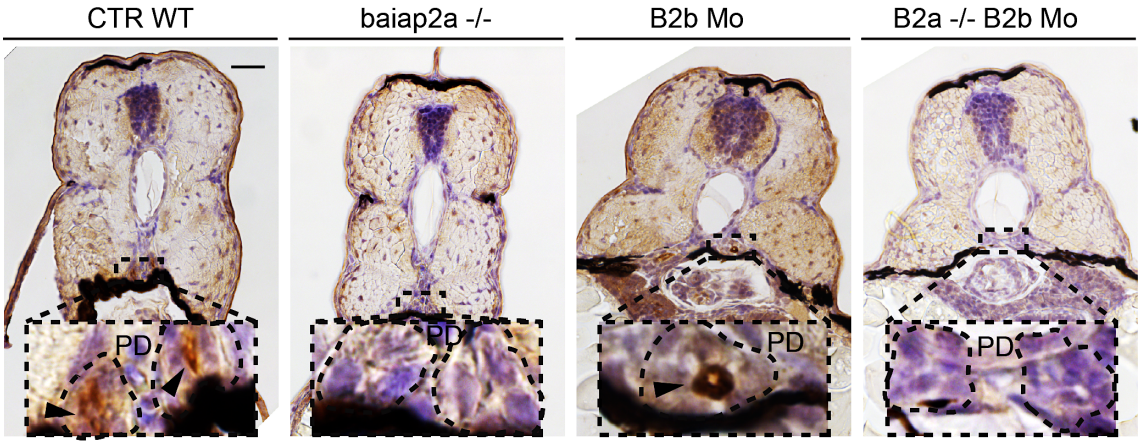

Fig. 1.2.2: IRSp53 is localised at the apical side of lumina in pronephric ducts of zebrafish embryos

IHC of 4dpf zebrafish WT, B2a null ($B2a^{-/-}$), B2b Knock down (B2b_MO) and B2b Knock down in B2a null ($B2a^{-/-}$B2b_MO) embryos using anti-IRSp53 antibody (Rab_IP_1335). The staining pattern brown (with arrowheads), showing IRSp53 localization at the lumina of the pronephric ducts. The staining is completely lost in $B2a^{-/-}$B2b embryos and is not detectable in $B2a^{-/-}$embryos as well. Scale bar = 50µm

The peculiar tissue distribution of IRSp53 across various luminal epithelia in different organisms and tissues supports the notion that this protein might be generally involved in the process of epithelial polarization. This latter possibility is further corroborated by a set of scattered and indirect evidences obtained in epithelial MDCK cell culture system [26]. In this system, the removal of the IRSp53 was shown to impair the proper formation of apical lumen [145], albeit neither the relevance of this finding in the physiological context, nor the underlying molecular mechanisms of IRSp53 action have been explored. Hence, we next set out to address these issues and assess the importance of IRSp53 in the process of epithelial polarization and tissues morphogenesis.

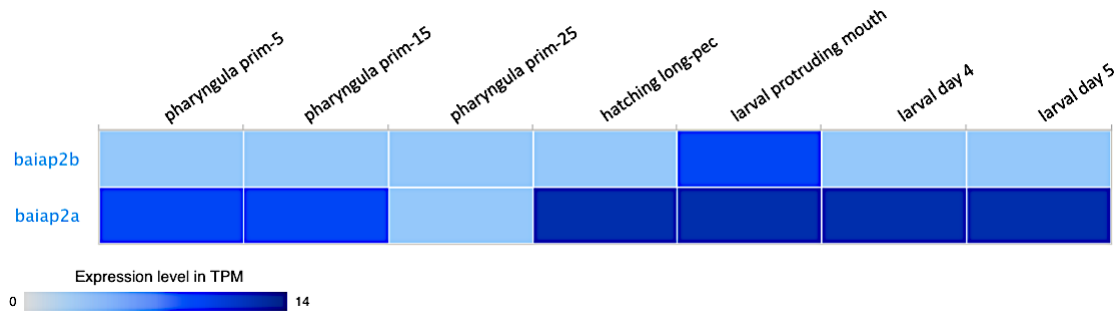

Fig. 1.2.3 Heat-map showing the expression pattern of B2a and B2b mRNAs during early stages of zebrafish development

Expression pattern of B2a and B2b in transcripts per million (TPM) through early stages of development in zebrafish shows relatively low mRNA levels of B2b as compared to B2a at the 4 days post fertilization. Figure generated using Expression Atlas (European Bioinformatics Institute, EBI).

1.3) IRSp53 co-localizes with the apical proteins, Podocalyxin and aPKC at the luminal membrane in the epithelial spheroids derived from either MDCK or Caco-2

To start gaining clues as to the role played by IRSp53 in lumenogenesis, we employed MDCK and Caco-2 cells. These epithelial cells when grown on top of or embedded in 3D matrices composed of basement membrane (Matrigel), undergo a step-wise process of polarisation and lumenogenesis that recapitulates the morphogenesis of renal and intestinal tubes. The polarized divisions and growth of these epithelial cells results, indeed, into the formation of hollow spheroids or cysts, consisting of a mono-layer of cells surrounding a single central lumen [60]. Caco-2 and MDCK cysts were fixed, stained for various apical and basal markers and for IRSp53, and imaged using confocal microscopy. We analysed the localisation of both endogenous, as well as of the ectopically expressed GFP-tagged IRSp53 protein. We found that the cysts formed from GFP-IRSp53-expressing MDCK cells showed a distinct localisation of the GFP signal along the apical side of the lumen. Whereas, the GFP, used as the negative control, was diffused in the cytoplasm of the cells forming the spheroids. Importantly, also the endogenous IRSp53 was specifically localised to the apical side of the lumen in the spheroids formed by WT MDCK cells (Fig.1.3), thus, validating the use of ectopically expressed EGFP-IRSp53. We also confirmed that IRSp53 co-localizes with the other canonical apical markers, including F-actin and Podocalyxin in the MDCK cysts. We performed a similar analysis in Caco-2 cysts. We found the enrichment of GFP-IRSp53 at the apical side of the lumen in these spheroids as well, whereas the EGFP alone was diffused (Fig. 1.3). These results are in line with our previous observations for different tissues *in vivo* (Fig 1.1 & 1.2.2), and provided us with relevant *in vitro* model systems to study in details the role, IRSp53 plays during the process of polarization and lumenogenesis.

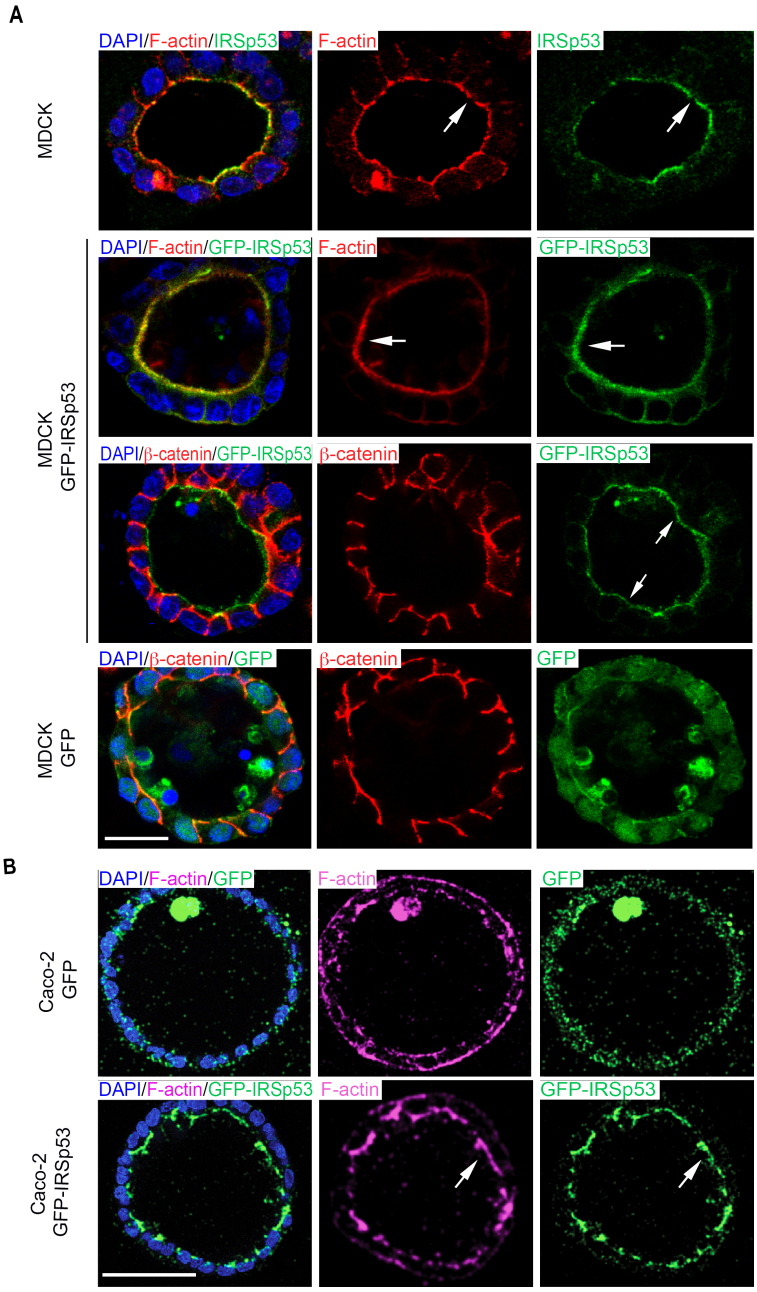

Fig.1.3: IRSp53 co-localizes with the apical proteins, Podocalyxin and aPKC at the luminal membrane in the epithelial spheroids derived from either MDCK or Caco-2

A) MDCK cells WT or infected with GFP or GFP-IRSp53 were resuspended as single cells and plated on a Matrigel layer for 6 days, to form polarized cysts. Cysts were then fixed and stained with rhodamine-phalloidin, anti-IRSp53 and DAPI or processed for epifluorescence to visualize GFP- or GFP-IRSp53 positive cells, stained with anti-β-catenin and DAPI, respectively. Images are confocal section of the central region of each cyst. Arrows point to the apical/luminal membranes. Scale bar = 18μm.

B) Caco-2 cells infected with GFP or GFP-IRSp53 encoding vectors were embedded in Matrigel-collagen mixture as single cells to form cysts. The cysts were then fixed, processed for epifluorescence to visualize GFP- or GFP-IRSp53 positive cells, stained with DAPI to detect nuclei and Phalloidin to

stain the lumina. Images are confocal section of the central region of each cyst. Arrows point to the apical/luminal membranes. Scale bar is 70 μm.

1.4) Depletion of IRSp53 causes an aberrant multi-lumen phenotype in MDCK & Caco-2 spheroids

An obvious question arising within this context is whether IRSp53 plays any significant role in the establishment of polarity and the process of lumenogenesis specifically during the spheroid formation *in vitro*. To address this point, we utilized distinct strategies to knock out or knock down IRSp53 in Caco-2 and MDCK cells. Using the former cells, we generated IRSp53 KO clones with the help of CRISPR-Cas9 system by using specific sgRNA targets. We selected a set of independent clones, identified the mutation by sequencing the loci (Fig. 1.4) and verified the loss of IRSp53 in these clones by western blotting. The protein levels were found to be severely downregulated in two of these clones (#3 and #12). Notably, Caco-2 cells are tetraploid and analysis of these clones indicated that at least three out of the four loci were successfully targeted by sgRNA in clone #3 resulting in non-sense mutations. These clones were used for further experiments to study the effect of IRSp53 depletion on the cystogenesis. Clone #2 did not show any downregulation of IRSp53 after the treatment with IRSp53 CRISPR-Cas9 and was, thus, used as a control in all the experiments involving Caco-2 clones #3 or #12.

Fig. 1.4: Genomic editing of MDCK and Caco-2 cell lines using CRISPR/Cas9 to KO IRSp53 gene function

IRSp53 locus of MDCK and Caco-2 cell lines was targeted using CRISPR/Cas9 technology to KO the gene function. *Upper panel* showing the guide RNA (gRNA) sequence (in red) used for targeting MDCK. Allele 1 and allele 2 below the gRNA show both the alleles of IRSp53 were successfully targeted resulting in the non-sense mutations in the IRSp53 KO MDCK clone. *Lower panel* showing the gRNA sequence (in red) used for targeting IRSp53 locus of Caco-2 cells. The sequences below, obtained from two independent clones (#3 and #12), show 2 out of 3 alleles in clone #3 resulting in premature termination of protein coding, while as, the mutation in the other allele of clone #3 resulted in loss of two amino-acids. One allele of Clone #12 had a non-sense mutation while as the other two resulted in the loss of 2 amino acids, each.

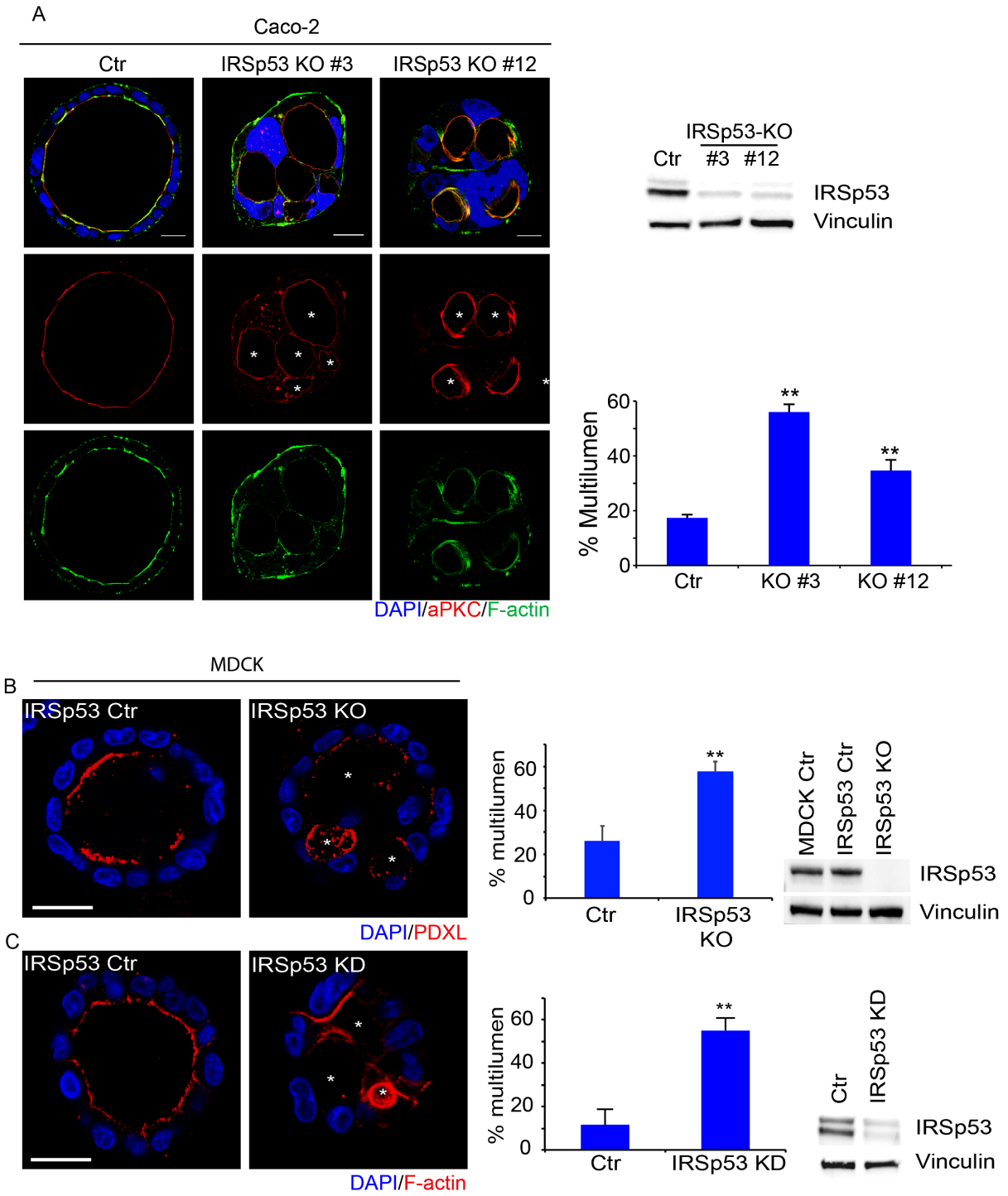

Fig. 1.4.1: Depletion of IRSp53 causes multi-lumen phenotype in Caco-2 and MDCK spheroids

A) Confocal images of Caco-2 WT (Ctrl #2) or IRSp53 KO (generated with CRISPR/Cas9 genome editing) cysts embedded in Matrigel-collagen matrix. Cysts were fixed and stained with anti-aPKC, phalloidin and DAPI. Images are confocal planes at the central region of each cyst. Scale bar = 20 µm. *Right upper panel.* Caco-2 WT (Ctrl #2) or IRSp53 KO (clones #3 and #12, generated by CRISPR/Cas9 genome editing) cells were lysed and immunoblotted with the indicated antibodies. *Right lower panel.* Percentage of multi-lumen cysts in Caco-2 WT (Ctrl #2) or IRSp53 KO (clones #3 and #12, generated by CRISPR/Cas9 genome editing). At least 30 cysts were analysed in 3 independent experiments. Data are mean ± S.D. T-test, **p<0.01.

B) MDCK IRSp53 Tet-off cells treated with or without doxycycline, to induce IRSp53 depletion. Single cells were plated on Matrigel to form cysts and fixed at day 6. Cysts were fixed and stained with phalloidin to highlight the lumen and DAPI to stain the nuclei. Images are confocal sections of the central region of each cyst. Scale bar = 18 μm. *Right panels.* Percentage of cyst presenting a multilumen phenotype, formed by MDCK IRSp53 Tet-off cells treated with or without doxycycline, to induce IRSp53 depletion. Experiments were performed in triplicate, counting at least 30 cysts for each condition. Data are mean ± S.D. T-test, **p<0.01. Levels of IRSp53 expression in MDCK IRSp53 Tet-off cells treated with or without doxycycline, to induce IRSp53 depletion.
C) Ctrl and IRSp53 KO MDCK cells (generated using CRISPR/Cas9 genome editing) plated on Matrigel to form cysts and fixed at day 6. Cysts were fixed and stained with phalloidin to highlight the lumen and DAPI to stain the nuclei. Images are confocal sections of the central region of each cyst. Scale bar = 18 μm. *Right panels.* Histogram showing the percentage of the multi-luminal cysts generated by Ctrl and IRSp53 KO MDCK cells. Experiments were performed in triplicate, counting at least 30 cysts for each condition. Data are mean ± S.D. T-test, **p<0.01. Western blot of MDCK Ctrl or IRSp53 KO cells showing the levels of IRSp53 expression.

We also employed MDCK cells for these studies. In this case, we used shRNA or siRNA as well as CRISPR-Cas9 system to silence the protein (Fig. 1.4). The levels of IRSp53 in the siRNA transfected cells were considerably reduced as compared to the control transfected cells (Fig.1.4.1).

Next, we employed these IRSp53 KO Caco-2 cells in our spheroid formation assay to study the effect of IRSp53 on the polarization and the lumen formation. We found that while a vast majority of spheroids derived from the control (Clone #2) cells formed a normal single lumen in ~80% of the cases, while as the spheroids from the cells deficient in IRSp53 developed a normal lumen only in ~40% (Clone #3) and ~60% (Clone #12) of the cases. The majority of the spheroids devoid of IRSp53 displayed an aberrant multi-lumen phenotype (Fig.1.4.1).

Next, we repeated the spheroid formation assays with WT or IRSp53 depleted (either by KD or KO) MDCK cells. Similarly, the depletion of IRSp53 resulted in a significantly higher number of multi-lumen spheroids as compared to the control spheroids (Fig.

1.4.1). Collectively, this finding indicates that IRSp53 is required in the formation of a proper lumen under these conditions.

Since, the establishment of a correct polarity program is essential for the normal lumenogenesis of these spheroids [60], a multi-luminal phenotype in IRSp53 depleted cysts indicate that the process of polarisation during the spheroid formation is perturbed begging the question in which step and processes IRSp53 might be involved.

1.5) Introducing GFP tagged IRSp53 back in the system completely rescues the multi-lumen phenotype in Caco-2 spheroids to the WT levels

To formally demonstrate the essential requirement of IRSp53 in cystogenesis, we reconstituted its expression by infecting IRSp53 KO Caco-2 cells either with GFP or GFP-IRSp53 using lentiviral vectors. The multi-lumen defective phenotype due to the lack of IRSp53 was completely rescued by the expression of GFP-IRSp53, but not by GFP alone. The spheroids expressing only GFP, indeed, presented a multi-lumen phenotype similar to that of the IRSp53 KO spheroids (>50%), whereas those re-expressing GFP-IRSp53 were indistinguishable from WT control cysts (Fig.1.5). These results clearly indicate that the significantly elevated multi-lumen phenotype observed in IRSp53 KO/KD spheroids is specifically due to the depletion of IRSp53.

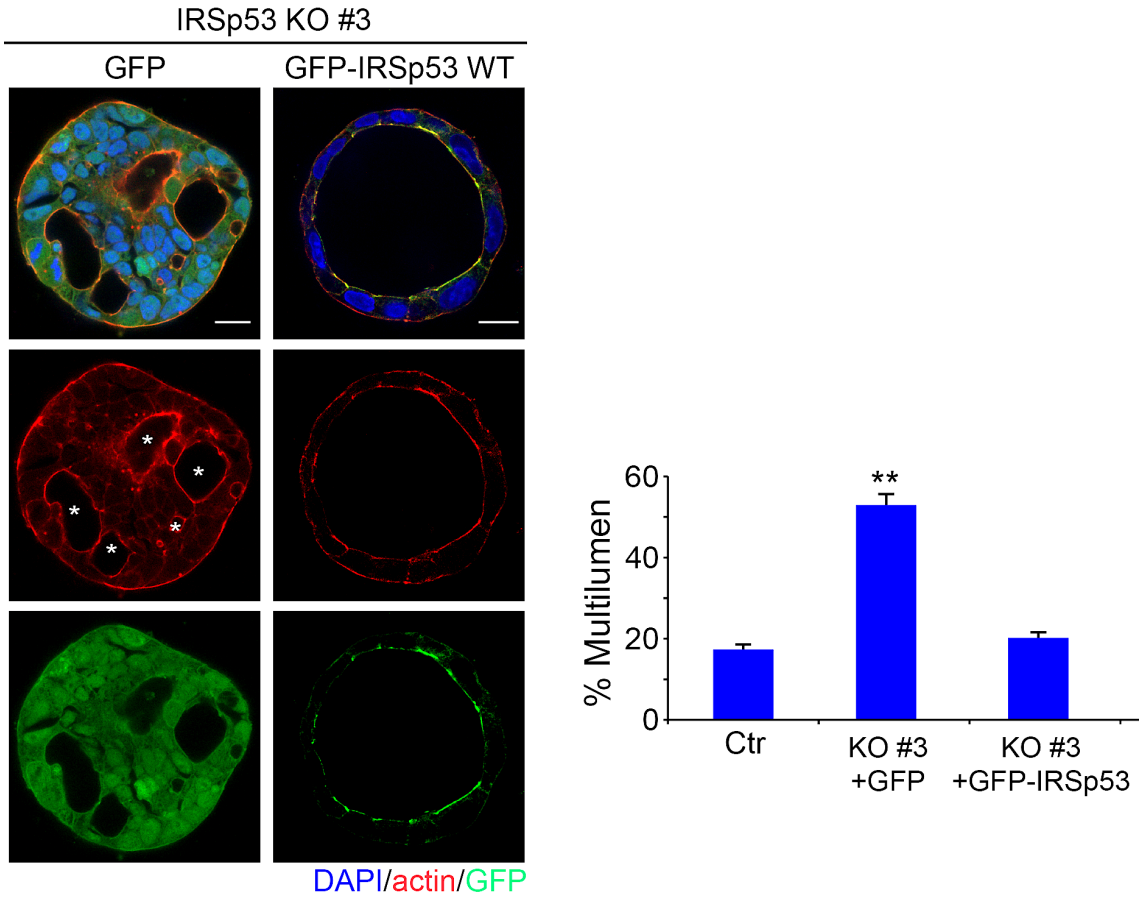

Fig. 1.5: Expression of GFP-IRSp53 in the KO cells reverses the multi-lumen phenotype back to the WT-levels in Caco-2 spheroids

Confocal analysis of Caco-2 IRSp53 KO cyst infected with either GFP or GFP-IRSp53. Caco-2 cells IRSp53 KO (CRISPR/Cas9 derived clone #3) were infected with lentiviral vectors encoding for GFP or GFP-IRSp53. Cells were then embedded in Matrigel-collagen matrix to form cysts. After 7 days cysts were fixed, processed for epifluorescence to visualize GFP or GFP-IRSp53 positive cells, stained with phalloidin to visualise the lumen and DAPI to detect nuclei. Images are confocal sections of the central region of each cyst. Scale bar = 20µm. *Right panel.* Histogram showing the percentage of multi-lumen phenotype in Ctrl (#2), IRSp53 KO spheroids reconstituted either with GFP or IRSp53-GFP. The experiments were done at least thrice. Data are mean ± S.D. T-test **p<0.01. Western blot analysis is shown in Fig. 1.12.1.

1.6) IRSp53 is localized at the intervening membrane between the cells right after the first division preceding the relocalization of canonical apical markers and the formation of AMIS

Next, we asked how IRSp53 could contribute to polarity and lumenogenesis programs. To begin addressing this question, we examined the localization and dynamics of IRSp53 in the very early phases of cystogenesis.

The polarity program in MDCK and Caco-2 spheroids follow a step-wise process which is hard wired and can be easily followed by tracking various apical markers. During the early steps of polarization, the formation of Apical Membrane Initiation site (AMIS) is critical as it leads to the formation of Pre-Apical Patch (PAP) between the daughter cells where the opposing cell membranes start drifting apart from each other to open up a space in between them [60]. This space starts growing due to the accumulation of ions which create a negative osmotic pressure and ultimately triggers the formation of an enclosed lumen which is usually filled with a fluid [60]. This structurally and temporally stereotypic morphogenetic process in MDCK and Caco-2 spheroids offered us the opportunity to investigate whether and when IRSp53 becomes asymmetrically distributed during the process of polarization and lumen formation.

Notably, various apical markers are initially localized isotropically along the entire cell membrane at the single cell stage. The first cell division acts as a symmetry breaking event in these unpolarised cells. This becomes obvious, right at the initiation of the cleavage furrow between the two cells during the cytokinesis. After the first division and the formation of an intervening membrane between the two newly formed cells, apical proteins are transported from the outer membrane to the intervening membrane at the AMIS. The transport of these proteins to the AMIS is primarily achieved through transcytosis of trafficking vesicles [60]. We monitored this process using confocal imaging of GFP-IRSp53 expressing MDCK cells along the very early

stages of the cyst formation. To this end, we plated cells on Matrigel in order to let them polarise and then fixed them at different time-points. We also analysed the cellular distribution of canonical apical markers, such as PDX. In the first 8-12 hours after plating cells, PDX localizes isotropically to the peripheral surface of single cells, before being internalized into vesicles and subsequently delivered to the membrane formed between the two dividing cells, where apical lumen is formed *de novo.*

We found that IRSp53 became prominently enriched at the cell-junction along the first cleavage furrow of a cell division well before PODXL recruitment. At later stages IRSp53 and PODXL concentrated at the AMIS and when cyst was formed the two proteins co-stained the lumen. Importantly, IRSp53 and PODXL could also be seen colocalizing in the early phases in vesicle-like structures (Fig. 1.6) which were subsequently targeted to the newly formed AMIS and lumen. The latter findings suggest that the two proteins may co-traffic to or from endosomal recycling compartments. They further raise the possibility that IRSp53 may be involved in trafficking or targeting of PODXL to the AMIS.

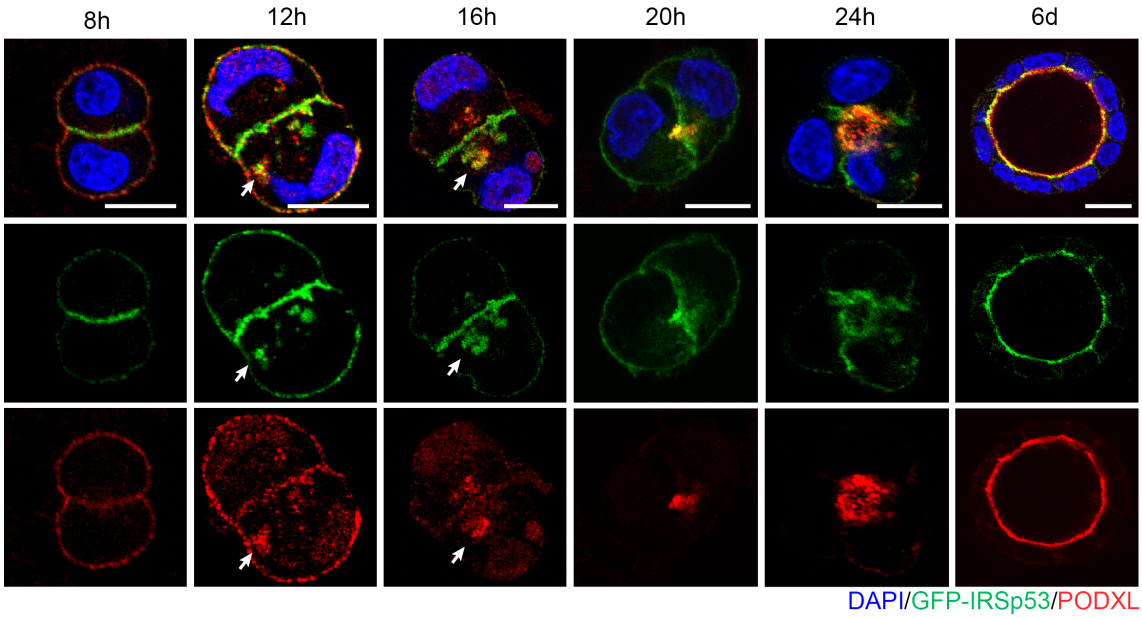

Fig. 1.6: IRSp53 is localized at the intervening membrane between the cells right after the division preceding the canonical apical markers and the formation of AMIS

Confocal analysis of early and late cystogenesis events. MDCK cells infected with GFP-IRSp53 were resuspended as single cells, plated on a Matrigel layer and fixed at the indicated time. Cysts were processed for epifluorescence to visualize GFP-IRSp53 and stained with anti-Podocalyxin antibody and DAPI to detect nuclei. Images are confocal section of the central region of each cyst. Arrows highlight vesicle-like structures where GFP-IRSp53 and Podocalyxin partially co-localize. Scale bar is 12 μm.

1.7) IRSp53 depletion leads to the formation of multi-focal AMIS-like apical domains (MAD) phenotype during early stages of polarisation

To understand whether IRSp53 is involved in the process of polarisation and the trafficking of apical proteins to the AMIS, we studied the initial phases of polarisation by looking at the formation of AMIS in IRSp53 depleted MDCK and Caco-2 cells. Depletion of IRSp53 using siRNA in MDCK cells resulted in the formation of aberrant multi-focal AMIS-like apical domains (MAD phenotype), in more than 60% of the cysts during the early stages of spheroid formation. While only about 30% of the control cells showed MAD phenotype (Fig.1.7).

We repeated this experiment with control and IRSp53 KO Caco-2 cysts during early stages of polarisation as well. We plated these Caco-2 cells in the Matrigel and let them polarise for 48 hours. The cells were analysed for canonical apical and basolateral markers, including aPKC and F-actin. We observed that the cells depleted of IRSp53 display a significant increase in MAD phenotype as compared to controls. Importantly, re-expressing a GFP-tagged IRSp53 in the KO cells reverted this phenotype (Fig. 1.7), formally demonstrating that IRSp53 is specifically required to form a single apical domain in the early stages of polarisation.

These findings indicate that IRSp53 is required for the proper polarisation of MDCK and Caco-2 cells at the early stages to form a single apical domain or AMIS during cystogenesis. Since, the normal process of polarisation requires the trafficking of apical proteins from the outer membrane to form a single AMIS [60], IRSp53 may play some role in this process. In the absence of IRSp53 the coordination of the trafficking machinery might be perturbed, resulting in the aberrant deposition of apical proteins at multiple foci and a MAD phenotype. These multi-focal apical domains may act as independent sites where lumina start expanding. Thus, the formation of MAD

phenotype may eventually result in the formation of multi-luminal spheroids during the process of cystogenesis.

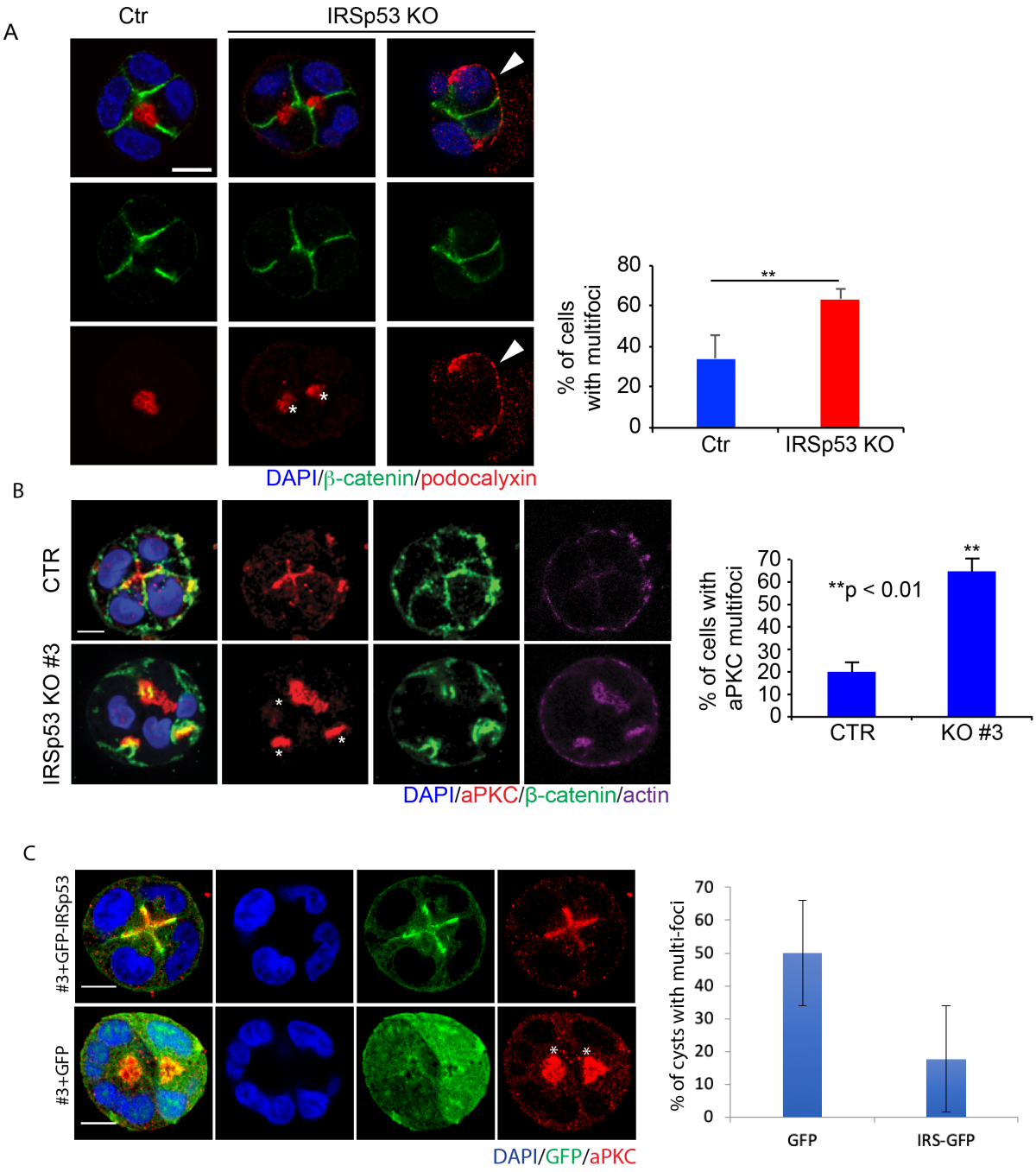

Fig. 1.7: IRSp53 depletion leads to the formation of multi-focal AMIS-like apical domains (MAD) phenotype during polarisation

A) Ctrl and IRSp53 KO MDCK were plated on Matrigel as single cells for 24-30 hrs to let them divide and polarise at 3-4 cell stages. The cells were fixed, stained for Podocalyxin (Red) and β-catenin (Green) and analysed for a MAD phenotype. The images are a single confocal section at the centre of the cells undergoing cystogenesis. Arrow heads indicate the mis-localisation of PDX at the basal side of the cysts. Scale bar = 10μm. Histogram on the right depicts the percentage of cells with MAD phenotype. Data are mean ± S.D. The experiment was repeated at least 5 times. T-test **p<0.01.
B) Single plane confocal images of Ctrl and IRSp53 KO Caco-2 cysts, embedded in Collagen-Matrigel matrix as single at early stages during cystogenesis. The cysts were fixed and stained with aPKC (Red), β-catenin (Green), Phalloidin (Magenta) and DAPI. Scale bar = 10μm. The histogram showing the percentage of cells with MAD phenotype in both the conditions. The experiment was done at least thrice. Data are mean ± S.D. T-test, **p<0.01.
C) IRSp53 KO #3 Caco-2 cells were reconstituted with either GFP or IRSp53-GFP. Single cells were embedded in Collagen-Matrigel matrix to let them undergo polarisation and cystogenesis for 48 hours. The cysts were fixed, processed for epifluorescence to visualize GFP or GFP-IRSp53 and stained for anti-aPKC and DAPI. Scale bar = 10μm. Histogram on the right depicts the percentage of cysts with MAD phenotype. Data are mean ± S.E.M of a single experiment.

1.8) IRSp53 colocalizes with apical trafficking proteins in vesicle-like structures during the early phases of polarisation

Careful analysis of the cellular distribution of IRSp53 in the initial process of polarisation leading to the formation of a single AMIS revealed that it also co-localizes with vesicles containing Podocalyxin, a prototypical marker of the apical domains (Fig. 1.6 and 1.8). These vesicles are trafficked through a CDC42 and RAB-GTPase dependent mechanism to the apical membrane to form the AMIS [146]. Therefore, we investigated the nature of IRSp53 carrying vesicles during the early stages of polarisation and AMIS formation.

We analysed IRSp53 cellular localization in relation to a variety of proteins that mark distinct trafficking compartments. We employed MDCK cell-lines stably expressing GFP-IRSp53, which we showed earlier, display a localization nearly identical to that of the endogenous protein. We let these cells to polarise on Matrigel for about 4 hours and analysed them by confocal microscopy in conjunction with vesicular trafficking

markers and cargos. We observed a partial co-localization of GFP-IRSp53 with PODXL and actin in vesicle-like structures that were also positive for RAB7, RAB11a and RAB35 (Fig. 1.8). These vesicles are known to be essential for the transport of apical proteins through recycling routes to the AMIS [60] [67]. To understand the specificity of this colocalization, we also stained these cells with the early endosome marker EEA1 (early endosome antigen 1), late endosome marker LAMP1 (lysosome-associated membrane glycoprotein 1) or the Golgi marker Giantin. We did not observe any colocalization of IRSp53 with any of these latter markers, thus confirming the specificity of IRSp53 colocalization with the apical protein transporting vesicles.

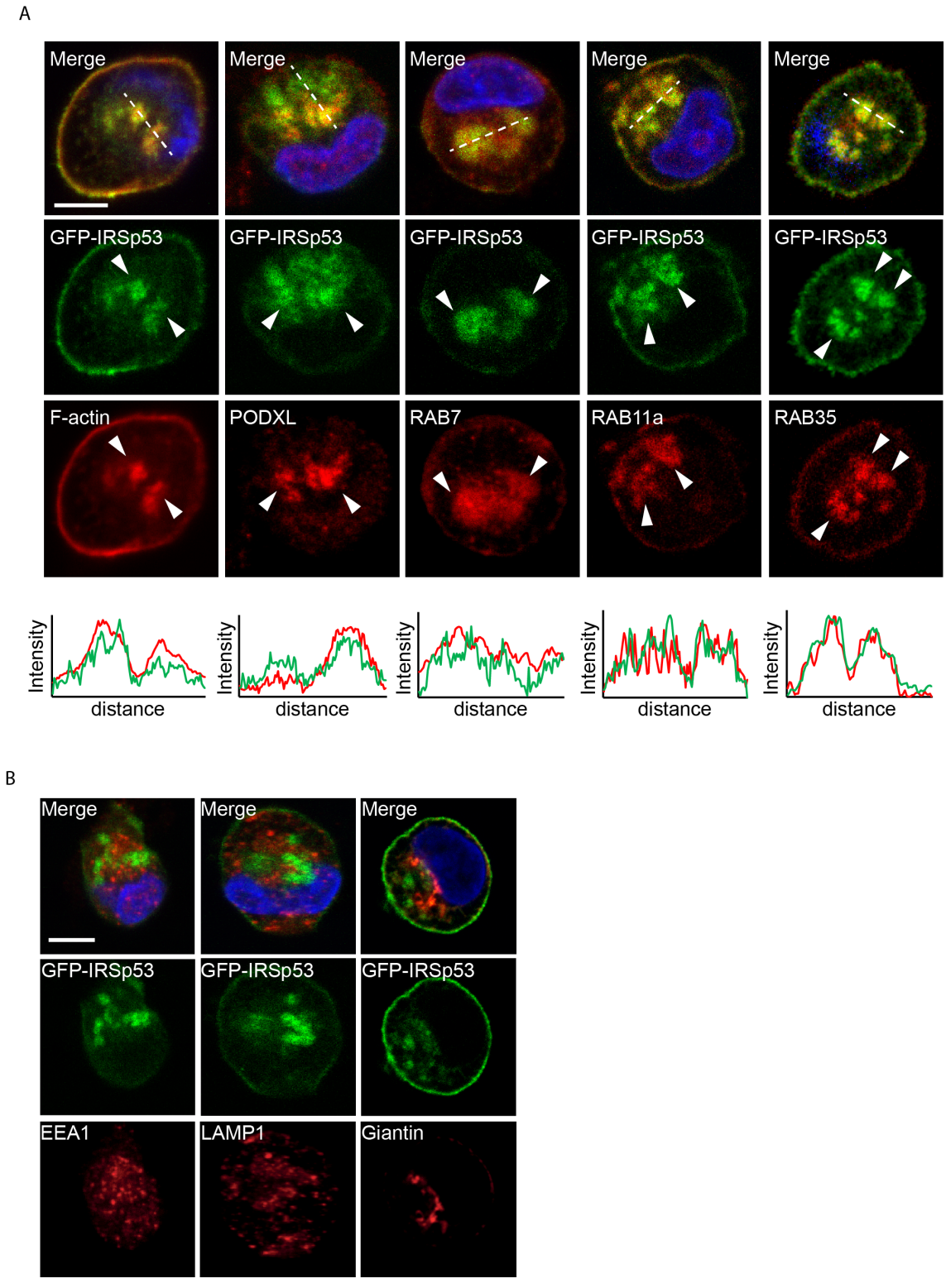

Fig.1.8: IRSp53 colocalizes with apical trafficking proteins in vesicle-like structures during the early phases of polarisation

A) MDCK cells infected with GFP-IRSp53, were resuspended as single cells and plated on a Matrigel layer to undergo cystogenesis. Cells were fixed at one-cell stage after 8 hours, processed for epifluorescence to visualize GFP-IRSp53 and stained with phalloidin, anti-PDX, anti-RAB7. For RAB11a and Rab35 analysis, MDCK GFP-IRSp53 cells were transfected with Apple-Rab11a and RFP-Rab35

plasmids respectively, fixed and processed for epifluorescence to visualize GFP-IRSp53 and Apple-Rab11a or GFP-IRSp53 and RFP-Rab35. DAPI was used to detect nuclei. Scale bar is 6 μm. *Lower panels.* Colocalization analysis. Intensity profiles of red and green signals across the line indicated in the respective merged images.

B) MDCK cells infected with GFP-IRSp53, were resuspended as single cells and plated on a Matrigel layer to undergo cystogenesis. Cells were fixed at one-cell stage after 8 hours, processed for epifluorescence to visualize GFP-IRSp53 and stained with Anti-EEA1, anti-LAMP1 or anti-Giantin. DAPI was used to detect nuclei. Scale bar is 6 μm.

1.9) IRSp53 depletion perturbs the trafficking of Podocalyxin during the early phases of polarisation

In addition, to being present in vesicles carrying the apical proteins, we also showed that IRSp53 accumulates at the adjacent membrane between the two cells, originating from the first cell division, destined to form a spheroid (Fig. 1.6). We also identified these vesicles as the ones carrying the apical proteins from the outer membrane to the AMIS. Additionally, the depletion of IRSp53 resulted in perturbation of a normal AMIS formation and a MAD phenotype. Altogether, these findings suggest that IRSp53 might be involved in the regulation of proper trafficking of critical apical proteins, necessary for the formation of a single AMIS, to the apical membrane. To verify this hypothesis, we took advantage of the fact that PDX re-localization to Vacuolar Apical Compartment (VAC) upon calcium depletion in 2-D monolayers. VACs are transient apical organelles formed in single cells in 2D monolayers upon disruption of cell-cell junction. The formation of these structures can be induced in a monolayer of cells by perturbing their cell-cell contacts via depletion of calcium [147]. VACs are known to contain many apical proteins that rapidly re-localize to the intercellular membranes upon re-establishing or properly functional, cell-cell contacts [147]. This process is thought to recapitulate the formation of proper apical membranes and the establishment of the polarity [147, 148]. To understand the role of IRSp53 in the trafficking of these apical

proteins, we monitored PDX localization to the VAC upon calcium depletion in normal or IRSp53 depleted MDCK monolayers. For this, we plated WT or IRSp53 KO MDCK cells as monolayers in normal calcium containing media. We then depleted calcium from these cells and fixed them at different timepoints to study the process of PDX cellular distribution and the formation of VAC. We found that IRSp53 KO cells had a significant delay in the relocalization of the PDX to VAC as compared to WT cells. At 5 hours post calcium depletion, the majority (~70%) of WT cells had re-localized their PDX to the VAC, while only 35% of IRSp53 KO cells had PDX re-localized to VAC (Fig. 1.9). This finding indicates that IRSp53 is involved in the proper trafficking and localization of PDX to the apical domains during polarization.

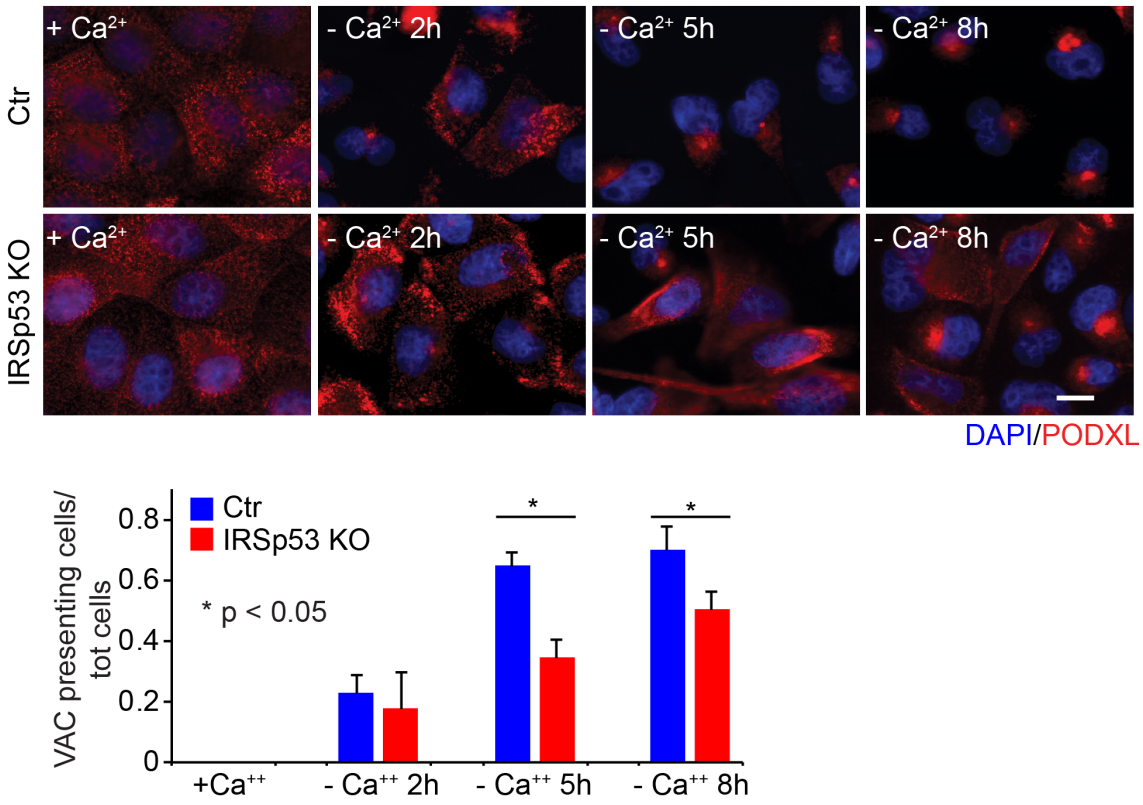

Fig.1.9: IRSp53 depletion perturbs the trafficking of Podocalyxin to VAC

Ctrl or IRSp53 KO MDCK cells were grown as monolayers, depleted of calcium and fixed at the indicated time points. The cells were stained for Podocalyxin and DAPI and imaged with a widefield fluorescent microscope. Scale Bar = 10μm

The histogram below shows the fraction of WT and IRSp53 KO cells containing a VAC after calcium depletion. Data are mean ± S.D. The experiment was repeated at least thrice. T-test, *p<0.05

1.10) IRSp53 binds to Rab35 that may explain it role in the trafficking of apical proteins during polarization

To further understand the molecular mechanism by which IRSp53 regulates the trafficking of apical proteins to the AMIS, we took a candidate-based approach to look at the interactors of IRSp53 that might be playing a key role in the trafficking of apical proteins. One such candidate, RAB35, has been recently shown to be present at the intervening membrane upon the first cell division in the polarizing cells in a 3D matrix [67, 68]. In addition, RAB35 depletion was reported to cause aberrant multi-lumen cyst formation, reversal of polarity, and altered Podocalyxin distribution [67]. Thus, recapitulating some of the defects seen upon the removal of IRSp53. Importantly, RAB35 has been shown to interact directly with Podocalyxin and proposed to facilitate the docking of trafficking vesicles to the apical membrane [67, 68]. These observations in the context of our results suggest that IRSp53 and RAB35 may directly interact with each other to facilitate the normal trafficking of the apical proteins to the AMIS. To investigate this possibility, firstly we performed co-immunoprecipitation studies in HeLa and MDCK cells stimulated or unstimulated with growth factors. We found that GFP-RAB35 and Flag-IRSp53 weakly, but reproducibly interacted with each other. Strikingly, the interaction was severely reduced upon GF stimulation (Fig. 1.10). To corroborate these results and assess whether the proteins interact directly, we performed dot blot assay using purified recombinant WT, dominant negative, RAB35S22N, and constitutively active, RAB35Q73L forms of RAB35 together with wild

type His-tagged IRSp53. We found that IRSp53 preferentially interacted with RAB35S22N as compared to its constitutively active form (Fig. 1.10). These results indicate that the IRSp53 directly binds to RAB35 in its GDP-bound inactive state. They further suggest the intriguing possibility that IRSp53 might be serving or facilitating the proper localization of this GTPase at the AMIS and possibly serving as a docking platform.

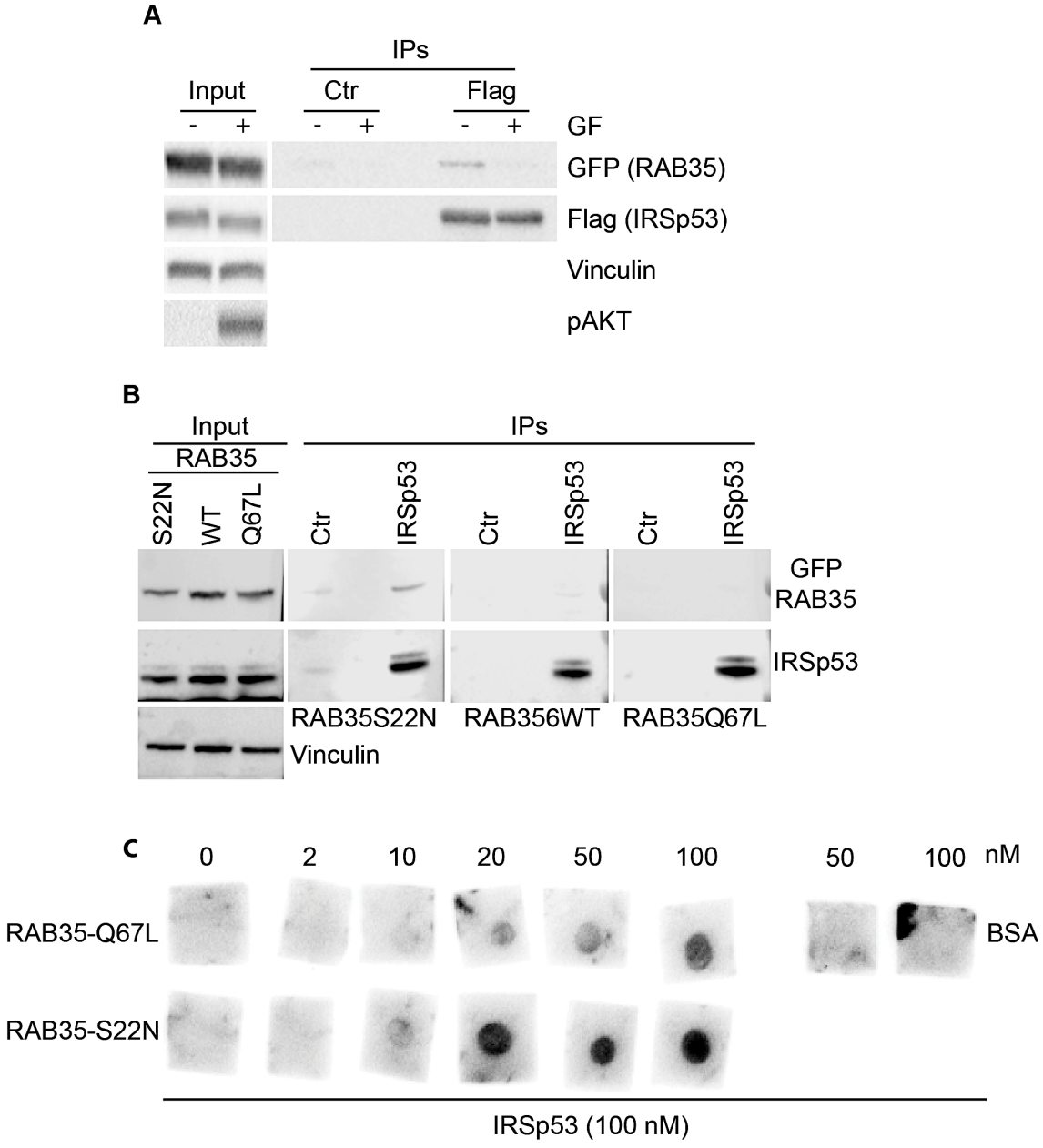

Fig. 1.10: IRSp53 interacts with Rab35.

A) Lysates (1mg) of Hela cells transfected with flag-IRSp53 and RFP-RAB35, serum-starved, mock treated (ss) or stimulated with Serum + EGF (100ng/ml) + HGF (100ng/ml) (S/G) were

immunoprecipitated with anti-flag or anti-HA (Ctr) antibodies. Lysates (25 µg) and immunoprecipitants (IP) were run on SDS-PAGE and immunoblotted with the indicated antibodies.
B) Lysates (1mg) of MDCK cells transfected with RFP-RAB35 WT, S22N and Q67L were immunoprecipitated with anti-IRSp53 or anti-HA (Ctr) antibodies. Lysates (25 µg) and immunoprecipitants (IP) were run on SDS-PAGE and immunoblotted with the indicated antibodies.
C) Recombinant purified GST-Rab35-Q67L or S22N were spotted on nitrocellulose membrane (as indicated) and overlaid with 100nM of recombinant purified IRSp53. Anti-IRSp53 antibody was used to detect the signal. BSA was spotted as negative ctrl.

1.11) IRSp53 binds to Rab35 through its I-BAR domain

To get further insights into the interaction between IRSp53 and RAB35, we mapped their interaction surfaces using various IRSp53 fragments or single point mutants and the dominant negative form of RAB35 (RAB35S22N) in various immunoprecipitation and *in vitro* binding assays. Firstly, we expressed RFP-tagged RAB35S22N in MDCK cells along with GFP-tagged IRSp53 either WT or I-BAR mutant form (IRSp53 IBAR*: K142E, K143E, K146E, K147E [106]). Only the WT IRSp53 could pull-down RAB35S22N from the lysates while as no signal was detected either in the I-BAR*-IRSp53 or the negative control, GFP alone (Fig. 1.11). We then investigated this by dot blot assay using WT or I-BAR* mutant forms of IRSp53. The results confirmed that the direct interaction of IRSp53 was disrupted by functional mutations in its I-BAR domain. These results suggest that the I-BAR domain of IRSp53 is necessary for its association with RAB35S22N (Fig. 1.11). We further repeated this assay using either full length IRSp53 or its various truncated forms to understand if I-BAR domain is sufficient for the interaction with RAB35. For this purpose, we employed WT IRSp53, its I-BAR domain only, or I-BAR deleted form (∆I-BAR), a truncation mutant lacking the PDZ binding motif (I-BAR-CRIB-SH3), and a single point mutant (W413G) impairing the function of the SH3 domain. The results showed that the I-BAR domain is sufficient

for the interaction with RAB35 and there is no significant contribution from the CRIB or SH3 domains.

In summary, these results indicated that the interaction with the inactive form of RAB35 is mediated through the I-BAR domain of IRSp53 and that this domain is sufficient for the interaction.

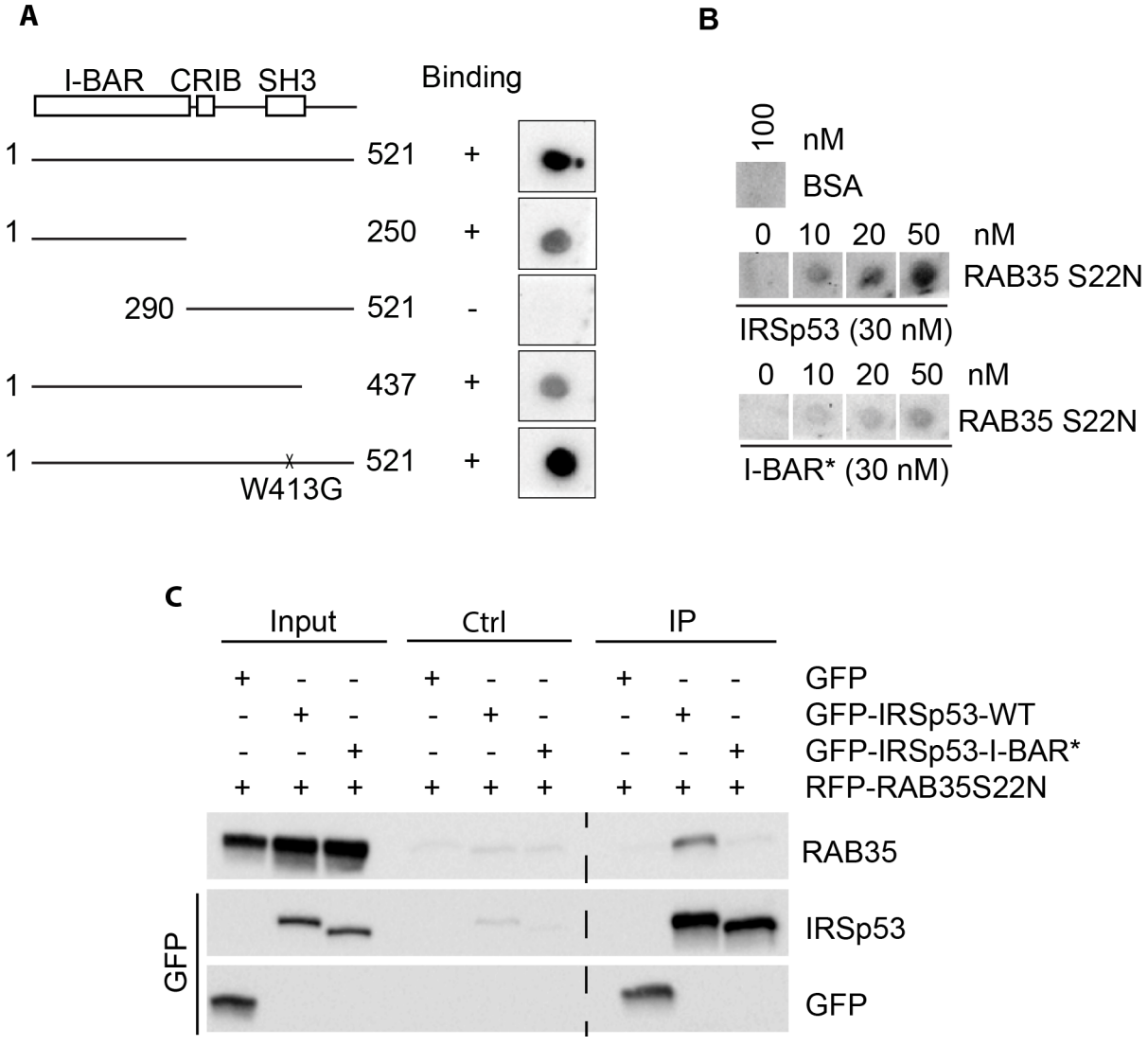

Fig. 1.11: IRSp53 binds to RAB35 through its I-BAR domain

A) Equal amounts of recombinant purified IRSp53 full length (FL) or the indicated fragments/mutants were spotted on nitrocellulose and overlaid with recombinant purified GST-RAB35-S22N (100nM). Anti-GST antibody was used to detect the signal. BSA was spotted as negative ctrl.

B) Recombinant purified GST-RAB35-S22N was spotted on nitrocellulose membrane (as indicated) and overlaid with the indicated amount of recombinant purified IRSp53 WT or the isolated I-BAR mutant (I-BAR*). Anti-IRSp53 antibody was used to detect the signal. BSA was spotted as negative ctrl.
C) Lysates (1mg) of MDCK cells transfected with GFP or GFP-IRSp53 WT or GFP-IRSp53 I-BAR* and RFP-Rab35 S22N were immunoprecipitated with anti-GFP or Ctr (HA) antibodies. Lysates (10 µg) and immunoprecipitants (IP) were run on SDS-PAGE and immunoblotted with the indicated antibodies.

1.12) I-BAR, CRIB & SH3 domains are all essential for proper polarization and lumenogenesis in 3-D spheroids

The direct interaction between IRSp53 and RAB35 suggest the possibility that the two proteins might co-operate in the regulation of PDX localization. Hence, hampering this interaction should affect PDX trafficking to AMIS and disrupt the correct polarity/lumenogenesis program. To asses if this was the case, we took advantage of mouse-IRSp53 lentiviral constructs carrying mutations in its critical domains (I-BAR, CRIB, SH3 and PDZ-binding domains) [54]. Single MDCK IRSp53-depleted cells, infected with GFP empty vector or with GFP-IRSp53 WT or mutants, were seeded onto Matrigel and developing cysts were fixed at 3-4 cell stages. We analysed PDX localization and rescue of the MAD phenotype in each case (Fig. 1.12). As predicted, at early phases of cystogenesis, a functional I-BAR domain, mediating the interaction between IRSp53 and RAB35, was required for the correct delivery of PDXL to a single focal spot (Fig. 1.12). Molecularly, both the ability to bind to negatively curved, PIP2-rich membrane, which is compromised by the mutations inserted [106], and to interact with RAB35 likely account for the finding observed. Mutations in the CRIB domain, required for IRSp53 binding to active CDC42 [116], or in the SH3 domain that mediates the interaction of IRSp53 with a variety of binding partners [54], could not rescue the defects in PODXL delivery due to IRSp53 depletion as well and gave rise to the MAD

phenotype (Fig. 1.12a). Conversely, the integrity of the PDZ binding motif was not required for this process.

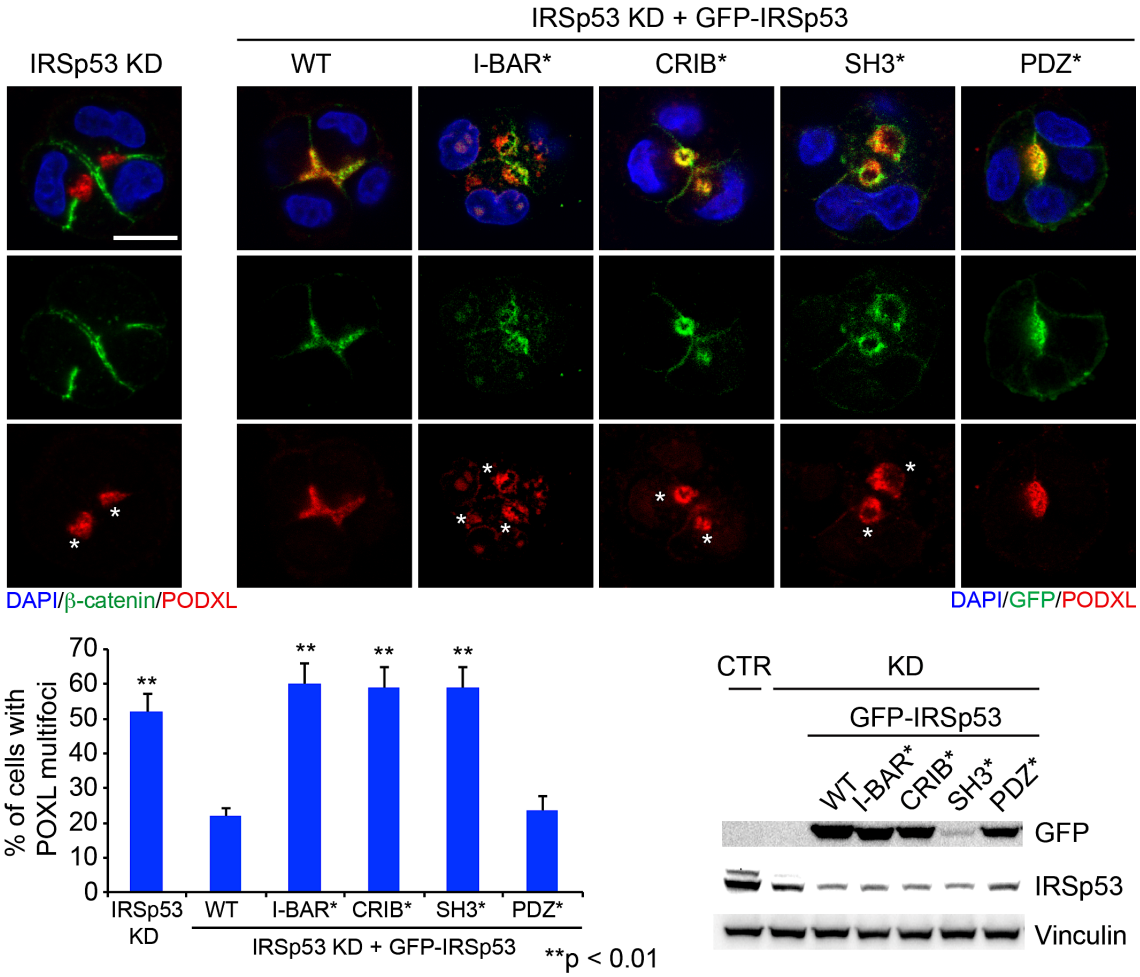

Fig. 1.12: I-BAR, CRIB and SH3 domains are all essential for proper polarization and lumenogenesis during spheroid formation

Confocal analysis of MDCK IRSp53 KD (siRNA) reconstituted with murine GFP-IRSp53 WT or mutants in different domains (as indicated). Single cells were plated on Matrigel to undergo cyst formation, fixed at 3-4 cell stages, processed for epifluorescence to visualize GFP-IRSp53 and stained with anti-Podocalyxin and DAPI. Scale bar = 10µm. *lower panels.* Histogram shows the percentage of cysts with a MAD phenotype. Data are mean ± S.D. The experiment was repeated at least 3 times. T-test, **p<0.01. Western blot of MDCK CTR or IRSp53 KD cells showing the levels of IRSp53 expression.

To get further insights into the molecular mechanisms and processes used by IRSp53 to regulate proper lumen formation, we repeated the structure-function analysis in Caco-2 cells as well. In this system, we focused on spheroid formation at later stages of lumen morphogenesis. To this end, we similarly expressed WT IRSp53

or its various mutant forms in IRSp53 KO Caco-2 cells and assessed their ability to rescue the multi-lumen phenotype caused by the depletion of the endogenous protein. Consistent with the results obtained in MDCK, we found that only WT IRSp53 and PDZ mutant forms fully rescued the defective multi-lumen phenotype in the IRSp53 depleted spheroids (Fig. 1.12b). These results show that the domains (I-BAR, SH3 and CRIB) which are essential to rescue the MAD phenotype are also required for the proper lumenogenesis of the spheroids. It also suggests the mechanism of action by IRSp53 underlying the process of polarisation at the early stages of cystogenesis is effectively the same at the later stages in the formation of a normal single lumen in the spheroids. We could further infer from these findings that one of the mechanisms by which IRSp53 depletion leads to the aberrant multi-lumen phenotype in mature spheroids is due to the development of a MAD phenotype at the early stages of polarisation. We will discuss this further in the discussions section.

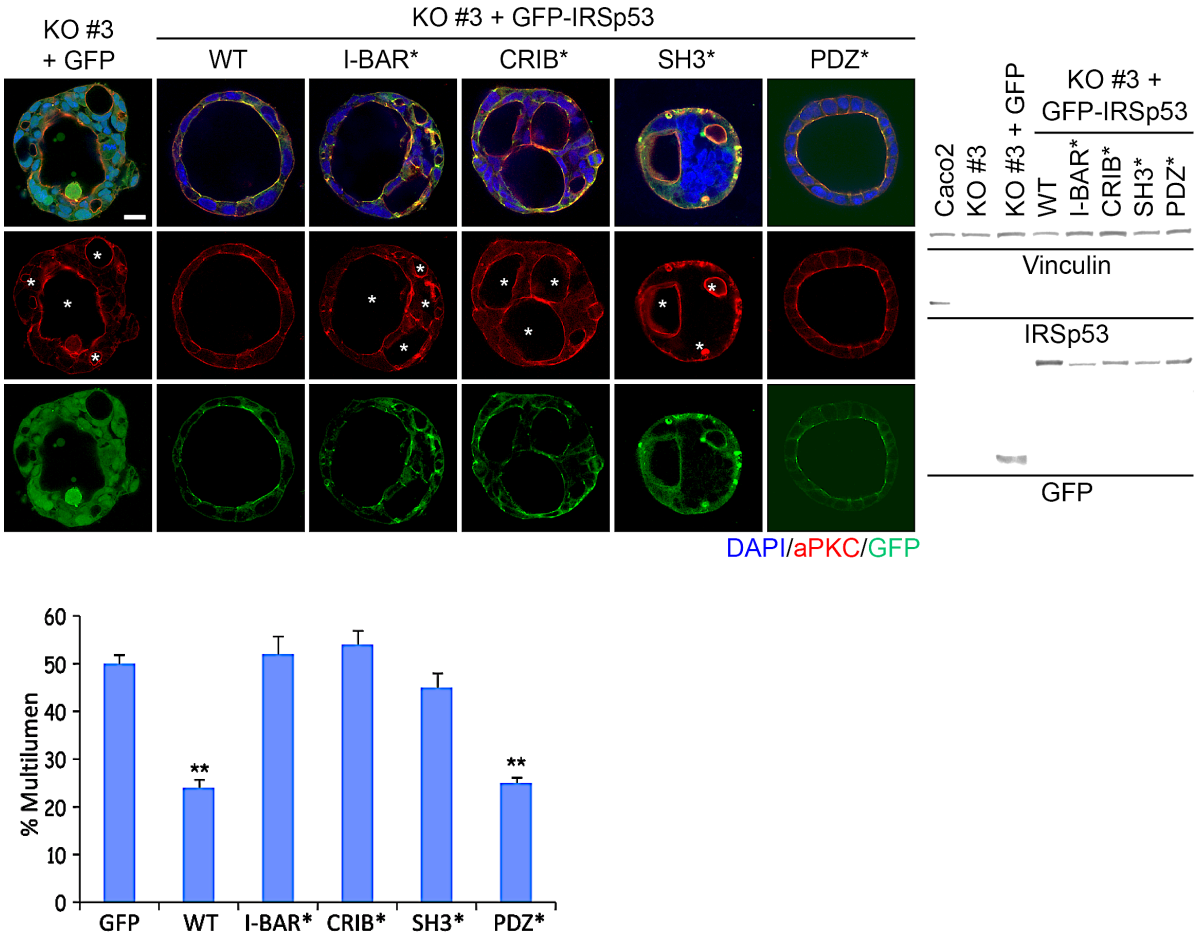

Fig. 1.12.1: I-BAR, CRIB & SH3 domains are all essential for proper polarization and lumenogenesis in 3-D spheroids

Caco-2 IRSp53 KO (#3) reconstituted with GFP tagged WT (Ctrl #2) or various mutants of IRSp53 in different domains were plated as single cells in Matrigel-collagen to undergo cyst formation. The cysts were fixed after 7 days, processed for epifluorescence to visualize GFP or GFP-IRSp53 and stained with anti-aPKC antibodies and DAPI. *Right*, western blot of the cells from the above experiment, with anti-vinculin, anti-IRSp53 for endogenous and anti-GFP antibodies for the ectopically expressed proteins in Caco-2 and IRSp53 KO Caco-2 (#3). *Lower panel*, histogram shows the percentage of cysts with a multi-lumen phenotype from the above experiment. The experiment was repeated at least 3 times. Data are mean ± S.D. T-test, **p<0.01.

Part 2: IRSp53 is involved in the proper orientation of mitotic spindle during cystogenesis

2.1) IRSp53 is enriched at the spindle poles both in 2-D monolayers and 3-D spheroids during cell division and is required for the correct orientation of the mitotic spindle during cystogenesis

From the part one of our results we obtained clues indicating that the multi-lumen phenotype in epithelial cysts results from the MAD phenotype due to the perturbation of trafficking machinery carrying the apical proteins to form the AMIS. These results however do not account for the complete picture of the mechanisms involved. An earlier study by Jaffe, et al. 2008 [82] found CDC42 depletion in Caco-2 resulted in a similar multi-lumen phenotype due to the perturbation of mitotic spindle orientation during cystogenesis. Since, IRSp53 is one of the effectors of CDC42 in regulating cytoskeleton dynamics in the cell [116], we asked if IRSp53 is also involved in the mechanism of proper spindle orientation in the mitotic cells undergoing cystogenesis.

First of all, we examined the cellular distribution of IRSp53 in further details. We found that IRSp53 also localizes at the spindle poles during mitosis in Caco-2 cells, both in monolayers as well as in 3D-cysts (Fig. 2.1). Co-staining of GFP-IRSp53 in Caco-2 cysts with the spindle marker, β-tubulin revealed a clear localization of this protein at the spindle poles (Fig.2.1). The correct orientation of the spindle has been shown to play an important role in the establishment and maintenance of polarity. This requires that dividing cells must keep a near perpendicular orientation of their mitotic spindle with respect to the centre of the cyst [82]. The study by Jaffe et al. described a method to measure the angle formed between the centre of the cyst and the spindle poles in the dividing cells. Importantly, in the same study it was reported that depletion of CDC42, a prominent interactor of IRSp53, caused a robust mis-orientation of spindle

pole angle of cell division, ultimately resulting in the formation of multiple luminal cysts (Fig 2.1).

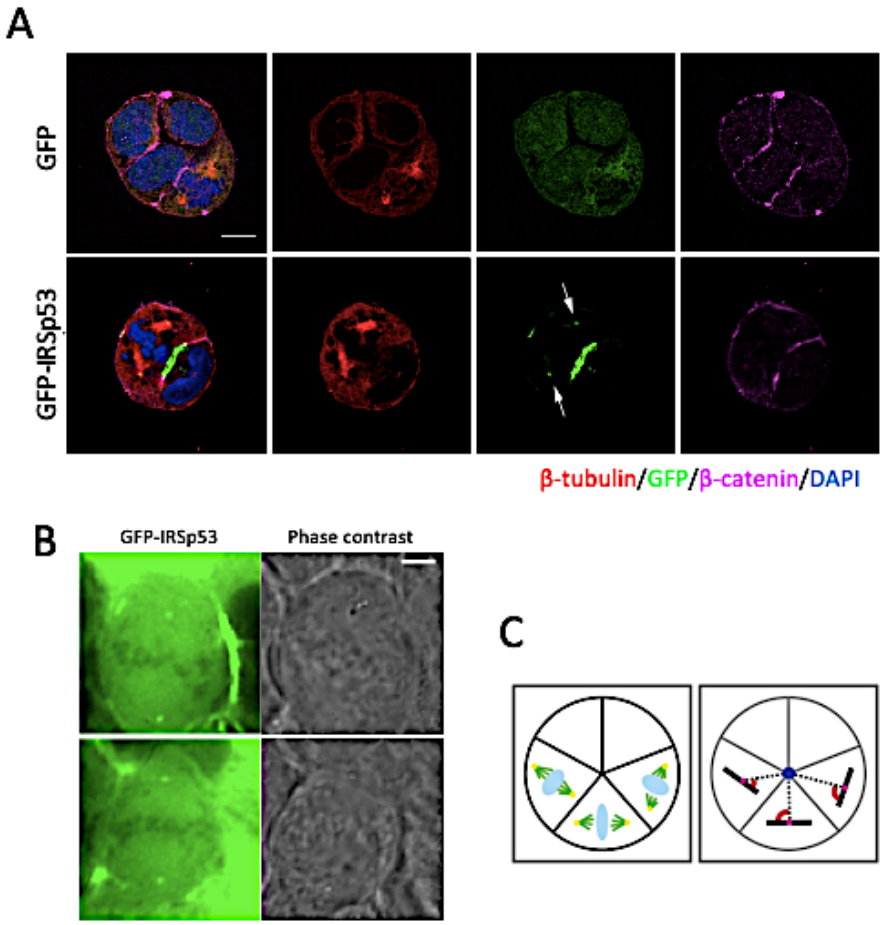

Fig. 2.1: IRSp53 is enriched at the spindle poles both in 2-D monolayers and 3-D spheroids during cell division

A) IRSp53 KO Caco-2 cells expressing GFP or IRSp53 GFP were plated as single cells in Matrigel-collagen matrix and let to undergo cystogenesis. The cysts were treated with mitotic inhibitor RO-3306 to arrest the cells in their mitotic stage (see Methods section for details). The cysts were fixed, processed for epifluorescence to visualize GFP or GFP-IRSp53 and stained with DAPI, anti-β-Tubulin and anti-β-catenin antibodies. Confocal images of a middle plane of the dividing cells were taken. Scale bar = 20μm

B) HaCat cells infected with GFP-IRSp53 in a normal 2-D culture and imaged live using DELTA vision™ microscope. The images are a screen shots of time-lapse movie frames. Scale bar = 20 μm

C) Cartoon depicting the orientation of spindle poles with respect to the centre of the cysts. Schematic of the method to measure the mitotic spindle angle is also depicted (modified from Jaffe, et al, 2008).

These results were quite unexpected and novel as there are no reports of IRSp53 localization in the spindle poles. This prompted us to further investigate the role of IRSp53 in the proper orientation of cell divisions during spheroid formation. We therefore asked whether IRSp53 might have any role in controlling the proper orientation of the mitotic spindle during the cyst formation. To this end, we measured the angle formed by mitotic spindle with respect to the centre of the cysts in control and IRSp53 depleted Caco-2 cysts. As expected, in control cysts the spindle oriented with respect to the centre of the cysts at an angle that was nearly close to 90^{o}. Conversely, loss of IRSp53 caused a significant mis-orientation of the spindle angle (Fig. 2.1.1). To check the specificity of this phenotype due to IRSp53 depletion, we took advantage of our IRSp53 KO Caco-2 cells expressing either GFP as a control or GFP-IRSp53 for the rescue. GFP-IRSp53 expression in the KO cysts completely rescued the defects in the spindle orientation (Fig.2.1.1), thus confirming the specificity of IRSp53 in this process as well. These results suggest that, in addition to control the trafficking of the apical proteins to a single apical focal point, IRSp53 is required to properly orient the mitotic cell divisions during spheroid formation. Thus, IRSp53 may play a central role by co-ordinating these two distinct mechanisms for the establishment of polarity and lumenogenesis during spheroid formation.

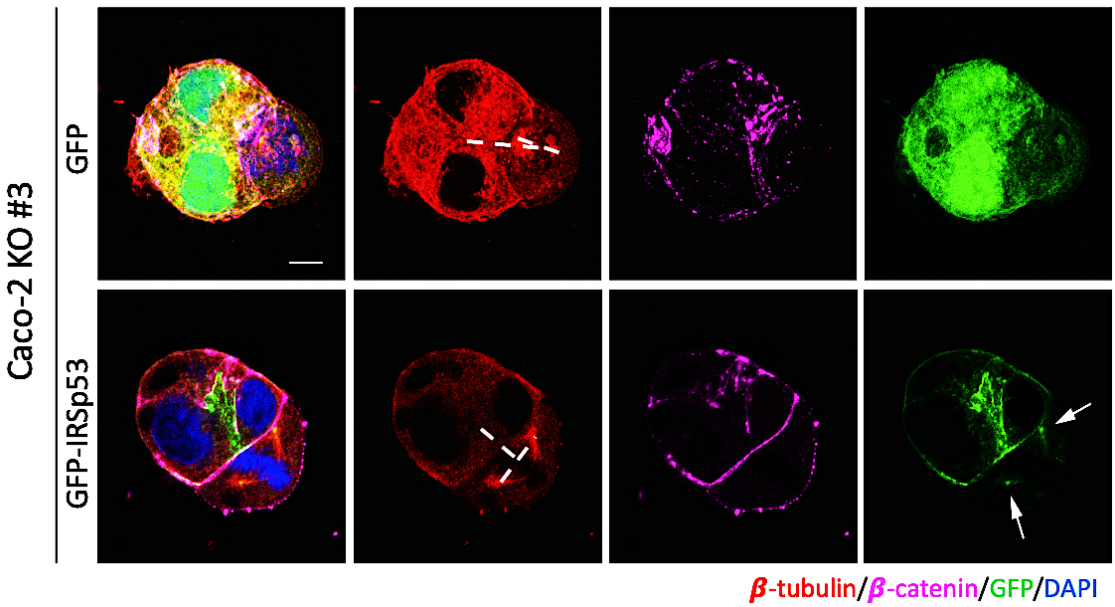

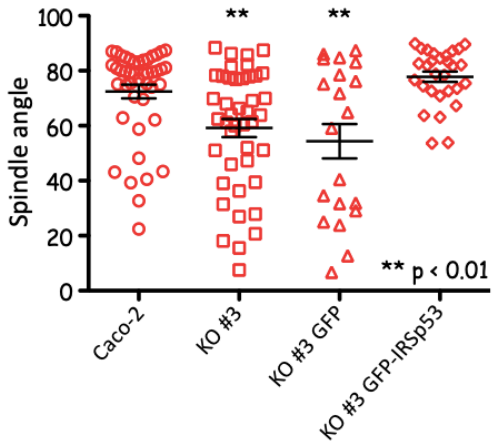

Fig. 2.1.1: IRSp53 is required for correct orientation of the mitotic spindle during cystogenesis
Caco-2 control (Caco-2) or IRSp53 KO (#3) (KO #3) (not shown) or IRSp53 KO (#3) infected with GFP (KO #3 GFP) or GFP-IRSp53 (KO #3 GFP-IRSp53) were plated as single cells in in Matrigel-collagen matrix and let to undergo cystogenesis. The cysts were treated with RO-3306 to arrest the dividing cells in mitosis. The cysts were fixed, processed for epifluorescence to visualize GFP or GFP-IRSp53 and stained with anti-β-tubulin and anti-β-catenin. Confocal images of the cysts were taken in the centre of the plane of mitotic cells. The angle of mitotic spindle axis with respect to the centre of the cysts was measured for these cells, across the different conditions. The graph shows the measure of the spindle angle obtained across different conditions. Data are mean ± S.D. T-test, **p<0.01. Scale bar = 10μm

2.2) I-Bar domain of IRSp53 is required for the localization at the spindle poles, but it is not sufficient for the proper orientation of the spindle

The atypical localization of IRSp53 at the mitotic spindle poles and its role in the proper orientation of cell divisions during cystogenesis, prompted us to further investigate the mechanism of this interaction. To answer this question, we took advantage of our GFP tagged IRSp53 constructs containing mutations in its critical domains (see section 1.12). We expressed these constructs in IRSp53 KO cells and let these cells undergo spheroid formation in 3-D matrices. We analysed these spheroids using confocal microscope and looked for the effect of these mutations on the localization of IRSp53 in the cells undergoing mitosis. The striking observation during this experiment came to light when we found that only GFP-IRSp53 I-BAR* mutant did not localize anymore at the spindle poles but was diffused all over the cytoplasm (Fig.2.2). This indicates that the localisation of IRSp53 at the spindle poles is mediated through its I-BAR domain. Thus, we wanted to study this in further details to understand if I-BAR domain was sufficient for the colocalization of IRSp53 at the spindle poles. To verify this possibility, we expressed the isolated I-BAR domain of IRSp53 tagged with GFP (or GFP alone as a control) in our KO Caco-2 cells and studied its localization during spheroid formation in mitotic cells. We found that the isolated I-BAR domain clearly localized at the spindle poles during mitosis. These results confirmed that the interaction of IRSP53 at the spindle poles is mediated through I-BAR domain and that this domain is sufficient for this interaction (Fig 2.2).

Another question that arises from these observations is whether I-BAR domain is sufficient to properly align the spindle poles in the dividing cells during cystogenesis. To address this question, we measured the angle of spindle axis in the IRSp53 depleted cysts, expressing either GFP or GFP I-BAR domain. However, the expression of isolated I-BAR domain of IRSp53 failed in rescuing the spindle pole

orientation defects. These results indicate that although the I-Bar domain of IRSp53 is sufficient to drive IRSp53 localization at the mitotic spindle, it is not sufficient to maintain the proper orientation of the spindle poles during mitosis. Although, the I-BAR domain aids IRSp53 in binding and localizing at the spindle poles, the other domains, including CRIB and SH3, may critically contribute to the functioning of this protein in this context as well. These domains may very likely be mediating interactions with other proteins or the assembly of yet to be defined protein complexes to properly orient the spindle poles during the cell divisions for normal polarization and lumenogenesis. To confirm the role of these domains in the process of polarisation through spindle pole orientation, we did a structure function analysis of IRSp53 in this context as well, which is further discussed below.

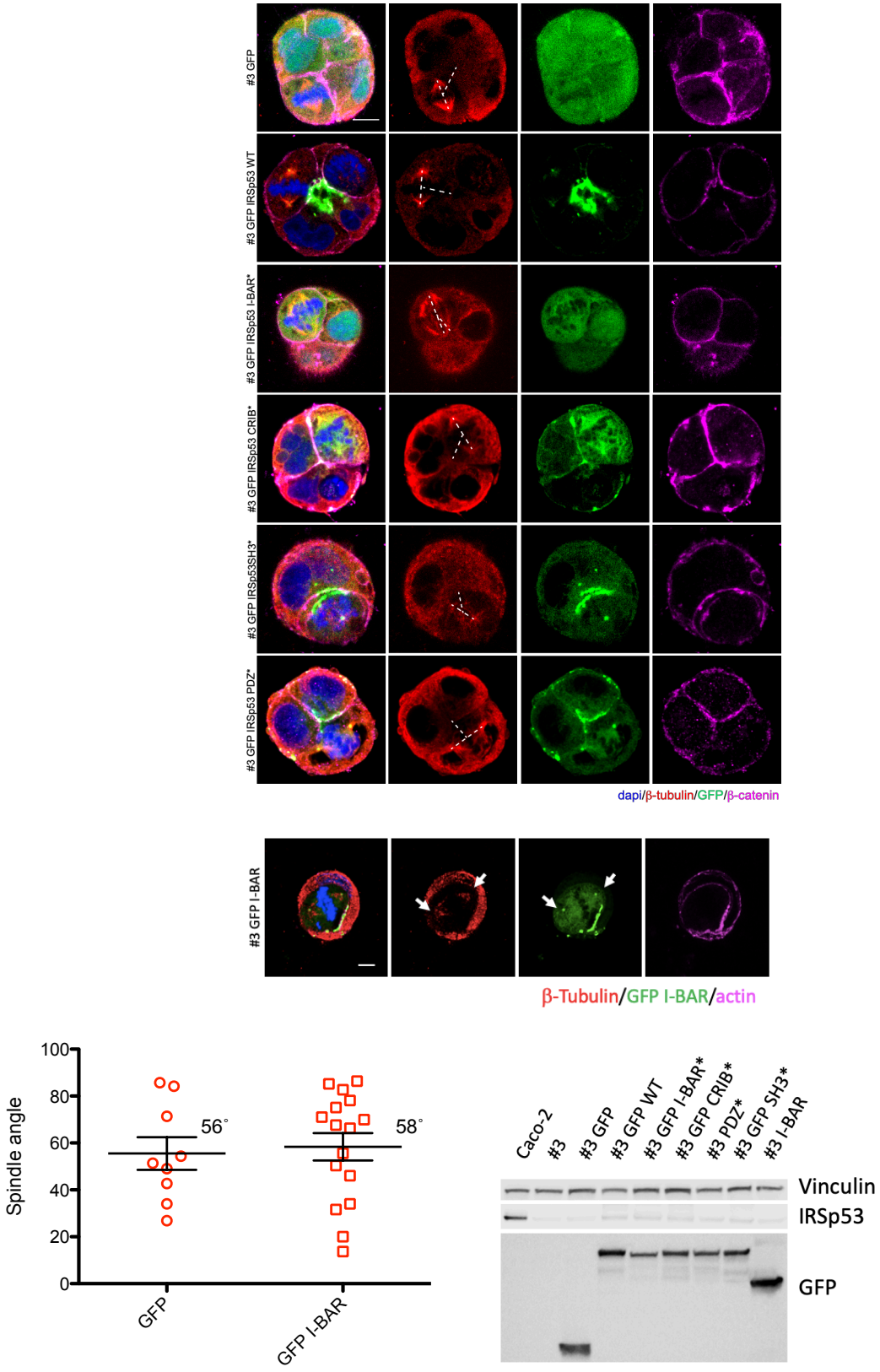

Fig. 2.2: I-Bar domain of IRSp53 is required for the localization at the spindle poles, but it is not sufficient for the proper orientation of the spindle

Caco-2 IRSp53 KO #3 cells reconstituted either with GFP, GFP-IRSp53 WT or its mutant versions (as indicated) were embedded in the matrix for cystogenesis and treated with RO-3306 to arrest the dividing cells in their mitotic phase. The cysts were fixed, processed for epifluorescence to visualize GFP or

GFP-IRSp53 and stained for nuclei (Blue), β-Tubulin (Red), β-catenin/actin (Magenta). The co-localisation of the GFP signal at the spindle poles was analysed using confocal imaging. Bottom panels. Caco-2 IRSp53 KO #3 expressing GFP-I-BAR domain were processed as described above. Localization of recombinant GFP-I-BAR domain the spindle poles is indicated by arrows. Scale Bar = 20μm.
Lower panels. Left, the graph shows the measure of the spindle angle in IRSp53 KO #3 reconstituted with either GFP or GFP-I-BAR only. *Right*, western blot shows the expression of IRSp53 in WT, IRSp53 KO #3 or #3 reconstituted with different versions of IRSp53 (as indicated).

2.3) I-BAR, CRIB & SH3 domains are all required to rescue the mis-orientation of spindle poles in IRSp53 depleted cysts

As discussed previously, CDC42 has been shown to play an important role in the proper alignment of spindle poles during mitosis in Caco-2 spheroids [82]. Since IRSp53 consists of a CDC42 binding CRIB domain [116] we wanted to understand if this domain along with the other critical domain SH3, contributes to the proper orientation of spindle poles in the spheroids. This could provide us with some important molecular cues regarding the mechanism of action of IRSp53 in controlling the spindle pole orientation. Thus, we performed a structure function analysis of IRSp53 in this context as well. For these experiments, we took advantage of our previous experiment in which we expressed different mutant forms of IRSp53 in the KO Caco-2 cells (Section 2.2). We let these cells undergo spheroid formation in a 3-D matrix and analysed, using a confocal microscope, the rescue in the spindle orientation (Fig.2.3). Notably, only WT and PDZ binding mutant IRSp53 could rescue the phenotype, while as, I-BAR, CRIB and SH3 mutants did not show any rescue (Fig.2.3). The results confirmed that the integrity of I-BAR, CRIB and SH3 domains is critical for the proper orientation of the mitotic spindle (Fig. 2.3). We will further discuss the possible role these domains may play in this context during the discussions section.

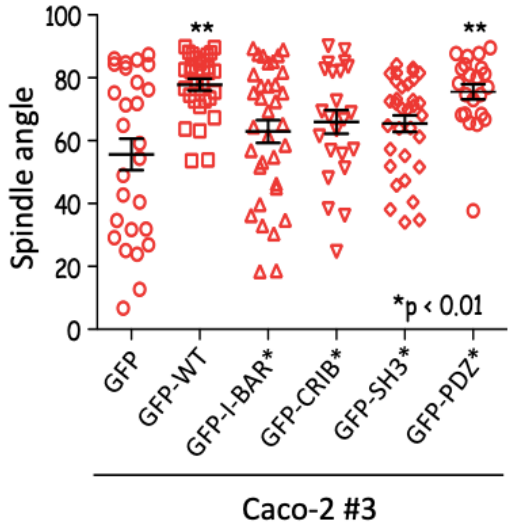

Fig. 2.3: I-BAR, CRIB & SH3 domains are all required to rescue the mis-orientation of the spindle poles in IRSp53 depleted spheroids

IRSp53 KO Caco-2 cells expressing GFP or IRSp53 GFP either WT or its different mutant forms (as indicated) were plated as single cells in Matrigel-collagen matrix and let to undergo cystogenesis. The cysts were treated with mitotic inhibitor RO-3306 to arrest the cells in the mitosis. The cysts were fixed and stained with DAPI, anti-β-Tubulin and anti-β-catenin antibodies. Confocal images of a plane in the middle of the dividing cells was taken (Fig. 2.2) and the spindle angle was calculated for each of the condition. At least 30 cysts were calculated in three independent experiments.

Quantification of the spindle angle in the different condition analysed. Data are mean ± S.D. T-test, **p<0.01

Part 3: Role of IRSp53 in proper tissue morphogenesis in vivo

3.1) IRSp53 is required for the proper tissue morphogenesis of zebrafish pronephric ducts during development

In the previous two parts of the results, we demonstrated that IRSp53 is important in the establishment of polarity and lumenogenesis during the development of 3-D spheroids. Since, these processes are also critically important in the development and functioning of various tissues in the animals, we investigated the physiological consequences of IRSp53 depletion *in vivo*.

We were particularly interested in analysing the phenotypes in the tissues where polarization and lumenogenesis are critical to execute their function during development and morphogenesis. Thus, we focused our attention on the epithelial tissues in our *in vivo* zebrafish models and specifically on the development of nephrotic organs. Indeed, the fish pronephric ducts which mark the early development of kidneys in zebrafish, display a localization of IRSp53 (B2a and B2b in zebrafish) restricted to the apical side of their lumen (Section 1.2). Relevantly, gene duplication in zebrafish has led to the formation of two distinct, but highly related IRSp53 paralogues named BAIAP2a (B2a) and BAIAP2b (B2b). Therefore, to assess the impact of a complete loss of function of IRSp53, both the genes have to be mutated. We also used morpholinos to target specifically B2a and B2b in zebrafish. This strategy allowed us to deplete either B2a and B2b in the WT background or B2b in the B2a$^{-/-}$ background.

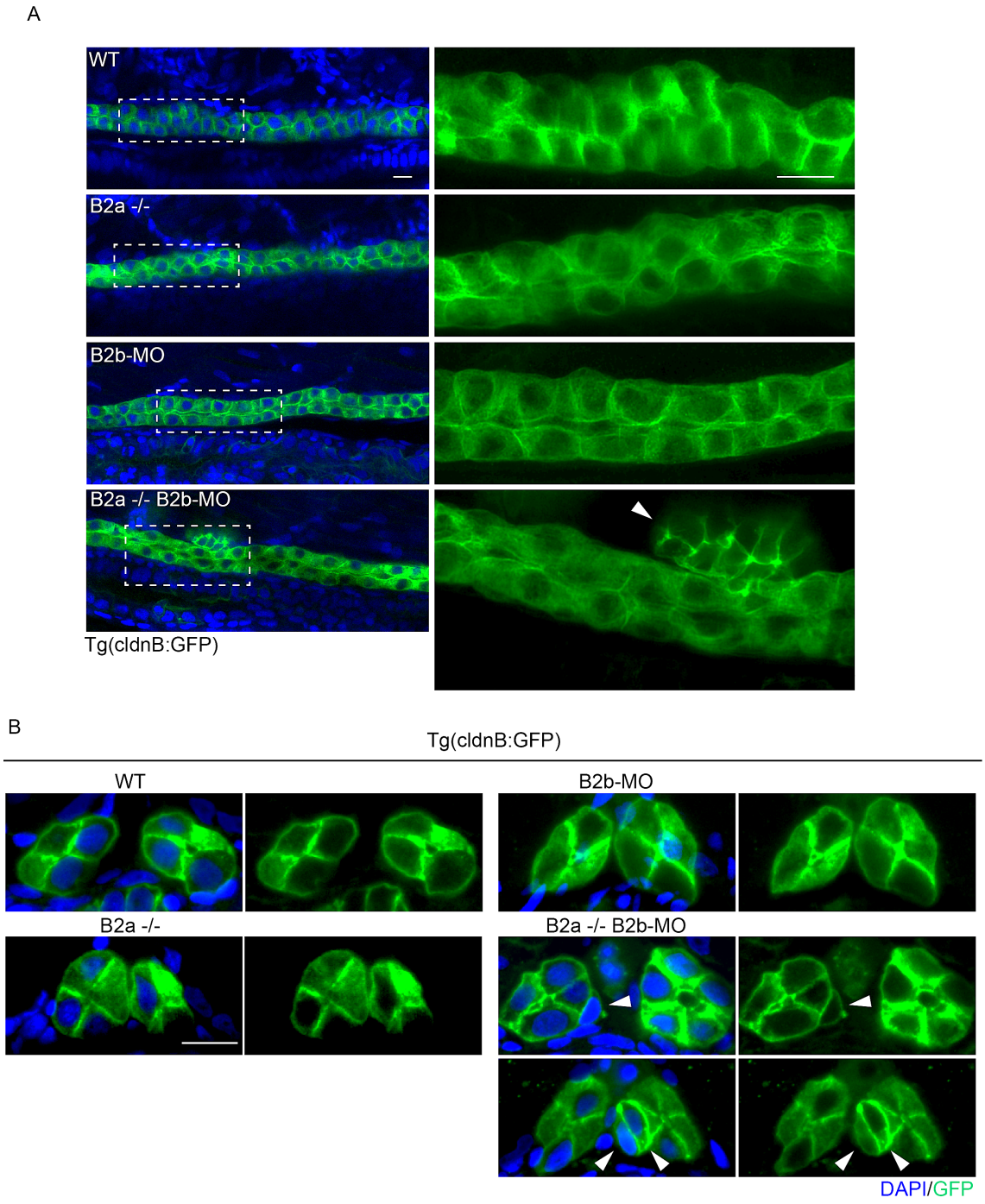

Fig. 3.1: IRSp53 is required for the proper morphogenesis of zebrafish pronephric ducts during development

Tg(CldnB:GFP) embryos, expressing GFP in their pronephric ducts, WT and B2a null, uninjected or injected with B2b Morpholinos were fixed at 4-dpf, stained with DAPI and anti-GFP antibodies. The embryos were mounted in agarose and imaged with an SP8 confocal microscope. Z-Stacks along the pronephric ducts were collected. The stacks were then merged into maximum projection images. The pronephric ducts of the B2a+B2b depleted embryos show ectopic structures as indicated by the arrows. Scale bar = 10µm.

Some of the embryos were sectioned before staining and the images of the cross-sectional area of the pronephric ducts were collected (as shown in the lower panel). The B2a+B2b depleted embryos show aberrant structures marked by delocalized CldnB:GFP signal outside the ducts. Scale bars = 10 μm

To analyse in more details the morphogenesis of the embryonic pro-nephric duct in our B2a and B2b KO/KD zebrafish models (Fig 1.2), we generated a B2a$^{-/-}$ line in Tg(CldnB:GFP) background. Tg(CldnB:GFP) is expressed in pro-nephric ducts where it specifically labels each of the epithelial-like cells forming these structures [149, 150] thus, making it easier to analyse any phenotype associated with IRSp53 depletion in this background, using a confocal microscope. We observed that upon the individual depletion of either B2a using morpholino or in the B2a$^{-/-}$ mutant embryos, the pronephric ducts developed normally until 4 days post fertilization (dpf) (Fig.3.1). Similarly the depletion of B2b by injecting a mix of B2b translation blocking and splice blocking morpholinos in freshly fertilized, WT Tg(CldnB:GFP) embryos, did not result in any observable phenotype in the pronephric ducts of these embryos until 4dpf. Conversely, when we simultaneously depleted B2a and B2b by morpholinos injections in the B2a$^{-/-}$ Tg(CldnB:GFP) background embryos, we observed aberrant ectopic structures forming on their pronephric ducts at 4dpf, which caused a disruption of the overall morphology of these pronephric ducts (Fig. 3.1 A). Remarkably, this phenotype resembles the aberrant multi-lumen phenotype that we observed following depletion of IRSp53 in mammalian epithelial spheroids (Fig. 3.1 B), suggesting that the aberrant development and morphogenesis of epithelial pronephric tissues in B2a+B2b depleted embryos might be caused by a perturbation of the polarity program.

3.2) B2a KO in zebrafish causes morphological defects in the adult kidneys

The alteration in the zebrafish pronephric ducts prompted us to have a closer look also at the morphology of the adult kidneys in our B2a null zebrafish models. During development, the expression of B2b in B2a-mutant animals might be sufficient to ensure the renal morphogenetic program. In adult animals, however, the sole deletion of B2a might be sufficient to cause alteration in the organization of fully functional tissue. To test this possibility, we fixed WT and B2a null adult zebrafish overnight in 4% PFA and embedded them in paraffin, after decalcifying them for 36 hours, for sectioning. Histological analysis of these sections revealed a set of severe morphological defects in the kidneys of B2a null adult zebrafish. The kidneys in these animals displayed areas of partial degeneration with a lot of infiltrating cells, the nature of which remains to be determined, covering most of these degenerated areas.
Additionally, the arrangement of epithelial cells that typically surround and enclose the distal tubules is not very uniform as in the WT kidneys and, frequently, the tubules in the mutant kidneys appear to be closed at their ends lacking a pervious lumen.

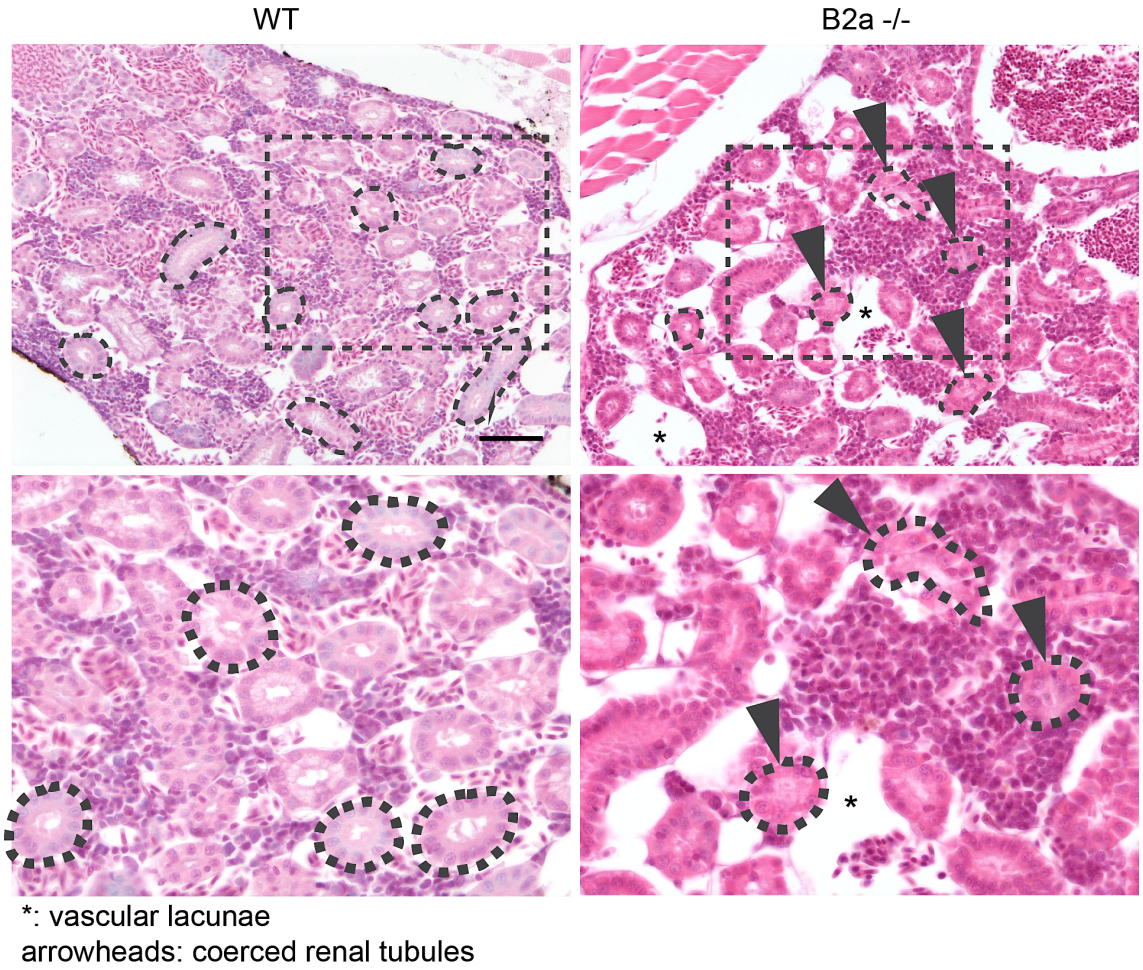

Fig. 3.2: BAIAP2a KO in zebrafish causes defects in the morphology of adult kidneys

Adult zebrafish either WT or B2a null were fixed, decalcified and embedded in paraffin for sectioning. The sections were stained with H&E to study the morphology of the kidneys. The lower images are the 2X zoomed in view of the boxed areas in the upper images. Some of the tubules are highlighted with the contours. The arrow heads indicate coerced renal tubules and the asterisks mark the vascular lacunae in the B2a null kidneys Scale bar = 100μm

3.3) IRSp53 KO in mice causes various defects in the adult kidneys

To understand the relevance of IRSp53 in the morphogenesis of epithelial tissues *in vivo*, in the mammalian models, we analysed our IRSp53 KO mice for any defects in their epithelial tissues.

Notably, IRSp53 KO mice show a partially penetrant mid-gestation lethality of about 80% from E11.5 – E14.5. The remaining 20%, however, develop normally without any obvious gross morphological phenotypes. The phenotypes detected in B2a$^{-/-}$ zebrafish promoted us to revisit in more detail the structural organization of murine kidney in IRSp53 null animals. We found that adult IRSp53 KO mice displayed many histological aberrations in their kidneys (Fig. 3.3). The overall morphology of the IRSp53 KO kidneys appeared to be defective in some areas. Detailed analysis of these areas revealed uneven distribution of epithelial cells in the tubules similar to the one detected in the kidney of adult B2a$^{-/-}$ zebrafish. As discussed previously, this may be an indication of the loss of polarity in these cells. We also found, the presence of coerced tubules and coerced glomeruli in the KO kidneys. Moreover, the vasculature of these kidneys seems to be perturbed in some areas, characterized by the presence of vascular dilations and large lacunae. All these defects indicate alteration of polarity as the underlying cause. Therefore, we performed IHC analysis using a number of polarity markers, including ZO-1 and aPKC which are apical markers, acetylated tubulin which marks the cilia on the apical membrane and endomucin, used as a basal marker. Remarkably, while ZO-1 demarked clearly the apical membrane of tubular lumina in kidney from WT control animal, it was absent or decreased in most of the tubules of kidneys from IRSp53 KO mice. Similarly, the endomucin in the WT kidneys decorated the basal side of the tubules uniformly in a continuous manner, while this pattern was completely lost in the kidneys of IRSp53 KO mice with discontinuous and intermittent staining of the tubules. Acetylated tubulin was mostly absent from the apical membrane

of the renal tubules in IRSp53 KO mice, revealing a drastic reduction in the presence of cilia in the lumen of the renal tubules of IRSp53 KO mice. These results indicate that the morphological and histological defects seen in the KO kidneys is due to the loss of polarity in these tissues (fig. 3.3.1).

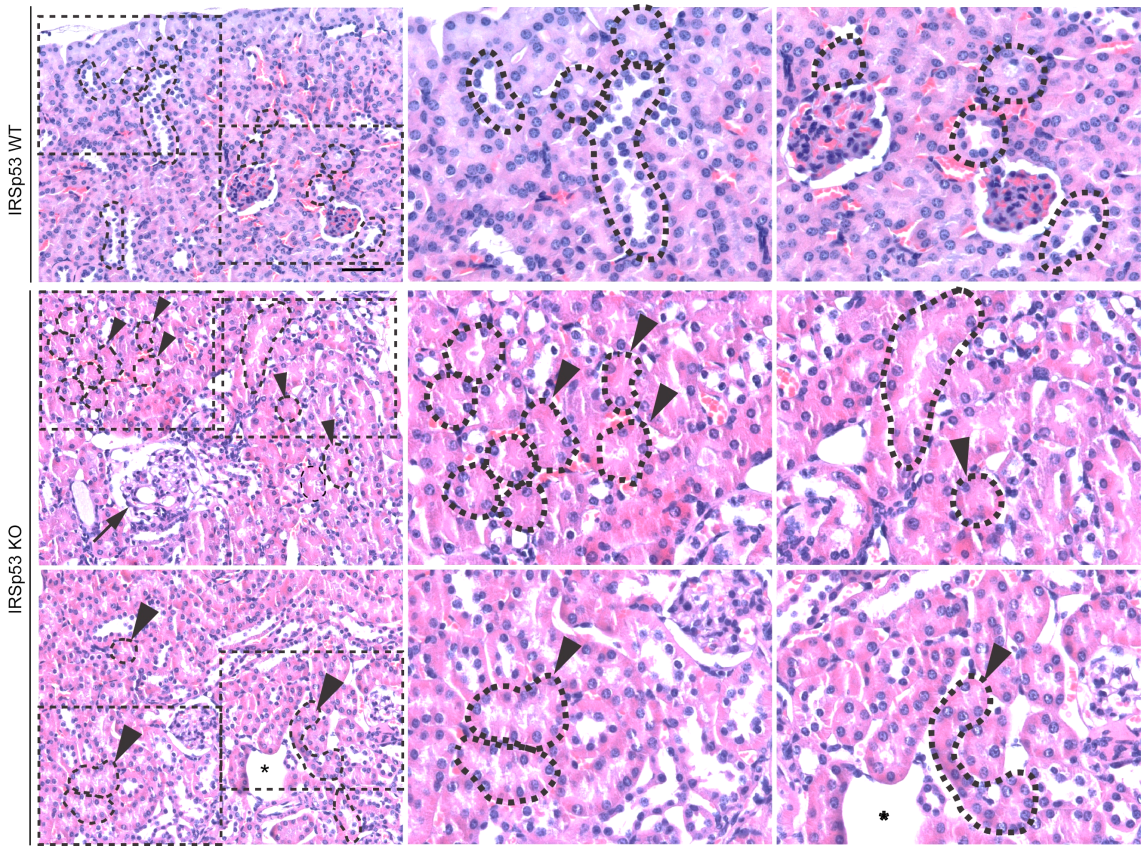

Fig. 3.3: IRSp53 KO in adult mice causes morphological defects in their kidneys

Kidneys were harvested from WT or IRSp53 KO adult mice, fixed and embedded in paraffin for sectioning. The sections were stained with H&E to study the morphology of the renal tissues. Images on the right are the 2X zoomed in view of the boxed areas in the corresponding image on the extreme left. Contours are drawn around some of the tubules to highlight them. The arrows indicate the microcystic alterations of the glomeruli in the IRSp53 KO kidneys, while as, arrow heads indicate coerced renal tubules and the asterisks indicate the vascular lacunae. Scale bar = 200μm

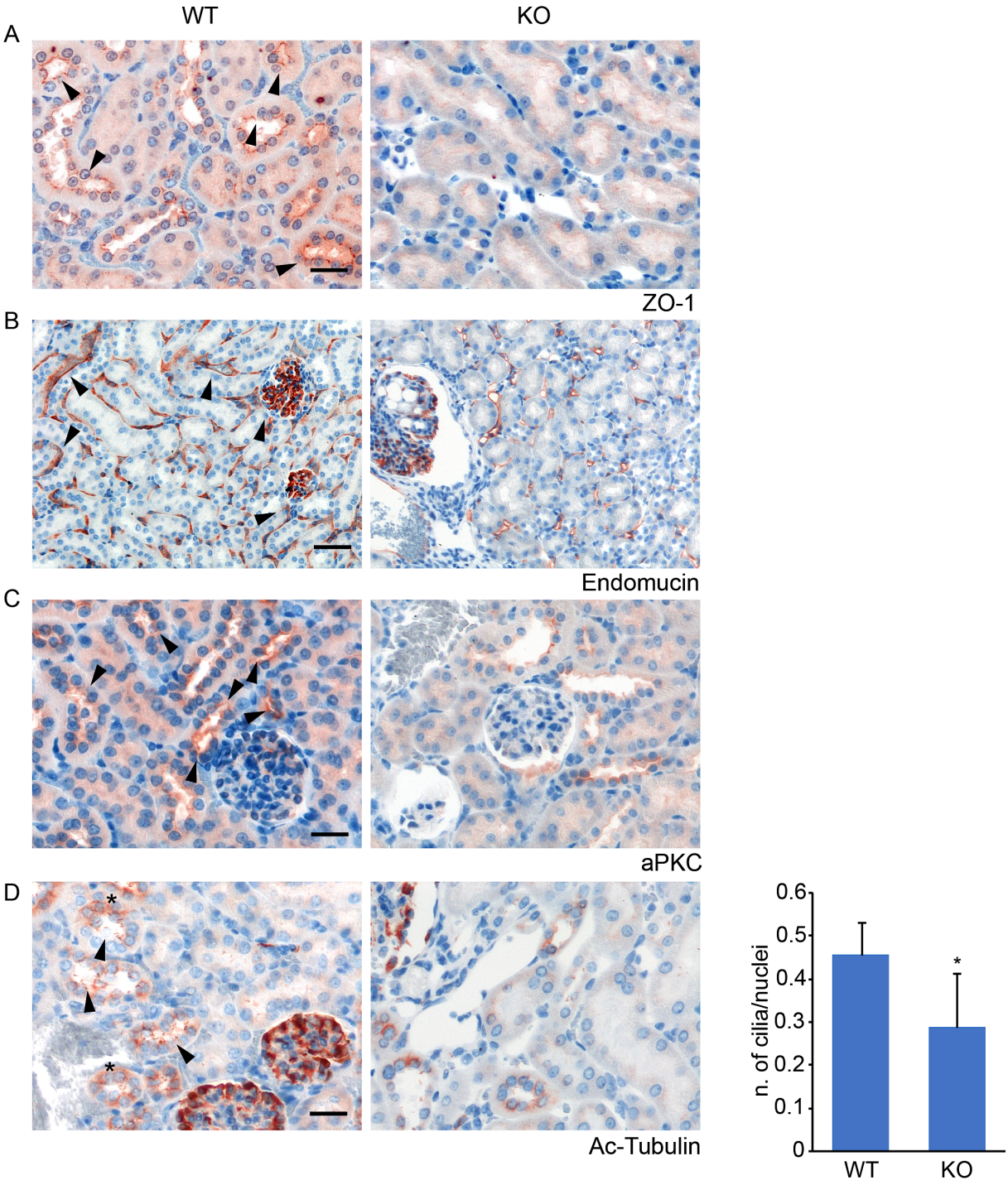

Fig. 3.3.1: IRSp53 depletion leads to the perturbation of apico-basal polarity in the kidneys of adult mice

Immunohistochemistry images of WT and IRSp53 KO mouse kidneys for ZO-1 (A), Endomucin (B), aPKC (C) and Acetylated Tubulin (D) show an overall reduction in the staining of these polarity markers in IRSp53 KO mice as compared to the WT. Endomucin staining shows a disrupted labelling pattern on the basal side of the renal tubules, whereas, Acetylated tubulin staining reveals reduction of the cilia inside the lumina of renal tubules in IRSp53 KO mice; Quantification of the same is shown in the graph on the right. Data are mean ± S.D. T-test *<0.05 Scale bar = 100μm

Conclusion and Discussions

This study provides a set of evidence in support of a critical role played by IRSp53 in the establishment of polarity and proper lumen formation during epithelial cystogenesis *in vitro* and of its physiological implications *in vivo* in the morphogenesis of murine and zebrafish kidneys.

We found that IRSp53 acts at the intersection of different molecular pathways involved in the trafficking of apical proteins to form a single AMIS, and also in the proper orientation of mitotic spindle poles during cystogenesis. Formation of a unifocal AMIS and a near perpendicular orientation of the mitotic spindle with respect to the centre of the cyst are vital for the proper polarisation and lumen morphogenesis in the epithelial spheroids [60] [82]. Thus, by controlling both these critical processes, IRSp53 can be regarded as a central player in orchestrating the overall polarity processes in epithelial spheroids. Consistently, the depletion of IRSp53 leads to the aberrant polarisation and multi-lumen formation in the epithelial cysts *in vitro* by perturbation of these processes. Furthermore, physiologically, IRSp53 depletion in whole organisms, from mice to fish, leads to severe morphological defects in their kidneys. While we have not been able to provide a direct demonstration that the latter alterations are due to the disruption of the IRSp53-RAB35 trafficking route and spindle orientation defects detected in organoids *in vitro*, we noticed that in both organisms, kidney dysmorphology and renal tubule defects are linked to altered polarity, reinforcing the notion that IRSp53 is a novel polarity determinant.

In keeping with this tenet, Immunohistochemistry (IHC) of human and mouse epithelial-glandular tissues revealed IRSp53 localisation specifically restricted to the apical side of their luminal membrane (Fig. 1.1). Similar localisation of IRSp53 paralogues was observed at the luminal side of the pronephric ducts in zebrafish

embryos during development (Fig.1.2.2). The asymmetric distribution of the canonical polarity determinants helps in the establishment and maintenance of overall polarity, and thus for the proper morphogenesis of epithelial tissues [12, 60]. This peculiar tissue distribution of IRSp53 across various luminal epithelia in different organisms, henceforth, further corroborates its possible role in the process of polarization. These findings and observations extend and are totally consistent with a set of scattered and previously reported indirect evidences obtained in epithelial MDCK cell culture systems [26]. In these systems, the removal of the IRSp53 was shown to impair the proper apical lumen formation [145], albeit neither the general relevance of this finding in physiological context nor the underlying molecular mechanisms of IRSp53 action have been explored.

We also found that in Caco-2 and MDCK derived epithelial spheroids, IRSp53 localises specifically at the apical side of the lumen along with other apical markers, including F-actin, aPKC or PDX. These spheroids undergo a process of polarisation and lumen formation when plated on pliable substrate and are bathed in Matrigel-containing media *in vitro,* thereby recapitulating the process of polarisation and lumenogenesis that epithelial tissues undergo *in vivo* during development and organogenesis. The majority of the cysts devoid of IRSp53 develop an aberrant multi-lumen phenotype (Fig.1.4.1), which is completely rescued upon ectopic expression of GFP-IRSp53. Since, normal lumenogenesis follows a proper polarity establishment program [60], the depletion of IRSp53 from the apical membrane in these cysts may likely cause a disruption of this process, resulting in aberrant lumenogenesis. If that were indeed the case, the question that arises is how does IRSp53 contribute to the establishment of a normal polarity process.

The polarity program in MDCK and Caco-2 spheroids follow a step-wise process which is hard wired and can be easily monitored by tracking various apical markers.

Notably, IRSp53 along with the other canonical apical proteins, such as PDX, localizes isotropically to the peripheral surface of single cells. At the first cell division, which acts as a symmetry breaking event in these cells, IRSp53 together with the other pioneering apical determinants is re-localised to the intervening membrane between the two daughter cells. The re-localisation of additional apical proteins to this membrane is subsequently required for the specification of AMIS, which is the site of *de novo* lumen formation [60].

We analysed this process in our systems in order to get clues as to the involvement of IRSp53 in the specification of this early apical domain. We observed that IRSp53 depletion leads to the formation of multi-focal AMIS-like apical domains (MAD) phenotype in these cysts, which is completely reversed upon complementation with GFP-IRSp53 (Fig. 1.7) Formation of a proper AMIS is critical for the normal lumenogenesis. AMIS is thought to eventually give rise to a Pre-Apical Patch (PAP) between the cells where the opposing cell membranes start drifting apart from each other, initiating the formation of intercellular lumen. The luminal space starts expanding, at least initially, due to a repulsive force between the negatively charged glycosylated proteins, like PDX, on the opposite membranes in case of MDCK cysts or due to the accumulation of ions, which create a negative osmotic pressure, in case of Caco-2 cysts. These events are thought to be the initial trigger for the formation of a fluid filled lumen [60, 82].

During the normal polarisation process, a single apical domain is specified at the centre of the developing cyst by the proper alignment of the apico-basal axes of all the constituent cells. This is achieved by a tight co-ordination of the polarity determinants to ensure the formation of a cyst with a single central lumen. This suggests that the MAD phenotype observed in IRSp53 depleted cysts is likely due to the perturbation of the co-ordinated polarity program, which leads to the formation of multiple apical

domains at the early stages of cystogenesis. These multiple apical domains then independently go on to form lumina, resulting in the multi-lumen phenotype. However, the mechanism by which IRSp53 contributes to the co-ordination of the polarity program between different cells of a cyst to form a single unifocal AMIS, remains unclear.

One of the mechanisms through which IRSp53 may co-ordinate the polarity program is by controlling the proper trafficking of the apical determinants to form a single unifocal AMIS. In our *in vitro* epithelial models, we observed that apart from localising to the earliest apical domain during cystogenesis, IRSp53 also impinges on the trafficking of vesicles containing actin, PDX and other apical markers towards the AMIS (Fig 1.6). These vesicles are trafficked through a CDC42 and RAB-GTPase dependent mechanism to the apical membrane to form a proper AMIS [60] [67]. Co-localization of GFP-IRSp53 with RAB7, RAB11a and RAB35 containing vesicles indicates that IRSp53 might be involved in the co-ordination of the apical trafficking machinery to specify a proper AMIS (Fig.1.8). We verified this latter contention, in part, in a set of independent experiments involving the role of IRSp53 in PDX trafficking to the Vacuolar Apical Compartment (VAC). VACs are transient apical domains formed in non-contacting single cells in 2D monolayers, induced by perturbing their cell-cell contacts via depletion of calcium [147]. VACs are known to contain many apical proteins that rapidly re-localize to the intercellular membranes upon re-establishing the cell-cell contacts [147]. This process is thought to be critical in the formation of proper apical membranes and the establishment of the polarity and thus, considered as a proxy for the formation of AMIS in 2-D cells and sometimes referred to as intracellular AMIS [147, 148]. IRSp53 KO cells, indeed, displayed a perturbed trafficking of PDX to the VAC, implying its role in the trafficking of proteins to the apical domains. Loss of

IRSp53 may thus, lead to interference with the normal trafficking mechanism of PDX, and potentially of the other apical determinants to AMIS, resulting in a MAD phenotype. Whether IRSp53 is directly involved in the co-ordination of the trafficking of other apical determinants to form a proper AMIS, remains to be determined.

To further understand the molecular mechanism by which IRSp53 regulates PDX trafficking to AMIS, we took a candidate-based approach. One potential candidate, RAB35 has recently been shown to interact directly with the PDX to facilitate its trafficking to the apical membrane [67, 68]. RAB35 depletion causes aberrant multi-lumen cyst formation, reversal of polarity and altered PDX distribution, similar to the defect caused by IRSp53 removal [67, 68]. RAB35 also co-localises with IRSp53, at PDX containing apical vesicles (Fig. 1.8). These observations in the context of our results suggest that IRSp53 and RAB35 may interact with each other to facilitate the normal trafficking of PDX to the AMIS. Co-immunoprecipitation studies in HeLa and HEK293 cells revealed that GFP-RAB35 and Flag-IRSp53 weakly, but reproducibly interacted with each other. Strikingly, the interaction was inhibited upon GF stimulation (Fig.1.10), suggesting that IRSp53 preferentially binds to the GDP-bound inactive form of RAB35. In fact, biochemical experiments using purified proteins indicate that IRSp53 preferentially interacted with the dominant negative form RAB35S22N as compared to its constitutively active form (Fig.1.10).

Thus, at least one of the mechanisms by which, IRSp53 helps in the coordination of the trafficking of PDX to form a proper AMIS is through its interaction with RAB35. However, how IRSp53 performs this function through RAB35 is yet to be clarified. The finding that IRSp53 interacts with the inactive form of RAB35 suggests that it may help in the proper localization of inactive RAB35 at the AMIS or in retaining the latter GTPase to this structure before it becomes activated and capable of recruiting additional key polarity determinants, such as PDX. Experiments to address this

question have, however, not been informative. Indeed, RAB35 can be seen at the AMIS also in IRSp53 depleted cells, likely by virtues of its prenylated c-terminal tail. Whether RAB35 dynamics at this site is affected by the loss of IRSp53 remain however a likely possibility that is worth to be further investigated. FRAP or fast spinning disk confocal analysis might be needed to precisely address this point.

IRSp53 may also facilitate the subsequent activation of RAB35 at the AMIS, possibly via stabilizing or facilitating the interaction between RAB35 and its activator guanine nucleotide exchange factors. Albeit evidence in favour of this latter possibility is still lacking, we are currently establishing a proteomic approach to identify interactors of IRSp53 in epithelial forming cysts that might illuminate on the biochemical function of the IRSp53::RAB35 interaction.

I-BAR domain of IRSp53 is sufficient for its interaction with RAB35. The interaction between IRSp53 and RAB35 is completely abolished in the absence of a functional I-BAR domain, leading to a MAD phenotype and eventually, multi-luminal cysts. The latter results are interesting in that the same residues are also required for enabling the interaction between IRSp53 and the PIP_2 rich plasma membrane. Hence, one possibility is that IRSp53 binds via its I-Bar domain to RAB35 in apical endosomal vesicles, from where it traffics to the PM, facilitating the re-localization of RAB35, which would then dissociate from IRSp53 because of the interaction of the latter protein with enriched PIP_2 at the AMIS. Within this scenario, IRSp53 might not only participate in the proper coordination of RAB35 activity or dynamic localization but also act as a critical scaffold aiding in the assembly of different complexes (IRSp53-RAB35, CDC42-IRSp53, IRSp53 and actin regulatory complex) whose fine regulated dynamics might be key in controlling where and how a central polarized lumen arises.

Consistent, with the latter possibility, structure function analysis of IRSp53 in 3D spheroids revealed that mutations in the CRIB domain, required for IRSp53 binding to

active CDC42 [116], or in the SH3 domain that mediates the interaction with a variety of IRSp53 binding partners [54] [109] [112], also resulted in a MAD phenotype (Fig1.12). and eventually to the formation of multi-luminal cysts (Fig.1.12.1). Conversely, the integrity of the PDZ binding motif was not required for these processes.

CDC42, an additional key component in the apical domain establishment and the formation of a central lumen epithelial cysts [59, 82] is recruited apically by the binding of Annexin2 (Axn2) to PIP_2 rich apical membrane in a PTEN dependant manner [59]. At this site, CDC42 is also activated by its GEF Tuba, leading, in turn, to the assembly of adherens junctions via Par3–Par6–aPKC [22, 23]. The assembly of the Par3–Par6–aPKC and the activation of the latter kinase also leads to the phosphorylation of Par3 and Lgl and to their exclusion from the apical domain [151]. LGL is a part of the basolateral Scribble complex, it's exclusion from the apical domain due to its phosphorylation by aPKC is one of the mechanisms to keep the Scribble complex out of the apical domains. This is important for the proper localisation and function of the polarity complexes to the establish of the apico-basal polarity [151]. What is the role, if any, of IRSp53 in this complex interplay remains to be assessed. Notably, IRSp53 displays high affinity for PIP_2 rich membranes via its I-BAR domain. This interaction is likely to be one of the mechanisms for IRSp53 recruitment to the apical domain. At this site, IRSp53, as it does on the extending filopodia in crawling cells, might associate with CDC42 via its CRIB domain. The ensuing structural changes are expected to lead to the opening of the close conformation of IRSp53, via liberation of its SH3 domain, which can become free to interact with a number of Proline rich interactors [112] [116] that might be important to assemble complexes at the apical domain. While more work would be needed to validate the relevance of this scenario, the finding that mutants of IRSp53 in the CRIB and SH3 domain are incapable of rescuing the MAD phenotype

and multiple lumina in IRSp53 depleted cysts lends support to this possibility. Similarly, along this line, are the observations that the SH3 domain of IRSp53 binds to various interactors like EPS8, mDia1, WAVE2, involved in the regulation of actin dynamics [116] [152]. Notably, recent data from our lab indicates that; i) EPS8 co-localises with IRSp53 at the apical membrane during early stages of cystogenesis; ii) Eps8 is involved in the proper polarisation and lumen morphogenesis since its molecular genetic removal causes the formation of multilumen phenotypes in MDCK and Caco-2 cysts; iii) EPS8 is also required for the proper localisation of IRSp53 at the apical membranes (Fig. D1). These findings altogether suggest that additional mechanisms, involving Eps8 and possibly additional SH3 interactors might be in play for achieving the correct arrangement of IRSp53 at the apical membrane for the establishment of proper polarity and lumen morphogenesis.

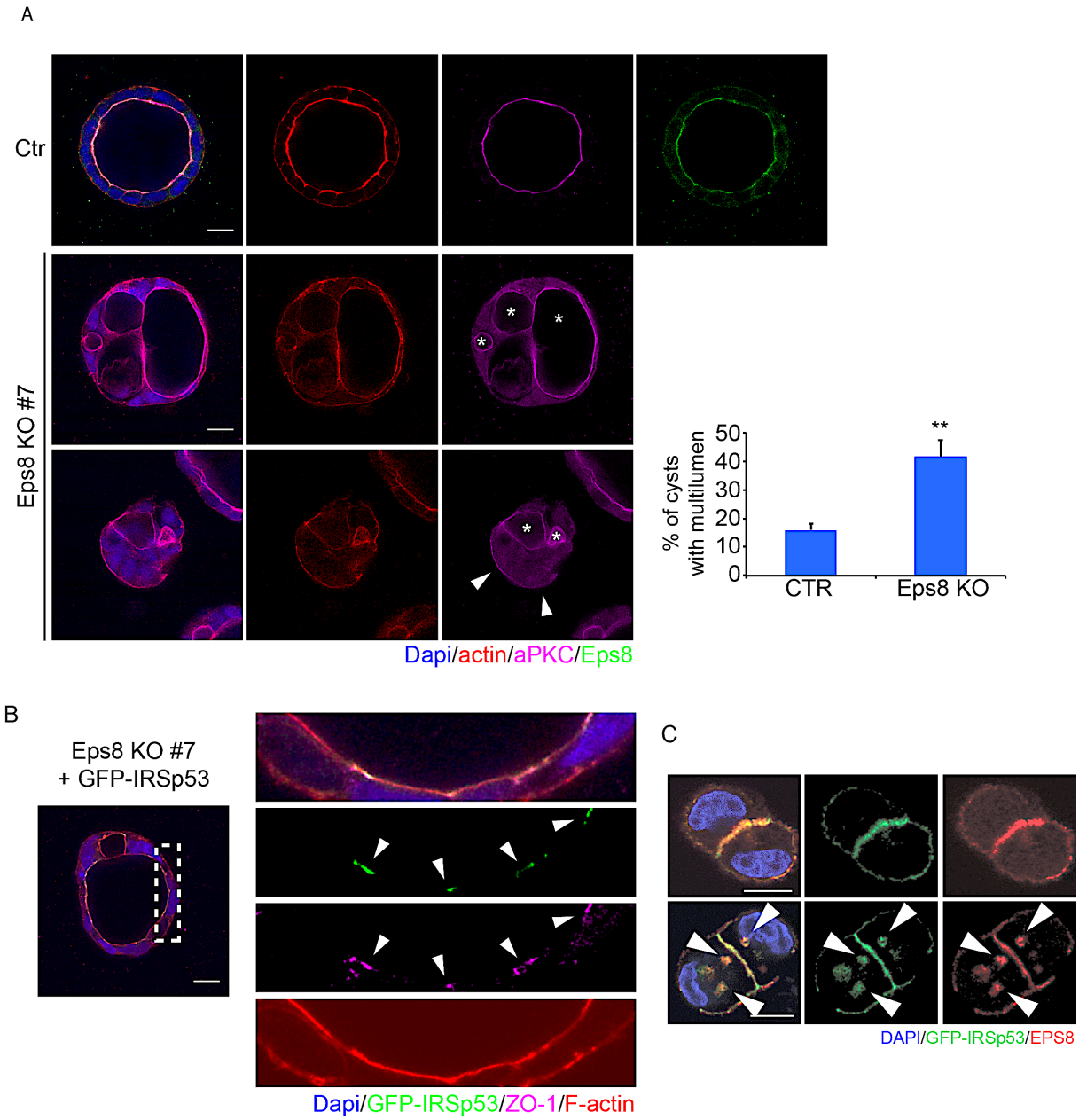

Fig. D1: EPS8 is localised to the apical lumen in Caco-2 cysts and its depletion leads to multilumen phenotype

A) Single plane confocal images of WT Ctrl and EPS8 KO Caco-2 cysts, embedded in Collagen-Matrigel matrix as single cells to undergo cystogenesis. The cysts were fixed and stained with anti-aPKC (Magenta), Phalloidin (Red), anti-EPS8 (Green), and DAPI. The control cysts display a normal central lumen with EPS8 decorated along the apical membrane. Its depletion in EPS8 KO (#7) leads to a multi-lumen phenotype. *Right*, Histogram showing the percentage of multi lumen phenotype in Ctr and #7 Caco-2 cysts. The data are mean ± S.D. T-test **p<0.01. Scale bar = 10µm.

B) Single plane confocal images of EPS8 KO Caco-2 infected with GFP-EPS8, embedded in Collagen-Matrigel matrix as single cells to undergo cystogenesis. The cysts were fixed and processed for epifluorescence to visualize GFP-IRSp53 positive cells, stained with anti-ZO1 (Magenta), Phalloidin (Red), and DAPI. The arrowheads indicate the localisation of IRSp53 to the tight junctions, marked by the ZO-1 staining. Scale bar = 10µm.

C) Confocal images of early stage MDCK cells undergoing cystogenesis on Matrigel coated slides and overlaid with Matrigel containing media. The cells were fixed, processed for epifluorescence to visualise GFP-IRSp53 and stained with anti-EPS8 and DAPI. EPS8 (Red) colocalises with GFP-IRSp53 (Green) at the apical membrane as well as in the trafficking vesicles containing IRSp53 (as shown by the arrows). Scale bar = 10μm

In summary, our data are consistent with the notion that IRSp53 is one of the early apical polarity determinants during epithelial cystogenesis and its localisation at the apical domains is critical for the normal polarisation and lumen morphogenesis of the epithelial cysts. IRSp53 also plays an important role in the development of normal single-luminal cysts by facilitating the process of early polarisation through proper trafficking of the apical proteins, to form a single AMIS. We also showed that the critical domains (I-BAR, SH3 and CRIB) of IRSp53 are all essential for the proper functioning of IRSp53 in the normal polarisation and lumenogenesis of epithelial cysts.

Apart from the role of IRSp53 in the trafficking of apical proteins to form a single AMIS, we also uncovered its role in maintaining a proper orientation of cell divisions during cystogenesis. While the cells are dividing to form a cyst, they should also maintain a proper plane of division with respect to the apical membrane for the maintenance of the overall polarity. This is achieved by a near perpendicular orientation of the mitotic spindle with respect to the apical domains in the dividing cells during the cyst formation [82]. IRSp53 localizes at the spindle poles through its I-BAR domain and helps in the maintenance of polarity during the cyst formation by properly orienting the mitotic spindle during cell divisions (Fig. 2.1). The isolated I-BAR domain of IRSp53 is, however, insufficient for the proper orientation of the mitotic spindle suggesting that other domains are critical in this process. Accordingly, a structure function analysis of IRSp53 in this context also revealed that I-BAR, CRIB and SH3 domains are all required for the proper orientation of the spindle poles during

cystogenesis. This is plausible as many of the molecular interactors of IRSp53, such as CDC42, have overlapping roles in controlling both the spindle orientation as well as the trafficking of the apical proteins.

While more work is needed to understand how IRSp53 acts in controlling spindle pole orientation, one intriguing possibility is that IRSp53 functions at this site in a fashion similar to what we discussed previously. IRSp53 may be independently localized at spindle pole through its I-BAR domain, where CDC42 may become locally activated by its GEF, Intersectin-2 or Tuba. Notably, Intersectin has been shown to be essential for controlling mitotic spindle orientation and local activation of the GTPase [153]. Activated CDC42 may interact with IRSp53 via its CRIB domain, causing conformational alteration of IRSp53, which might become a platform for the assembly of complexes needed to regulate the proper orientation of the mitotic spindle.

Centrosomes have also been shown to be site of actin nucleators in the cells. This centrosomal actin nucleation activity was shown to be strictly Arp2/3 dependant [154]. Notably, the SH3 domain of IRSp53 is known to interact with different actin modulators including the Arp2/3 activating WAVE complex at the membranes [137]. Whether IRSp53 helps in the proper orientation of the spindle poles via modulating actin polymerisation at these sites, however, has not been established and remains a line of investigation worth pursuing. The identification of direct interactors of IRSp53 at the spindle poles will be critical in establishing whether this speculative model is correct. To this end, we are undertaking an unbiased approach using mass spectrometry to find new interactors of IRSp53 at the spindle poles which mediate its interaction through its I-BAR domain.

This nevertheless, in the context of our results suggest that, in addition to controlling the trafficking of apical proteins to a single AMIS, IRSp53 is also required to properly orient the mitotic cell divisions during cystogenesis. Thus, IRSp53 appears to play a

central role by co-ordinating these two distinct processes for the establishment of polarity and lumenogenesis during spheroid formation.

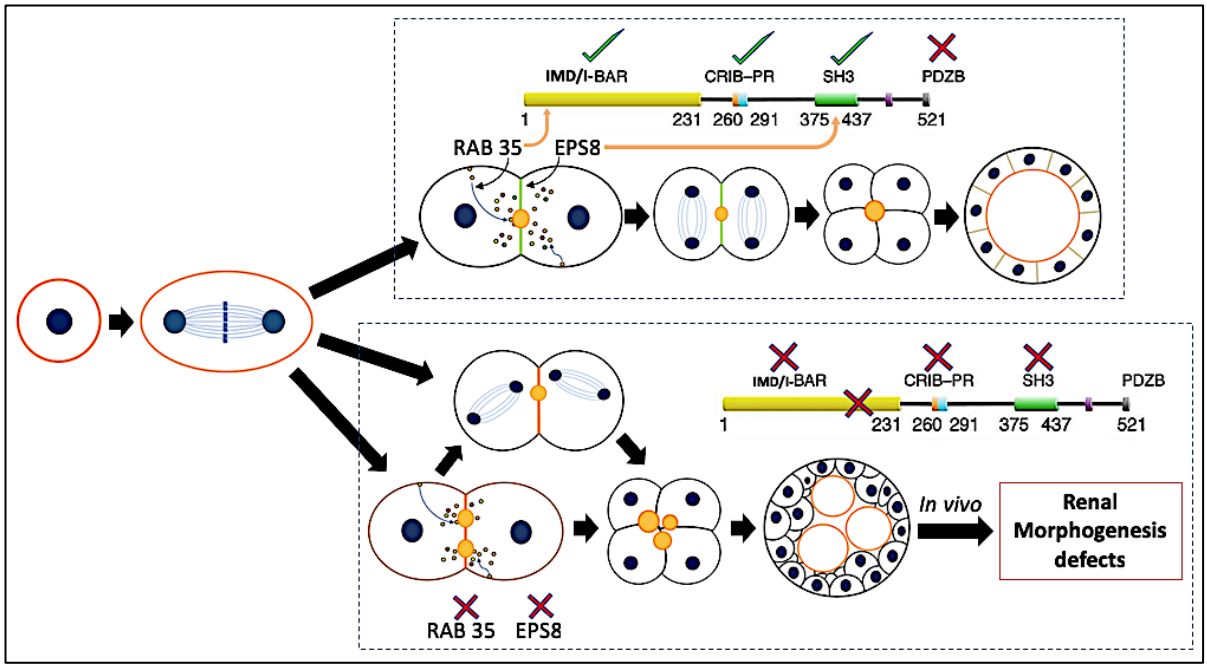

Fig. D2: Working model showing the role of IRSp53 in epithelial polarisation and lumen morphogenesis

Epithelial cells (MDCK or Caco-2) when plated as single cells in a 3-D matrix containing Matrigel™ undergo a process of polarisation and lumenogenesis. The normal process of polarisation and lumen morphogenesis, as depicted in the upper boxed area, is achieved with the help of IRSp53 containing functional I-BAR, CRIB-PR and SH3 domains. This process is perturbed, either in the absence of IRSp53 or functional mutations of any of its critical domains, as depicted in the lower boxed area, which leads to a MAD phenotype and aberrant multi-luminal cyst formation *in vitro*. While as depletion of IRSp53 in mice and zebrafish models lead to severe renal morphogenesis defects *in vivo.*

The establishment of polarity and lumenogenesis are also very important in the development and functioning of various epithelial and glandular tissues in the animals. One such tissue where IRSp53 showed a remarkably prominent expression and apically polarised localisation across many species is the Kidney. Kidney development in zebrafish starts as pronephric ducts, consisting of two simple tubules to a more complex mesonephros. The addition of tubules in the mesonephros continues till very late adult phases of the development [155], [156]. In Tg(CldnB:GFP) zebrafish

embryos, simultaneous depletion of both the paralogues of IRSp53 (B2a and B2b) leads to the formation of aberrant ectopic structures on their pronephric ducts. These ectopic, lumenised structures are reminiscent of the extra-lumens observed in mammalian cysts devoid of IRSp53, pointing to the notion that perturbation of the polarity program might be one of the underlying consequences of IRSp53 depletion *in vivo*. This is further corroborated by a disrupted tissue architecture of the kidneys in B2a KO adult zebrafish (Fig.3.2).

Mesonephric kidneys in adult zebrafish are complex dynamic and expanding structures, which keep on adding new tubules throughout the life-time of the zebrafish as it grows. They also possess a remarkable capacity to regenerate their tubules in case of an acute kidney injury [157]. In this regard, B2b alone may not be sufficient to sustain proper functioning and maintenance of the normal tissue morphology in B2a null zebrafish kidneys. In fact, B2a mutant kidneys display areas of partial degeneration, filled by infiltrating cells replacing the normal tissue. This is accompanied by the presence of vascular lacunae and defects in the architectural organization of renal tubules. It must be stressed, however, that the nature of infiltrating cells and the underlying cause of this degeneration in the tissues remains to be fully established. It will be interesting to understand if these infiltrating cells arise by morphological disruption of renal tubules due to the loss of apico-basal or planar cell polarity in the tubular epithelial cells. We are also currently generating a B2a/b double mutant line to understand whether these phenotypes are worsened upon complete removal of IRSp53 in the zebrafish.

The defects in B2a KO kidneys of adult zebrafish also prompted us to perform a detailed analysis of IRSp53 KO in the mouse models. Likewise, in zebrafish, we observed severe morphological defects in the kidneys of these mice (Fig. 3.3). Detailed analysis of these tissues revealed an uneven distribution of epithelial cells in the

tubules, reminiscent of what we observe in zebrafish. IHC analysis using the apical marker, ZO-1 and the basal marker endomucin in the kidneys further revealed a decreased and an irregular staining pattern in the IRSp53 KO renal tubules. Furthermore, reduction of cilia in the tubular lumen and the loss of aPKC staining from the apical membranes of these tubules in IRSp53 KO kidneys indicate that the perturbation of apico-basal polarity is likely the underlying cause of the observed defects. We also note, that the vasculature of these kidneys is perturbed in some areas, with vascular dilations and the presence of large lacunae. All these observations point towards the loss of polarity as the underlying cause of these gross morphological defects in the kidneys. We are currently trying to understand the implications of these defects in the proper functioning of the kidneys in IRSp53 null mice. Notably, the loss of CDC42 has been reported to cause severe kidney defects in mice due to perturbation of cell proliferation, polarity and actin cytoskeleton in their epithelial cells [158]. Moreover, CDC42 has been proposed to regulate the localisation of the co-transcriptional regulator YAP1 in kidney epithelial cells in response to N-WASP mediated actin cytoskeletal modulation [159]. IRSp53 is also known to mediate actin dynamics downstream of CDC42 through N-WASP in response to TGFβRIII signalling in epithelial cells [160]. Thus, IRSp53 may act as a scaffold to relay upstream polarity cues into a proper organisation of the actin cytoskeleton, which is important for the establishment of polarity. Whether the morphological defects in IRSp53 depleted epithelia are a consequence of disrupted signalling to the actin cytoskeleton would require a more in-depth analysis of actin architecture and dynamics in these tissues.

References

1. Treuner-Lange, A. and L. Sogaard-Andersen, *Regulation of cell polarity in bacteria.* J Cell Biol, 2014. **206**(1): p. 7-17.
2. Tahirovic, S. and F. Bradke, *Neuronal polarity.* Cold Spring Harb Perspect Biol, 2009. **1**(3): p. a001644.
3. Ngok, S.P., W.H. Lin, and P.Z. Anastasiadis, *Establishment of epithelial polarity--GEF who's minding the GAP?* J Cell Sci, 2014. **127**(Pt 15): p. 3205-15.
4. Cheng, J., et al., *A Golgi-associated PDZ domain protein modulates cystic fibrosis transmembrane regulator plasma membrane expression.* J Biol Chem, 2002. **277**(5): p. 3520-9.
5. Forbes, J.R. and D.W. Cox, *Copper-dependent trafficking of Wilson disease mutant ATP7B proteins.* Hum Mol Genet, 2000. **9**(13): p. 1927-35.
6. Charron, A.J., et al., *Compromised cytoarchitecture and polarized trafficking in autosomal dominant polycystic kidney disease cells.* J Cell Biol, 2000. **149**(1): p. 111-24.
7. Macara, I.G. and L. McCaffrey, *Cell polarity in morphogenesis and metastasis.* Philos Trans R Soc Lond B Biol Sci, 2013. **368**(1629): p. 20130012.
8. Kemphues, K.J., et al., *Identification of genes required for cytoplasmic localization in early C. elegans embryos.* Cell, 1988. **52**(3): p. 311-20.
9. Tepass, U., C. Theres, and E. Knust, *crumbs encodes an EGF-like protein expressed on apical membranes of Drosophila epithelial cells and required for organization of epithelia.* Cell, 1990. **61**(5): p. 787-99.
10. Bilder, D. and N. Perrimon, *Localization of apical epithelial determinants by the basolateral PDZ protein Scribble.* Nature, 2000. **403**(6770): p. 676-80.
11. Etemad-Moghadam, B., S. Guo, and K.J. Kemphues, *Asymmetrically distributed PAR-3 protein contributes to cell polarity and spindle alignment in early C. elegans embryos.* Cell, 1995. **83**(5): p. 743-52.
12. Bryant, D.M. and K.E. Mostov, *From cells to organs: building polarized tissue.* Nat Rev Mol Cell Biol, 2008. **9**(11): p. 887-901.
13. Kemphues, K., *PARsing embryonic polarity.* Cell, 2000. **101**(4): p. 345-8.
14. Macara, I.G., *Par proteins: partners in polarization.* Curr Biol, 2004. **14**(4): p. R160-2.
15. Ebnet, K., et al., *The cell polarity protein ASIP/PAR-3 directly associates with junctional adhesion molecule (JAM).* EMBO J, 2001. **20**(14): p. 3738-48.
16. Ebnet, K., et al., *The junctional adhesion molecule (JAM) family members JAM-2 and JAM-3 associate with the cell polarity protein PAR-3: a possible role for JAMs in endothelial cell polarity.* J Cell Sci, 2003. **116**(Pt 19): p. 3879-91.
17. Hirose, T., et al., *Involvement of ASIP/PAR-3 in the promotion of epithelial tight junction formation.* J Cell Sci, 2002. **115**(Pt 12): p. 2485-95.
18. Martin-Belmonte, F., et al., *PTEN-mediated apical segregation of phosphoinositides controls epithelial morphogenesis through Cdc42.* Cell, 2007. **128**(2): p. 383-97.

19. Otani, T., et al., *Cdc42 GEF Tuba regulates the junctional configuration of simple epithelial cells.* J Cell Biol, 2006. **175**(1): p. 135-46.
20. Suzuki, T., et al., *Neural Wiskott-Aldrich syndrome protein (N-WASP) is the specific ligand for Shigella VirG among the WASP family and determines the host cell type allowing actin-based spreading.* Cell Microbiol, 2002. **4**(4): p. 223-33.
21. Hirano, Y., et al., *Structure of a cell polarity regulator, a complex between atypical PKC and Par6 PB1 domains.* J Biol Chem, 2005. **280**(10): p. 9653-61.
22. Nagai-Tamai, Y., et al., *Regulated protein-protein interaction between aPKC and PAR-3 plays an essential role in the polarization of epithelial cells.* Genes Cells, 2002. **7**(11): p. 1161-71.
23. Morais-de-Sa, E., V. Mirouse, and D. St Johnston, *aPKC phosphorylation of Bazooka defines the apical/lateral border in Drosophila epithelial cells.* Cell, 2010. **141**(3): p. 509-23.
24. Smith, C.A., et al., *aPKC-mediated phosphorylation regulates asymmetric membrane localization of the cell fate determinant Numb.* EMBO J, 2007. **26**(2): p. 468-80.
25. Suzuki, A., et al., *aPKC acts upstream of PAR-1b in both the establishment and maintenance of mammalian epithelial polarity.* Curr Biol, 2004. **14**(16): p. 1425-35.
26. Cohen, D., et al., *The serine/threonine kinase Par1b regulates epithelial lumen polarity via IRSp53-mediated cell-ECM signaling.* J Cell Biol, 2011. **192**(3): p. 525-40.
27. Lemmers, C., et al., *CRB3 binds directly to Par6 and regulates the morphogenesis of the tight junctions in mammalian epithelial cells.* Mol Biol Cell, 2004. **15**(3): p. 1324-33.
28. Hurd, T.W., et al., *Phosphorylation-dependent binding of 14-3-3 to the polarity protein Par3 regulates cell polarity in mammalian epithelia.* Curr Biol, 2003. **13**(23): p. 2082-90.
29. Wang, Y., et al., *Platelet-derived growth factor receptor-mediated signal transduction from endosomes.* J Biol Chem, 2004. **279**(9): p. 8038-46.
30. Makarova, O., et al., *Mammalian Crumbs3 is a small transmembrane protein linked to protein associated with Lin-7 (Pals1).* Gene, 2003. **302**(1-2): p. 21-9.
31. Roh, M.H., et al., *The Crumbs3-Pals1 complex participates in the establishment of polarity in mammalian epithelial cells.* J Cell Sci, 2003. **116**(Pt 14): p. 2895-906.
32. Wang, Y., et al., *N-ethylmaleimide-sensitive factor regulates beta2 adrenoceptor trafficking and signaling in cardiomyocytes.* Mol Pharmacol, 2007. **72**(2): p. 429-39.
33. Lemmers, C., et al., *hINADl/PATJ, a homolog of discs lost, interacts with crumbs and localizes to tight junctions in human epithelial cells.* J Biol Chem, 2002. **277**(28): p. 25408-15.
34. Roh, M.H., et al., *The carboxyl terminus of zona occludens-3 binds and recruits a mammalian homologue of discs lost to tight junctions.* J Biol Chem, 2002. **277**(30): p. 27501-9.
35. Michel, D., et al., *PATJ connects and stabilizes apical and lateral components of tight junctions in human intestinal cells.* J Cell Sci, 2005. **118**(Pt 17): p. 4049-57.
36. Navarro, C., et al., *Junctional recruitment of mammalian Scribble relies on E-cadherin engagement.* Oncogene, 2005. **24**(27): p. 4330-9.
37. Muller, U., et al., *Integrin alpha 8 beta 1 promotes attachment, cell spreading, and neurite outgrowth on fibronectin.* Mol Biol Cell, 1995. **6**(4): p. 433-48.
38. Musch, M.W., et al., *T cell activation causes diarrhea by increasing intestinal permeability and inhibiting epithelial Na+/K+-ATPase.* J Clin Invest, 2002. **110**(11): p. 1739-47.

39. Kallay, L.M., et al., *Scribble associates with two polarity proteins, Lgl2 and Vangl2, via distinct molecular domains.* J Cell Biochem, 2006. **99**(2): p. 647-64.
40. Mathew, D., et al., *Recruitment of scribble to the synaptic scaffolding complex requires GUK-holder, a novel DLG binding protein.* Curr Biol, 2002. **12**(7): p. 531-9.
41. Laprise, P., A. Viel, and N. Rivard, *Human homolog of disc-large is required for adherens junction assembly and differentiation of human intestinal epithelial cells.* J Biol Chem, 2004. **279**(11): p. 10157-66.
42. Tanentzapf, G. and U. Tepass, *Interactions between the crumbs, lethal giant larvae and bazooka pathways in epithelial polarization.* Nat Cell Biol, 2003. **5**(1): p. 46-52.
43. Yamanaka, T., et al., *Mammalian Lgl forms a protein complex with PAR-6 and aPKC independently of PAR-3 to regulate epithelial cell polarity.* Curr Biol, 2003. **13**(9): p. 734-43.
44. Yurchenco, P.D., *Basement membranes: cell scaffoldings and signaling platforms.* Cold Spring Harb Perspect Biol, 2011. **3**(2).
45. Streuli, C.H. and N. Akhtar, *Signal co-operation between integrins and other receptor systems.* Biochem J, 2009. **418**(3): p. 491-506.
46. Myllymaki, S.M., T.P. Teravainen, and A. Manninen, *Two distinct integrin-mediated mechanisms contribute to apical lumen formation in epithelial cells.* PLoS One, 2011. **6**(5): p. e19453.
47. Li, B., et al., *Mesenchymal stem cells exploit extracellular matrix as mechanotransducer.* Sci Rep, 2013. **3**: p. 2425.
48. Miner, J.H. and P.D. Yurchenco, *Laminin functions in tissue morphogenesis.* Annu Rev Cell Dev Biol, 2004. **20**: p. 255-84.
49. Benton, R. and D. St Johnston, *Drosophila PAR-1 and 14-3-3 inhibit Bazooka/PAR-3 to establish complementary cortical domains in polarized cells.* Cell, 2003. **115**(6): p. 691-704.
50. Retta, S.F., F. Balzac, and M. Avolio, *Rap1: a turnabout for the crosstalk between cadherins and integrins.* Eur J Cell Biol, 2006. **85**(3-4): p. 283-93.
51. Li, R. and A.M. Pendergast, *Arg kinase regulates epithelial cell polarity by targeting beta1-integrin and small GTPase pathways.* Curr Biol, 2011. **21**(18): p. 1534-42.
52. O'Brien, L.E., et al., *Rac1 orientates epithelial apical polarity through effects on basolateral laminin assembly.* Nat Cell Biol, 2001. **3**(9): p. 831-8.
53. Yu, W., et al., *Beta1-integrin orients epithelial polarity via Rac1 and laminin.* Mol Biol Cell, 2005. **16**(2): p. 433-45.
54. Scita, G., et al., *IRSp53: crossing the road of membrane and actin dynamics in the formation of membrane protrusions.* Trends Cell Biol, 2008. **18**(2): p. 52-60.
55. Levi, B.P., A.S. Ghabrial, and M.A. Krasnow, *Drosophila talin and integrin genes are required for maintenance of tracheal terminal branches and luminal organization.* Development, 2006. **133**(12): p. 2383-93.
56. Lee, J.L. and C.H. Streuli, *Integrins and epithelial cell polarity.* J Cell Sci, 2014. **127**(Pt 15): p. 3217-25.

57. Moore, K.A., et al., *Control of basement membrane remodeling and epithelial branching morphogenesis in embryonic lung by Rho and cytoskeletal tension.* Dev Dyn, 2005. **232**(2): p. 268-81.
58. Montesano, R., G. Schaller, and L. Orci, *Induction of epithelial tubular morphogenesis in vitro by fibroblast-derived soluble factors.* Cell, 1991. **66**(4): p. 697-711.
59. Martin-Belmonte, F. and K. Mostov, *Phosphoinositides control epithelial development.* Cell Cycle, 2007. **6**(16): p. 1957-61.
60. Bryant, D.M., et al., *A molecular network for de novo generation of the apical surface and lumen.* Nat Cell Biol, 2010. **12**(11): p. 1035-45.
61. Bryant, D.M., et al., *A molecular switch for the orientation of epithelial cell polarization.* Dev Cell, 2014. **31**(2): p. 171-87.
62. Yu, D. and J.R. Turner, *Stimulus-induced reorganization of tight junction structure: the role of membrane traffic.* Biochim Biophys Acta, 2008. **1778**(3): p. 709-16.
63. Overeem, A.W., D.M. Bryant, and I.S.C. van, *Mechanisms of apical-basal axis orientation and epithelial lumen positioning.* Trends Cell Biol, 2015. **25**(8): p. 476-85.
64. Monteleon, C.L., et al., *Establishing epithelial glandular polarity: interlinked roles for ARF6, Rac1, and the matrix microenvironment.* Mol Biol Cell, 2012. **23**(23): p. 4495-505.
65. Akhtar, N. and C.H. Streuli, *An integrin-ILK-microtubule network orients cell polarity and lumen formation in glandular epithelium.* Nat Cell Biol, 2013. **15**(1): p. 17-27.
66. Apodaca, G., L.I. Gallo, and D.M. Bryant, *Role of membrane traffic in the generation of epithelial cell asymmetry.* Nat Cell Biol, 2012. **14**(12): p. 1235-43.
67. Klinkert, K., et al., *Rab35 GTPase couples cell division with initiation of epithelial apico-basal polarity and lumen opening.* Nat Commun, 2016. **7**: p. 11166.
68. Mrozowska, P.S. and M. Fukuda, *Regulation of podocalyxin trafficking by Rab small GTPases in 2D and 3D epithelial cell cultures.* J Cell Biol, 2016. **213**(3): p. 355-69.
69. Madrid, R., et al., *The formin INF2 regulates basolateral-to-apical transcytosis and lumen formation in association with Cdc42 and MAL2.* Dev Cell, 2010. **18**(5): p. 814-27.
70. de Marco, M.C., et al., *MAL2, a novel raft protein of the MAL family, is an essential component of the machinery for transcytosis in hepatoma HepG2 cells.* J Cell Biol, 2002. **159**(1): p. 37-44.
71. Martin-Belmonte, F. and K. Mostov, *Regulation of cell polarity during epithelial morphogenesis.* Curr Opin Cell Biol, 2008. **20**(2): p. 227-34.
72. Roland, J.T., et al., *Rab GTPase-Myo5B complexes control membrane recycling and epithelial polarization.* Proc Natl Acad Sci U S A, 2011. **108**(7): p. 2789-94.
73. Kravtsov, D., et al., *Myosin 5b loss of function leads to defects in polarized signaling: implication for microvillus inclusion disease pathogenesis and treatment.* Am J Physiol Gastrointest Liver Physiol, 2014. **307**(10): p. G992-G1001.
74. Li, D., et al., *FIP5 phosphorylation during mitosis regulates apical trafficking and lumenogenesis.* EMBO Rep, 2014. **15**(4): p. 428-37.
75. Joberty, G., et al., *The cell-polarity protein Par6 links Par3 and atypical protein kinase C to Cdc42.* Nat Cell Biol, 2000. **2**(8): p. 531-9.

76. Dhekne, H.S., et al., *Myosin Vb and Rab11a regulate phosphorylation of ezrin in enterocytes.* J Cell Sci, 2014. **127**(Pt 5): p. 1007-17.
77. Fogh, J., W.C. Wright, and J.D. Loveless, *Absence of HeLa cell contamination in 169 cell lines derived from human tumors.* J Natl Cancer Inst, 1977. **58**(2): p. 209-14.
78. Hidalgo, I.J., T.J. Raub, and R.T. Borchardt, *Characterization of the human colon carcinoma cell line (Caco-2) as a model system for intestinal epithelial permeability.* Gastroenterology, 1989. **96**(3): p. 736-49.
79. Meunier, V., et al., *The human intestinal epithelial cell line Caco-2; pharmacological and pharmacokinetic applications.* Cell Biol Toxicol, 1995. **11**(3-4): p. 187-94.
80. Angelis, I.D. and L. Turco, *Caco-2 cells as a model for intestinal absorption.* Curr Protoc Toxicol, 2011. **Chapter 20**: p. Unit20 6.
81. Zhang, J., et al., *Regulation of the intestinal epithelial response to cyclic strain by extracellular matrix proteins.* FASEB J, 2003. **17**(8): p. 926-8.
82. Jaffe, A.B., et al., *Cdc42 controls spindle orientation to position the apical surface during epithelial morphogenesis.* J Cell Biol, 2008. **183**(4): p. 625-33.
83. Engevik, A.C. and J.R. Goldenring, *Modeling Microvillus Inclusion Formation In Vitro.* Cell Mol Gastroenterol Hepatol, 2018. **6**(4): p. 472-473.
84. Morin, X. and Y. Bellaiche, *Mitotic spindle orientation in asymmetric and symmetric cell divisions during animal development.* Dev Cell, 2011. **21**(1): p. 102-19.
85. Zheng, Z., et al., *LGN regulates mitotic spindle orientation during epithelial morphogenesis.* J Cell Biol, 2010. **189**(2): p. 275-88.
86. Hao, Y., et al., *Par3 controls epithelial spindle orientation by aPKC-mediated phosphorylation of apical Pins.* Curr Biol, 2010. **20**(20): p. 1809-18.
87. Manahan, C.L., et al., *Dual lipid modification motifs in G(alpha) and G(gamma) subunits are required for full activity of the pheromone response pathway in Saccharomyces cerevisiae.* Mol Biol Cell, 2000. **11**(3): p. 957-68.
88. Du, Q. and I.G. Macara, *Mammalian Pins is a conformational switch that links NuMA to heterotrimeric G proteins.* Cell, 2004. **119**(4): p. 503-16.
89. Kotak, S., C. Busso, and P. Gonczy, *Cortical dynein is critical for proper spindle positioning in human cells.* J Cell Biol, 2012. **199**(1): p. 97-110.
90. Goldstein, B. and I.G. Macara, *The PAR proteins: fundamental players in animal cell polarization.* Dev Cell, 2007. **13**(5): p. 609-22.
91. Kiyomitsu, T. and I.M. Cheeseman, *Chromosome- and spindle-pole-derived signals generate an intrinsic code for spindle position and orientation.* Nat Cell Biol, 2012. **14**(3): p. 311-7.
92. Bagnat, M., et al., *Genetic control of single lumen formation in the zebrafish gut.* Nat Cell Biol, 2007. **9**(8): p. 954-60.
93. Riordan, J.R., *CFTR function and prospects for therapy.* Annu Rev Biochem, 2008. **77**: p. 701-26.
94. Husain, N., et al., *The agrin/perlecan-related protein eyes shut is essential for epithelial lumen formation in the Drosophila retina.* Dev Cell, 2006. **11**(4): p. 483-93.

95. Tonning, A., et al., *A transient luminal chitinous matrix is required to model epithelial tube diameter in the Drosophila trachea.* Dev Cell, 2005. **9**(3): p. 423-30.
96. Devine, W.P., et al., *Requirement for chitin biosynthesis in epithelial tube morphogenesis.* Proc Natl Acad Sci U S A, 2005. **102**(47): p. 17014-9.
97. Lowery, L.A. and H. Sive, *Initial formation of zebrafish brain ventricles occurs independently of circulation and requires the nagie oko and snakehead/atp1a1a.1 gene products.* Development, 2005. **132**(9): p. 2057-67.
98. Lee, Y.G., et al., *MIM, a potential metastasis suppressor gene in bladder cancer.* Neoplasia, 2002. **4**(4): p. 291-4.
99. Peter, B.J., et al., *BAR domains as sensors of membrane curvature: the amphiphysin BAR structure.* Science, 2004. **303**(5657): p. 495-9.
100. Bockmann, J., et al., *ProSAP/Shank postsynaptic density proteins interact with insulin receptor tyrosine kinase substrate IRSp53.* J Neurochem, 2002. **83**(4): p. 1013-7.
101. Kim, M.H., et al., *Enhanced NMDA receptor-mediated synaptic transmission, enhanced long-term potentiation, and impaired learning and memory in mice lacking IRSp53.* J Neurosci, 2009. **29**(5): p. 1586-95.
102. Sawallisch, C., et al., *The insulin receptor substrate of 53 kDa (IRSp53) limits hippocampal synaptic plasticity.* J Biol Chem, 2009. **284**(14): p. 9225-36.
103. Choi, J., et al., *Regulation of dendritic spine morphogenesis by insulin receptor substrate 53, a downstream effector of Rac1 and Cdc42 small GTPases.* J Neurosci, 2005. **25**(4): p. 869-79.
104. Kang, J., H. Park, and E. Kim, *IRSp53/BAIAP2 in dendritic spine development, NMDA receptor regulation, and psychiatric disorders.* Neuropharmacology, 2016. **100**: p. 27-39.
105. Offenhauser, N., et al., *Increased ethanol resistance and consumption in Eps8 knockout mice correlates with altered actin dynamics.* Cell, 2006. **127**(1): p. 213-26.
106. Suetsugu, S., et al., *Optimization of WAVE2 complex-induced actin polymerization by membrane-bound IRSp53, PIP(3), and Rac.* J Cell Biol, 2006. **173**(4): p. 571-85.
107. Mattila, P.K., et al., *Missing-in-metastasis and IRSp53 deform PI(4,5)P2-rich membranes by an inverse BAR domain-like mechanism.* J Cell Biol, 2007. **176**(7): p. 953-64.
108. Krugmann, S., et al., *Cdc42 induces filopodia by promoting the formation of an IRSp53:Mena complex.* Curr Biol, 2001. **11**(21): p. 1645-55.
109. Disanza, A., et al., *Regulation of cell shape by Cdc42 is mediated by the synergic actin-bundling activity of the Eps8-IRSp53 complex.* Nat Cell Biol, 2006. **8**(12): p. 1337-47.
110. Saarikangas, J., et al., *Molecular mechanisms of membrane deformation by I-BAR domain proteins.* Curr Biol, 2009. **19**(2): p. 95-107.
111. Yamagishi, A., et al., *A novel actin bundling/filopodium-forming domain conserved in insulin receptor tyrosine kinase substrate p53 and missing in metastasis protein.* J Biol Chem, 2004. **279**(15): p. 14929-36.
112. Disanza, A., et al., *CDC42 switches IRSp53 from inhibition of actin growth to elongation by clustering of VASP.* EMBO J, 2013. **32**(20): p. 2735-50.
113. Millard, T.H., et al., *Structural basis of filopodia formation induced by the IRSp53/MIM homology domain of human IRSp53.* Embo J, 2005. **24**(2): p. 240-50.

114. Prevost, C., et al., *IRSp53 senses negative membrane curvature and phase separates along membrane tubules.* Nat Commun, 2015. **6**: p. 8529.
115. Chen, C.J., et al., *SH2B1 and IRSp53 proteins promote the formation of dendrites and dendritic branches.* J Biol Chem, 2015. **290**(10): p. 6010-21.
116. Kast, D.J., et al., *Mechanism of IRSp53 inhibition and combinatorial activation by Cdc42 and downstream effectors.* Nat Struct Mol Biol, 2014. **21**(4): p. 413-22.
117. Lim, K.B., et al., *The Cdc42 effector IRSp53 generates filopodia by coupling membrane protrusion with actin dynamics.* The Journal of biological chemistry, 2008. **283**(29): p. 20454-72.
118. Miki, H. and T. Takenawa, *WAVE2 serves a functional partner of IRSp53 by regulating its interaction with Rac.* Biochem Biophys Res Commun, 2002. **293**(1): p. 93-9.
119. Funato, Y., et al., *IRSp53/Eps8 complex is important for positive regulation of Rac and cancer cell motility/invasiveness.* Cancer Res, 2004. **64**(15): p. 5237-44.
120. Fujiwara, T., et al., *Rho small G-protein-dependent binding of mDia to an Src homology 3 domain-containing IRSp53/BAIAP2.* Biochem Biophys Res Commun, 2000. **271**(3): p. 626-9.
121. Sekerkova, G., et al., *Novel espin actin-bundling proteins are localized to Purkinje cell dendritic spines and bind the Src homology 3 adapter protein insulin receptor substrate p53.* J Neurosci, 2003. **23**(4): p. 1310-9.
122. Soltau, M., D. Richter, and H.J. Kreienkamp, *The insulin receptor substrate IRSp53 links postsynaptic shank1 to the small G-protein cdc42.* Mol Cell Neurosci, 2002. **21**(4): p. 575-83.
123. Yanagida-Asanuma, E., et al., *Synaptopodin protects against proteinuria by disrupting Cdc42:IRSp53:Mena signaling complexes in kidney podocytes.* Am J Pathol, 2007. **171**(2): p. 415-27.
124. Teodorof, C., et al., *SPIN90-IRSp53 complex participates in Rac-induced membrane ruffling.* Exp Cell Res, 2009. **315**(14): p. 2410-9.
125. Okamura-Oho, Y., et al., *Dentatorubral-pallidoluysian atrophy protein interacts through a proline-rich region near polyglutamine with the SH3 domain of an insulin receptor tyrosine kinase substrate.* Hum Mol Genet, 1999. **8**(6): p. 947-57.
126. Oda, K., et al., *Identification of BAIAP2 (BAI-associated protein 2), a novel human homologue of hamster IRSp53, whose SH3 domain interacts with the cytoplasmic domain of BAI1.* Cytogenet Cell Genet, 1999. **84**(1-2): p. 75-82.
127. Weiss, S.M., et al., *IRSp53 links the enterohemorrhagic E. coli effectors Tir and EspFU for actin pedestal formation.* Cell Host Microbe, 2009. **5**(3): p. 244-58.
128. Sanda, M., et al., *The postsynaptic density protein, IQ-ArfGEF/BRAG1, can interact with IRSp53 through its proline-rich sequence.* Brain Res, 2009. **1251**: p. 7-15.
129. Misra, A., et al., *The mammalian verprolin, WIRE induces filopodia independent of N-WASP through IRSp53.* Exp Cell Res, 2010. **316**(17): p. 2810-24.
130. Tourette, C., et al., *A large scale Huntingtin protein interaction network implicates Rho GTPase signaling pathways in Huntington disease.* J Biol Chem, 2014. **289**(10): p. 6709-26.
131. Barilari, M. and L. Dente, *The neuronal proteins CIPP, Cypin and IRSp53 form a tripartite complex mediated by PDZ and SH3 domains.* Biol Chem, 2010. **391**(10): p. 1169-74.

132. Chou, A.M., et al., *Dynamin1 is a novel target for IRSp53 protein and works with mammalian enabled (Mena) protein and Eps8 to regulate filopodial dynamics.* J Biol Chem, 2014. **289**(35): p. 24383-96.
133. Robens, J.M., et al., *Regulation of IRSp53-dependent filopodial dynamics by antagonism between 14-3-3 binding and SH3-mediated localization.* Mol Cell Biol, 2010. **30**(3): p. 829-44.
134. Hori, K., et al., *MALS is a binding partner of IRSp53 at cell-cell contacts.* FEBS Lett, 2003. **554**(1-2): p. 30-4.
135. Soltau, M., et al., *Insulin receptor substrate of 53 kDa links postsynaptic shank to PSD-95.* J Neurochem, 2004. **90**(3): p. 659-65.
136. Govind, S., et al., *Cdc42Hs facilitates cytoskeletal reorganization and neurite outgrowth by localizing the 58-kD insulin receptor substrate to filamentous actin.* J Cell Biol, 2001. **152**(3): p. 579-94.
137. Miki, H. and T. Takenawa, *[WASP-family, a critical signal transducer linking various signals to rapid actin-polymerization].* Seikagaku, 2000. **72**(7): p. 550-4.
138. Ahmed, S., W.I. Goh, and W. Bu, *I-BAR domains, IRSp53 and filopodium formation.* Semin Cell Dev Biol, 2010. **21**(4): p. 350-6.
139. Sathe, M., et al., *Small GTPases and BAR domain proteins regulate branched actin polymerisation for clathrin and dynamin-independent endocytosis.* Nat Commun, 2018. **9**(1): p. 1835.
140. Connolly, B.A., et al., *Tiam1-IRSp53 complex formation directs specificity of rac-mediated actin cytoskeleton regulation.* Mol Cell Biol, 2005. **25**(11): p. 4602-14.
141. Disanza, A., et al., *Eps8 controls actin-based motility by capping the barbed ends of actin filaments.* Nat Cell Biol, 2004. **6**(12): p. 1180-8.
142. Vaggi, F., et al., *The Eps8/IRSp53/VASP network differentially controls actin capping and bundling in filopodia formation.* PLoS Comput Biol, 2011. **7**(7): p. e1002088.
143. Abou-Kheir, W., et al., *Membrane targeting of WAVE2 is not sufficient for WAVE2-dependent actin polymerization: a role for IRSp53 in mediating the interaction between Rac and WAVE2.* J Cell Sci, 2008. **121**(Pt 3): p. 379-90.
144. Cohen, D., et al., *Mammalian PAR-1 determines epithelial lumen polarity by organizing the microtubule cytoskeleton.* J Cell Biol, 2004. **164**(5): p. 717-27.
145. Massari, S., et al., *LIN7 mediates the recruitment of IRSp53 to tight junctions.* Traffic, 2009. **10**(2): p. 246-57.
146. Parker, S.S., C. Cox, and J.M. Wilson, *Rabs set the stage for polarity.* Small GTPases, 2018. **9**(1-2): p. 116-129.
147. Vega-Salas, D.E., P.J. Salas, and E. Rodriguez-Boulan, *Exocytosis of vacuolar apical compartment (VAC): a cell-cell contact controlled mechanism for the establishment of the apical plasma membrane domain in epithelial cells.* J Cell Biol, 1988. **107**(5): p. 1717-28.
148. Brignoni, M., et al., *Exocytosis of vacuolar apical compartment (VAC) in Madin-Darby canine kidney epithelial cells: cAMP is involved as second messenger.* Exp Cell Res, 1993. **205**(1): p. 171-8.

149. Haas, P. and D. Gilmour, *Chemokine signaling mediates self-organizing tissue migration in the zebrafish lateral line.* Dev Cell, 2006. **10**(5): p. 673-80.
150. Agarwala, S., et al., *Amotl2a interacts with the Hippo effector Yap1 and the Wnt/beta-catenin effector Lef1 to control tissue size in zebrafish.* Elife, 2015. **4**: p. e08201.
151. Rodriguez-Boulan, E. and I.G. Macara, *Organization and execution of the epithelial polarity programme.* Nat Rev Mol Cell Biol, 2014. **15**(4): p. 225-42.
152. Goh, W.I. and S. Ahmed, *mDia1-3 in mammalian filopodia.* Commun Integr Biol, 2012. **5**(4): p. 340-4.
153. Rodriguez-Fraticelli, A.E., et al., *The Cdc42 GEF Intersectin 2 controls mitotic spindle orientation to form the lumen during epithelial morphogenesis.* J Cell Biol, 2010. **189**(4): p. 725-38.
154. Farina, F., et al., *The centrosome is an actin-organizing centre.* Nat Cell Biol, 2016. **18**(1): p. 65-75.
155. Drummond, I.A. and A.J. Davidson, *Zebrafish kidney development.* Methods Cell Biol, 2010. **100**: p. 233-60.
156. Gerlach, G.F. and R.A. Wingert, *Zebrafish pronephros tubulogenesis and epithelial identity maintenance are reliant on the polarity proteins Prkc iota and zeta.* Dev Biol, 2014. **396**(2): p. 183-200.
157. McCampbell, K.K. and R.A. Wingert, *New tides: using zebrafish to study renal regeneration.* Transl Res, 2014. **163**(2): p. 109-22.
158. Elias, B.C., et al., *Cdc42 regulates epithelial cell polarity and cytoskeletal function during kidney tubule development.* J Cell Sci, 2015. **128**(23): p. 4293-305.
159. Reginensi, A., et al., *Yap- and Cdc42-dependent nephrogenesis and morphogenesis during mouse kidney development.* PLoS Genet, 2013. **9**(3): p. e1003380.
160. Oh, S.Y., et al., *The type III TGFbeta receptor regulates filopodia formation via a Cdc42-mediated IRSp53-N-WASP interaction in epithelial cells.* Biochem J, 2013. **454**(1): p. 79-89.

Acknowledgements

I would like to thank my supervisor Prof. Giorgio Scita for his continuous support and encouragement throughout my PhD.

I would also like to thank Sara Bisi and Andrea Disanza for their valuable help with some of the experiments and analysis.

Furthermore, I want to thank:

My internal advisor Prof. Elisabetta Dejana and my external advisor Prof. Holger Gerhardt for helpful discussions and evaluating my project reports.

Prof. Fernando Martin-Belmonte and Prof. Marina Mapelli for a detailed review of this manuscript.

Prof. Colin Jamora, my past supervisor and mentor, whom I continue to collaborate with and to learn from even to this day. I hope to continue this collaboration in future as well.

All ‘grumpy-bumpy’ and ‘sunny-funny’ members of the Scita group.

Other members of Lab B, who I shared the common lab space with.

Facilities at the campus for - Zebrafish, Imaging, Histopathology, DNA Sequencing, qPCR, Flow Cytometry and Tissue culture.

Friends at the campus, especially, among the small international community for scientific and non-scientific discussions over lunch/coffee. I have learned a lot from all of you during this time.

All friends outside the campus for the memorable moments we shared together. I hope we stay in touch and our paths keep intersecting in future.

All the members of *'Panin Keashir Baraderi'* in Europe especially, Irshad Mir, Zeeshan Hamid and Mohsin Hassan, for the adventurous trips we undertook together and for our intense discussions about Kashmir and beyond. I hope we continue these adventures in future as well.

International student's welcome office at IFOM for taking care of all the bureaucratic procedures and documentation to make my stay in Italy comfortable.

Università degli Studi di Milano (UniMi) for fellowship throughout my PhD and contribution by Fondazione Umberto Veronesi (FUV) to this fellowship during the initial years of my PhD.

Family and friends in Kashmir for always believing in me and bearing with the long intervals of my absence from home. I apologise for missing out on many important events of your life.

A special thanks to Marina Properzi, 'My Italian Mamma', for teaching me Italian and always being there for me especially during my ups and downs of health. I wish to be your Kashmiri son forever.